https://doi.org/10.1016/j.tws.2021.107573

DESIGN OF COLD-FORMED HIGH STRENGTH STEEL TUBULAR T-JOINTS UNDER COMPRESSION LOADS

Madhup Pandey*, Kwok-Fai Chung and Ben Young

Department of Civil and Environmental Engineering, The Hong Kong Polytechnic University, Hong Kong, China

Abstract

This study presents a comprehensive finite element (FE) analysis of cold-formed high strength steel (CFHSS) tubular T-joints. The brace members of tubular T-joints were made up of rectangular (including square) and circular hollow sections (RHS and CHS), whereas the chord members were made up of RHS. The nominal yield strengths (i.e. 0.2% proof stresses) of the tubular members were 900 and 960 MPa for S900 and S960 steels, respectively. Finite element (FE) models were developed and verified against the tests conducted by Pandey and Young [1], showing the capability of reciprocating the experimental joint strengths, failure modes and load-deformation histories. The material properties and test results used for the validations of the FE models are reported in Pandey and Young [1]. The tubular T-joints were tested under axial compression through the brace members, while the ends of the chord members were supported on rollers. Upon validations of the FE models, a parametric study comprised of 285 FE analyses was carried out. The validity ranges of governing parameters in this study exceeded the current validity ranges given in the EC3 [2] and CIDECT [3]. A total of 309 joint strengths obtained from the tests [1] and parametric study were compared with the nominal strengths obtained from the EC3 [2] and CIDECT [3]. In this study, three failure modes were observed, namely chord face failure, chord side wall failure and combined failure. The applicability of current chord stress function given in the CIDECT [3] was also evaluated for cold-formed tubular T-joints of S900 and S960 steel grades. It is shown that the existing design rules given in the EC3 [2] and CIDECT [3] are not directly suitable for T-joints of S900 and S960 steels with validity ranges of governing parameters exceeding the limits specified in these specifications [2,3] and their modifications are needed. Therefore, using two approaches, i.e. semi-empirical and by applying correction factors on the latest equations given in the EC3 [2,59], design rules are proposed in this study for cold-formed tubular T-joints of S900 and S960 steel grades. In addition, reliability analyses were also performed to check the reliability levels of the existing and proposed design rules.

Keywords: Cold-formed steel; Design rules; Finite element analysis; High strength steel; Hollow section joints; Tubular T-joints.

*Corresponding author. (e-mail: madhup.pandey@polyu.edu.hk)

1. Introduction

Over the last few years, the construction sector has noticed a sharp increase in the structural applications of cold-formed high strength steel (CFHSS) tubular members due to their superior strength-to-weight ratio, which eventually result in material saving and easier handling. The recent growths in manufacturing and metallurgical sectors facilitated high strength steel (HSS) production with reduced carbon content and improved toughness. Owing to these merits, the production and application of HSS material (yield strength greater than 460 MPa) are in-line with the sustainable development practice laid down by many countries and organisations. CFHSS tubular members with nominal yield strengths (i.e. 0.2% proof stresses) of 900 and 960 MPa are now commercially available, however, their structural applications are rather quite scant due to limited research findings. The validity of current design provisions in many international codes and guidelines are generally restricted for steels with the nominal yield strengths up to 460 MPa, except the Eurocode 3 (EC3) wherein the applicability of the design rules has been extended up to 700 MPa. Therefore, to bridge the gap between the industry and current design provisions, the potential exploration of CFHSS tubular joints needs urgent research attention. Pandey and Young [1,4,5] conducted a series of experimental investigation on CFHSS tubular T-joints, T-joints with fully supported chords and X-joints made up of S900 and S960 steel grades with square and rectangular hollow section (RHS) chords. Li and Young [6] conducted tests on concrete-filled RHS X-joints of S700 and S900 steel grades. Lan et al. [7] numerically investigated the structural performance of built-up RHS X-joints made up of S460, S690 and S960 steel grades. Feldmann et al. [8] conducted tests on RHS X- and K-joints made up of S500, S700 and S960 steel grades to examine the applicability of the existing reduction factors. Havula et al. [9] experimentally examined the behaviour of RHS T-joints under brace in-plane bending using S420, S500 and S700 steel grades.

This study presents a numerical investigation on the behaviour of CFHSS tubular T-joints. The numerical investigation was performed using finite element (FE) analysis, which is now increasingly employed to extend the size of the data pool, and thus, to have a broader understanding on the structural behaviour. The FE models developed in this study were calibrated against the tests conducted by Pandey and Young [1]. Using the validated FE models, a comprehensive parametric study, comprised of 285 tubular T-joints, was undertaken to broaden the test database by duly considering a wider range of governing geometrical parameters. The joint failure strengths obtained from the tests [1] and parametric study were compared with the nominal strengths obtained from the EC3 [2] and CIDECT [3]. It is shown that the existing design provisions in these specifications [2,3] are not directly suitable for T-joints made up of S900 and S960 steels and their modifications are needed. Hence, design rules are proposed for CFHSS tubular T-joints made up of RHS and circular hollow section (CHS) braces and RHS chords of S900 and S960 steel grades.

2. Summary of experimental programme

The experimental investigation on CFHSS tubular T-joints was conducted by Pandey and Young [1]. The joint failure strengths, failure modes and load-deformation histories reported in Pandey and Young [1] were used to validate the FE models of this study. The tubular T-joints in the test programme [1] were fabricated from CFHSS tubular members of S900 and S960 steel grades. The RHS and CHS used in the tests [1] were produced through the thermo-mechanically controlled process (TMCP). In the test programme [1], two types of T-joint configurations were investigated. First, RHS-RHS, wherein both brace and chord members were made up of RHS, and second, CHS-RHS, wherein brace members were made up of CHS and chord members were made up of RHS. The nominal yield strength of the RHS-RHS configuration was 960 MPa, while the nominal yield strength of the CHS-RHS configuration was 900 MPa. A total of 24 T-joint tests was conducted. Axial compression load was applied through the brace members keeping the ends of the chord members resting on rollers. It should be noted that during the tests, the chord ends were remained open. In the experiments [1], the chord members were not subjected to any external applied axial preload. In the test programme [1], brace-to-chord width ratio ($\beta=b_1/b_0$) ranged from 0.34 to 1, brace-to-chord thickness ratio ($\tau=t_1/t_0$) ranged from 0.52 to 1.27, chord width-to-chord thickness ratio ($2\gamma=b_0/t_0$) ranged from 20.6 to 38.6 and chord side wall slenderness ratio (h_0/t_0) ranged from 12.7 to 38.8. The chord length-to-chord width ratio (L_0/b_0) of test specimens ranged from 3.74 to 5.64, chord length-to-chord depth ratio (L_0/h_0) ranged from 4.61 to 8.11 and chord length-to-maximum of chord width and depth ($L_0/\max[b_0,h_0]$) ratio of test specimens ranged from 3.74 to 5.64. The average measured dimensions of braces, chords and welds can be obtained from Pandey and Young [1]. In order to determine the material properties, tensile tests were conducted on coupons extracted from the flat, corner and curved regions of the tubular members. The 0.2% proof stresses (adopted as yield strengths) of flat, corner and curved regions were ranged from 910.4 to 1059.1, 1042.2 to 1125.6 and 978.6 to 1006.7 MPa, respectively. The ultimate strengths of flat, corner and curved regions were ranged from 1051.1 to 1180.5, 1139.3 to 1249.4 and 1097.3 to 1105.3 MPa, respectively. For all tensile coupons, 80% of ultimate strengths were lesser than their corresponding 0.2% proof stresses. The material property of the weld metal was determined by conducting all-weld metal tensile coupon tests, as detailed in Pandey and Young [4]. The material properties and joint strengths reported in Pandey and Young [1] were obtained from the static curves, which in turn were obtained from their respective test curves by pausing the tests at different predetermined locations for 2 minutes. In the test programme [1], three types of failure modes were obtained, namely, chord face failure (F), chord side wall failure (S) and combined failure (F+S). With regard to the labelling of the test specimens, the general form of the label T-50×100×4-150×150×6 can be written as T-$b_1\times h_1\times t_1$-$b_0\times h_0\times t_0$, where the definition of symbols can be obtained from Fig. 1. In this numerical investigation, the labelling scheme for T-joints was kept identical to the experimental investigation [1]. For more details

regarding the test-setup, test procedure and analyses of results, reference can be made to Pandey and Young [1].

3. Numerical programme

3.1. Finite element models

3.1.1. General

The commercially available FE package ABAQUS [10] was used in this study to develop FE models. The measured tubular member dimensions and material properties, reported in Pandey and Young [1], were used to develop these FE models. In this study, the (*STATIC) general solver of the ABAQUS [10] was used for the analysis. The isotropic strain hardening and Von-Mises yield criterion rules were adopted in the FE models. For each FE model, a nonlinear time step analysis was used in conjunction with a full Newton-Raphson frontal equation solver. In order to provide accurate results, both geometric and material non-linearities were included in the FE models together with the allowance for large deformation. The joint strengths, failure modes and load-deformation histories, obtained from the FE models, were used to validate the test results reported in Pandey and Young [1]. In addition, the FE sensitivity analyses were performed to investigate the effects of element types, mesh size, through-thickness division, corner region extension and contact interaction between the chord and bearing plates.

3.1.2. Element types and mesh sizes

Based on the FE sensitivity analyses, hexahedral elements were used throughout the FE models except for the welds. Owing to the complex weld profiles, tetrahedral elements were used for the welds in this study. A 20-node quadratic hexahedral solid element without reduced integration (C3D20) was used for all elements except the welds, whereas a 10-node quadratic tetrahedral solid element (C3D10) was used for the welds. The built-in structured and free mesh techniques of ABAQUS [10] were respectively used for the meshing of C3D20 and C3D10 elements. Many previous numerical studies on tubular joints [11-16] advocated the selection of solid elements over shell elements in order to reflect actual joint behaviour and realistic fusions of weld-chord and weld-brace interface regions. By duly taking account of the accuracies and convergence studies of the FE models, 4 mm × 4 mm (length : width) mesh size was used for all the chord members and 7 mm × 7 mm (length : width) mesh size was used for all the brace members. However, the mesh size of the welds was kept as 7 mm. The corner regions of brace and chord members were respectively divided into 6 and 10 elements to ensure a smooth transition of the load. Various trials were conducted to investigate the effect of through-thickness division, wherein the chord member was divided along its thickness direction by up to three layers. The results of these simulations showed no noticeable

difference in the load vs chord face indentation curves of the typical RHS-RHS and CHS-RHS T-joints, as shown in Figs. 2 and 3, respectively. The use of tubular members with small thicknesses ($t \leq 6$ mm) in the tests [1] and the use of second-order solid element (i.e. C3D20) in the FE models could be the possible reasons behind these observations. Moreover, Crockett [16] numerically investigated the effects of through-thickness divisions and found negligible through-thickness stress variation in thin-walled structures modelled with C3D20 elements. Therefore, for the validation of the tests [1], brace and chord members of the FE models were not divided along the thickness direction.

3.1.3. Material properties

In this investigation, the material properties assigned to the FE models were obtained from the tensile coupon tests conducted by Pandey and Young [1]. Due to the cold-forming process, the corner and curved regions of the tubular members were work-hardened, and thus, exhibited different material properties compared to their respective flat regions. Therefore, measured static tensile material properties were obtained from the flat, corner and the curved regions of the tubes, as detailed in Pandey and Young [1]. The measured tensile stress-strain curves were converted into the static stress-strain curves using the load drops obtained by respectively pausing the tensile coupon tests near the 0.2% proof stress, ultimate strength and in the post-ultimate region for 2 minutes. The conversion of test stress-strain curves into static stress-strain curves eliminated the influence of loading rate from the obtained material properties. All the experimentally obtained measured static stress-strain curves were converted into true stress-logarithmic plastic strain curves using the recommendations given in the ABAQUS [10]. The true stress-logarithmic plastic strain curves from the flat, corner and curved regions of tubular members were then assigned into their respective locations in the FE models. As the cold-forming effect generally does not confine to the corner regions only, thus, the corner material properties were extended to the adjacent flat regions by a distance of $2t$, which was consistent with the recommendations of other studies [6,17,18]. In this study, the Poisson's ratio of steel was taken as 0.3. The material properties of the weld metal were obtained by conducting all-weld metal tensile coupon tests, as detailed in Pandey and Young [4]. The measured average values of 0.2% proof stress, ultimate strength and fracture strain of the weld metal were 965.2 MPa, 1023.4 MPa and 17.2%, respectively [4]. The measured static stress-strain curve of the weld metal was converted into true stress-logarithmic plastic strain curve before assigning it to the weld parts of the FE models. Furthermore, the material properties assigned to the weld heat affected region (WHAR) of the FE models are detailed in Section 3.1.8 of this paper.

3.1.4. Boundary conditions and loading

The boundary conditions at the reference points (RP) of the FE models were exactly assigned in accordance with the test setup [1], as shown in Fig. 4. The reference point, RP-1, was kinematically coupled to the cross-sectional nodes of the top brace end, and its movement was restrained against all degrees of freedom, thereby making it as a fixed end. In the experimental programme [1], T-joints were tested under pure chord in-plane bending, wherein the chord ends were resting on the rollers. Thus, in FE models, reference points (RP-2 and RP-3) were assigned at a vertical distance of 20 mm, equal to half of the diameter of rollers used in the tests [1], from the bottom surfaces of both the end bearing plates. Each bottom surface of the end bearing plate was then kinematically coupled to its respective reference point. In order to reciprocate the pin-end boundary condition, the movement of RP-2 and RP-3 were restrained against all degrees of freedom, except for the displacement along the brace axial direction (i.e. the direction of the applied load) and rotation about the chord transverse direction. It should be noted that the nodes other than these reference points (RP-1, RP-2 and RP-3) were free to translate and rotate in any direction. The loads were applied in the form of axial compressions at RP-2 and RP-3 reference points by specifying incremental axial displacements along the brace axial direction, which was identical to the movement of the loading ram in the tests [1]. In order to consider large displacement analysis, the non-linear geometry (*NLGEOM) parameter was enabled in all the simulations. Moreover, in order to establish the initial contact interaction, an initial load step was created before the application of actual displacement-controlled loading.

3.1.5. Modelling of weld sizes

In this study, welds were included in all the calibrated, and subsequent, parametric FE models. The weld geometries were based on the measured average weld leg sizes as detailed in Pandey and Young [1]. In tests [1], the average dimensions of the welds were obtained by taking mean of 20 weld measurements taken around the perimeter of the joint region. The welds were modelled for all RHS-RHS and CHS-RHS T-joints. Due to complex weld profiles, particularly for RHS-RHS and CHS-RHS T-joints with large values of β ratio, C3D10 element with free mesh technique was used to simulate the welds. It should be noted that the main objective of the present investigation was to focus on the member failure of the joints with weld being treated as non-critical elements. However, the inclusions of measured weld profiles and measured weld material properties in the FE models helped in achieving the accuracy of simulations in terms of joint stiffness, joint strength, failure mode and load-deformation history. In addition to the ability of C3D10 element of taking complicated shapes, its selection also helped in maintaining the flexibility of the welds under joint deformation, and thus, achieving the realistic joint strengths. For RHS-RHS and CHS-RHS T-joints with $\beta \leq 0.80$, the weld was modelled as fillet weld (FW) all around the joint perimeter. However, for RHS-RHS and CHS-RHS T-joints with $\beta > 0.80$, the weld was modelled as FW along the chord transverse direction and as partial joint penetration flare bevel groove weld (GW), without brace connecting end

chamfer, along the chord longitudinal direction. The fillet weld leg size (w) was designed as $1.5t_{min}$ (where t_{min} was taken as the minimum of brace and chord thickness) as per the recommendations given in the AWS D1.1/D1.1M [19], which was identical with the measured values in the tests [1].

3.1.6. Contact interactions

The contact interactions play a vital role in the load transfer mechanism of an FE model, and thus, requires a correct modelling approach. The surface-to-surface discretization contact approach, without any friction penalty and with finite sliding, was used to establish the contact between the connecting regions of brace and chord members. The 'master-slave' algorithm of the analytical rigid-deformable contact interaction from the ABAQUS [10] library was used to fuse the surfaces between weld-brace and weld-chord. This contact interaction algorithm does not allow the fused surfaces to penetrate each other under compression, while the fused surfaces can separate each other under tension. The 'master-slave' contact interaction facilitated the welds in transferring the loads from the brace member on to the wider area of the chord connecting face under brace axial compression, thereby reflecting the real joint behaviour. The welds, being non-critical, were assigned as the master surfaces, whereas the connecting parts of brace and chord members were assigned as the slave surfaces. This selection of master and slave surfaces also helped in avoiding the overlapping of the slave nodes, if assigned otherwise. The surface-to-surface discretization contact approach, with finite sliding and friction penalty along the tangential direction, was used to fuse the surfaces between the chord and the bearing plates. For this interaction, the chord (deformable member) was assigned as the slave surface, and the bearing plates (strong member) were assigned as the master surfaces. Various trials were made to select an optimum value of the friction coefficient in order to impose a friction penalty along the tangential direction. Finally, a friction coefficient of 0.3 had shown a good agreement with the test results. In this study, the surface-to-surface discretization contact was established using a 'hard' contact pressure overclosure along the normal direction, which also allowed the separation of contact surfaces.

3.1.7. Effect of weld modelling

The weld modelling has an important contribution in the numerical investigation of tubular joints. Notable numerical studies which investigated the effect of weld modelling on the behaviour of tubular joints, include Crockett [16], Reimer et al. [20], Bhuyan et al. [21], van der Vegte et al. [22] and de Koning et al. [23]. In these studies, Crockett [16] conducted FE analysis on tubular joints by considering both shell and solid elements for welds; Reimer et al. [20] conceptualised the weld modelling using 2-dimensional (2D) shell elements; Bhuyan et al. [21] used 6-noded solid elements for welds; van der Vegte et al. [22] and de Koning et al. [23] modelled welds using 8-noded shell

elements. There are various concerns associated with the modelling of welds as shell elements. First, the selection of correct optimum thickness for the weld shell element, second, the correct positioning of the weld shell element with respect to the brace-chord intersection, third, the presence of unrealistic 'air-gap' between the weld shell element and brace-chord intersection, fourth, the incapability of the shell elements to analyse stress and strain in 3-dimensional (3D) region, and fifth, the buckling of the weld shell element. On the other hand, the numerical incompatibility is very likely to arise with solid weld elements and shell tubular member elements due to the overlapping of their interaction regions, which could lead to poor calibration. All these concerns could simply be overcome by modelling welds and tubular members using solid tetrahedral and hexahedral elements, respectively. The weld modelling with shell elements was done when the computational possibilities were quite limited. Due to recent computational advancements, it is now possible to perform such numerical simulations using solid elements.

The practise of keeping a simple joint model by entirely excluding the welds eventually leads to an unrealistic FE model. It is now a proven fact that the lack of accounting for the welds in FE models yields conservative results [16,24]. In addition, the presence of welds in FE models has a significant effect in re-defining the effective β ratio which in turn is responsible for the load transfer mechanism of the joint and hence affects the joint failure strength. This explanation is in good agreement with the yield line models proposed by Packer [25] and Davies et al. [26], which included the effect of weld leg sizes in their proposed models. The influence of weld leg size on the static joint strength and overall joint behaviour was investigated by Yu and Wardenier [27]. In order to make the design recommendations simple and suitable for full penetration welds and also conservatively for fillet welded joints, the welds were neglected. The effects of weld modelling on the overall behaviour of CFHSS tubular T-joints was also investigated in this study. In total, 5 typical FE models covering different failure modes and joint configurations of this study were re-run by excluding the welds. The load vs chord face indentation curves obtained from this comparison are shown in Figs. 5-7 and 8-9 for RHS-RHS and CHS-RHS T-joints, respectively. The joint strengths obtained corresponding to this comparison are summarised in Table 1. It can be noticed that the FE models with welds provide a much closer correlation, both in terms of the joint strengths and load-deformation histories, to the experimental results, compared to the FE models without welds. The degree of conservatism increased with the increase of β value up to the extent that for equal-width (β=1) tubular T-joint, welds have to be included in the FE model to yield sensible numerical outcomes. It can be noticed that the ignorance of weld and WHAR in FE models underestimated the joint strengths by 6 to 32%.

3.1.8. Weld heat affected region (WHAR)

HSS is produced through different production processes, mainly by the quenched process (Q) and TMCP. Although the current international standards do not differentiate HSS by the production

process, however, when subjected to welding, HSS produced through different production processes behave differently [28]. During welding, the heat energy causes a phase transition in the semi-solid state, thereby significantly altering the virgin microstructure of the parent material. The most severe WHAR during the welding is the region where the weld metal gets fused with the parent metal (i.e. fusion zone, FZ) followed by the immediate region surrounding the freshly deposited weld material (i.e. heat affected zone, HAZ). The HSS produced using TMCP have relatively lower carbon equivalents compared to similar quenched HSS. Consequently, TMCP steels can be welded at a lower pre-heat temperature using the same welding process parameters [29]. Moreover, the original microstructure of TMCP steel and its associated mechanical properties are a result of the thermomechanical rolling process performed at low rolling temperatures. Due to the high welding heat energy, the original microstructure and the effect of the rolling process in TMCP steel get lost. The reduction of material strength in WHAR depends on many factors, such as parent metal thickness, parent metal type, parent metal steel grade, welding process type, welding process parameters (arc voltage, current and weld deposition speed) and so on [30,31,32,33]. Stroetmann et al. [28] discovered a relatively larger strength reduction in the HAZ of TMCP HSS compared to quenched HSS. Javidan et al. [30] observed around 30% strength reduction in the HAZ region of TMCP tubular members made up of S960 steel grade. For S960 steel, Amraei et al. [31] reported that the yield stress reduction is about 13%, and the ultimate tensile strength reduction is about 21%. Amraei et al. [32] reported that the yield stress reduction ranged from 20% to 37%, whereas the ultimate tensile strength reduction ranged from 16% to 32%, for S960 steel. Pandey and Young [33] concluded that the reduction in ultimate tensile strengths of S960 TMCP tubular members of 3 to 6 mm thicknesses were ranged from 3% to 32%. Therefore, during the welding process, TMCP HSS needs careful attention in order to prevent the excessive softening of the fusion and heat affected zones.

Pandey and Young [1] conducted various welding trials with different welding process parameters to control welding heat input and at the same time to achieve the desired weld profile and weld leg size. In order to investigate the material properties of the HAZ of S960 steel grade TMCP tubular members, Pandey and Young [33] prepared 3 T-joints with RHS chords of different thicknesses (t=3, 4 and 6 mm). Subsequently, 4 tensile coupons, each of 6 mm gauge width and 25 mm gauge length, were extracted from the HAZ of each of these 3 T-joints. These tensile coupons were extracted from the first 24 mm region from the fillet weld toe. Further, for comparison, a tensile coupon of similar dimension was also extracted from the non-HAZ region (i.e. parent metal). Fig. 10 presents a representative photo showing the extracted location of these tensile coupons. The test-setup, test procedure and the obtained material properties are detailed in Pandey and Young [33]. It should be noted that due to fabrication restraints, no tensile coupons were extracted from the FZ (i.e. t_1+w), where the material strength is expected to reduce significantly. It should be noted that although the HAZ coupons were extracted from the RHS-RHS T-joints, however, the obtained tensile stress-

strain curves of WHAR can also be used for the CHS-RHS T-joints, as the RHS chords of RHS-RHS and CHS-RHS T-joints belong to the identical mill batch. In addition, the CHS-RHS T-joints were welded using the identical welding process parameters, as used for the welding of RHS-RHS T-joints. Furthermore, the brace and chord thicknesses of CHS-RHS T-joints are similar to that of RHS-RHS T-joints. In the absence of material properties of the FZ and also to keep the FE models simple, a linear strength reduction (S_{rl}) for the WHAR (=FZ+HAZ) was proposed in this study. The definitions of WHAR and proposed linear strength reduction model are explained in Figs. 11 and 12, respectively. The proposed linear strength reduction (S_{rl}) values for the WHAR of 3, 4 and 6 mm thicknesses were 50%, 40% and 20%, respectively, which showed a good agreement for the validation of tests [1]. In order to reciprocate the real post-weld conditions of T-joints, the WHAR was modelled in both brace and chord members. In this study, the spread of WHAR was kept as w+6+6 mm and t_1+w+6+6 mm for all the brace members and along the longitudinal direction of all the chord members, respectively. However, along the transverse direction of the chord members, the spread of WHAR was kept as t_1+w+12 mm for $\beta \leq 0.75$, t_1+corner region for $0.75<\beta<1$ and corner region+2t_0 for $\beta=1$, for both RHS-RHS and CHS-RHS T-joints. The spreads of WHAR for T-joints of different β ranges are shown in Figs. 13-15. Furthermore, the material properties of WHAR were completely extended along the thickness direction of the brace and chord members. In order to investigate the effects of WHAR on the behaviour of CFHSS tubular T-joints, a total of 5 typical FE models, covering different failure modes and joint configurations of this study, were re-run by ignoring the WHAR. The comparisons of load vs chord face indentation curves from these simulations are shown in Figs. 5-7 and 8-9 for RHS-RHS and CHS-RHS T-joints, respectively. It is evident from these comparison curves that the WHAR has a significant impact on the structural performance of cold-formed tubular T-joints of S900 and S960 steel grades. The adverse effect of WHAR increased with the increase of β ratio and affected both the joint failure strength and initial stiffness. The joint failure strengths of typical RHS-RHS and CHS-RHS T-joints with and without considering the WHAR are presented in Table 1. It can be noticed that the ignorance of WHAR in FE models overestimated the joint strengths in the range of 12 to 34%.

3.1.9. Effect of initial geometrical imperfections

The acceptable tolerances on various dimensions of RHS and CHS tubular members are given in the EN 10219-2 [34]. However, whether these tolerance limits can be applied for S900 and S960 steel grades tubes, needs further confirmation. Garifullin et al. [35] carried out a numerical study to investigate the effect of initial geometric imperfections on the structural behaviour of T-joints with steel grades ranged from S355 to S700. Imperfections were simulated, using the conventional approach for thin-walled structures, by applying corresponding buckling modes to the perfect

geometry [35]. It should be noted that the scaling of imperfections by Garifullin et al. [35] was only limited up to the maximum tolerance limits specified in the EN 10219-2 [34]. They observed trivial effect of initial geometric imperfections, when restricted up to the tolerance limits given in the EN 10219-2 [34], on the T-joint behaviour, and concluded that its effect could be safely ignored in computational analysis. Pandey and Young [1] comprehensively measured the dimensions of the tubular members by taking 8 measurements, for each tubular member, recorded along the cross-sectional and longitudinal directions of that tubular member. However, compared to the nominal dimensions, the measured maximum cross-sectional widths and depths of the tubular members ($b_{0,max}$ and $h_{0,max}$), significantly exceeded the existing tolerance limits specified in the EN 10219-2 [34]. The average of the maximum convex bulge of all the chord members, used in tests [1], was 2.9%, as shown in Table 2. It is therefore imperative to include this initial imperfection in FE models in the form of a three-point convex arc and to investigate its effect on the T-joint behaviour. The failure modes observed in tests [1] and in the parametric study were chord face failure (F), chord side wall failure (S) and combined failure (F+S). In all these observed failure modes, the governing local deformations in the joint region were only confined in the chord members. Thus, in the FE models, this initial geometrical imperfection was only taken as the convex bulge in the flat region(s) of the chord members. For this investigation, 5 typical FE models, covering different failure modes and joint configurations of this study, were re-run by two methods. First, when the flat regions of the chord members were modelled straight using the measured average cross-sectional widths (b_0) and depths (h_0). Second, when the governing convex region(s) of the chord members were modelled as a three-point arc using the maximum convex bulge of that chord member. The governing convex region(s) of the chord member was chord flanges for chord face failure; chord webs for chord side wall failure; and both chord flanges and webs for combined failure, as shown in Fig. 16. The load vs chord face indentation curves obtained from these simulations are shown in Figs. 17 and 18 for typical RHS-RHS and CHS-RHS T-joints, respectively. From these curves, it can be noticed that the effect of modelling the flat region as straight or curve is only critical for equal-width (β=1) T-joints. For chord face failure, the effect is trivial with the difference of 0.6% and 0.9% in the joint failure strengths of typical RHS-RHS and CHS-RHS T-joints, respectively. For combined failure, the effect is quite small with the difference of 1.0% and 3.2% in the joint failure strengths of typical RHS-RHS and CHS-RHS T-joints, respectively. However, for chord side wall failure, the effect is significant with the difference of 9.5% in the joint failure strengths, and thus, cannot be ignored.

The main reason behind this observation is the nature of the involved failure mode. For chord face failure, the joint failed due to the yielding of the chord connecting face. The out-of-plane stiffness of the chord connecting face is quite small when subjected to brace concentrated load, thus, an imperfection in the form of convex bulging of the chord connecting face had an insignificant effect for this failure mode. For chord side wall failure, the chord webs behaved like a column, and thus,

they were quite sensitive towards the convex chord web bulge. The incorporation of convex bulge imperfection in the chord webs has an effect identical to the introduction of a global imperfection in the column analysis. For combined failure, the effect due to convex chord flange has an explanation similar to that of chord face failure, whereas the chord webs in combined failure cases were already out-of-plane of the load coming from the brace member. Therefore, irrespective of the introduction of convex chord web bulge, the chord webs were already resisting end bending moments and axial force. This proved that any controlled increase in the convex chord web bulge has a marginal effect on the joint failure strengths of T-joints failed in combined failure mode. Finally, in order to keep the FE models realistic and simple, the measured values of the convex bulges were only introduced in the chord webs of equal-width (β=1) tubular T-joints using a three-point arc.

3.2. Verification of finite element models

Using the guidelines and techniques detailed in Section 3.1 of this paper, FE models were prepared to simulate the test results [1] by duly validating the joint failure strengths, failure modes and load-deformation histories. In total 24 T-joints, including 16 RHS-RHS and 8 CHS-RHS, were modelled using the measured dimensions and material properties detailed in Pandey and Young [1]. The joint failure strengths (N_f) obtained from the tests were compared with the joint failure strengths obtained from the FE analyses (N_{FE}). The joint failure strengths, both experimentally and numerically, were obtained by using load and deformation limit criteria. The comparisons of N_f/N_{FE} for RHS-RHS and CHS-RHS T-joints are shown in Tables 3 and 4, respectively. The mean values of N_f/N_{FE} ratios are 1.00 and 1.02 and corresponding coefficients of variation (COV) are 0.014 and 0.018 for RHS-RHS and CHS-RHS T-joints, respectively. The load-deformation histories obtained from the FE analyses, including load vs chord face indentation curves, load vs chord side wall deformation curves and load vs axial shortening curves were compared with the corresponding experimental static curves for the typical cases of both RHS-RHS and CHS-RHS T-joints, as shown in Figs. 19 and 20, respectively. The failure modes obtained from the FE analyses were compared with the typical failure modes observed in the tests [1] for both RHS-RHS and CHS-RHS T-joints, as shown in Figs. 21-23 and 24-25, respectively. It is, therefore, demonstrated that the FE models developed in this numerical study are well capable of replicating the overall structural performance of both RHS-RHS and CHS-RHS CFHSS tubular T-joints of S900 and S960 steel grades.

3.3. Parametric study

3.3.1. Scope

The experimental programme conducted by Pandey and Young [1] included 24 T-joints and covered β ratio ranged from 0.34 to 1, 2γ ratio ranged from 20.6 to 38.6, h_0/t_0 ratio ranged from 12.7

to 38.8 and τ ratio ranged from 0.52 to 1.27. However, only the existing test database was not enough to develop a comprehensive understanding of the structural behaviour of CFHSS tubular T-joints. Therefore, an extensive parametric study was conducted, using the validated FE models, to enlarge the numerical database by duly covering the wider range of governing geometrical parameters. A total of 285 T-joints, including 189 RHS-RHS and 96 CHS-RHS, was analysed in the parametric study. In an attempt to extend the present validity limits of governing geometrical parameters in the EC3 [2] and CIDECT [3], the validity limits of the governing geometrical parameters in this parametric study were purposely designed beyond their current validity ranges. For RHS-RHS T-joints, β ratio ranged from 0.3 to 1, 2γ ratio ranged from 16.67 to 50, h_0/t_0 ratio ranged from 10 to 60, η ($=h_1/b_0$) ratio ranged from 0.3 to 1.2 and τ ratio ranged from 0.75 to 1.25. For CHS-RHS T-joints, β ratio ranged from 0.3 to 0.9, 2γ ratio ranged from 16.67 to 50, h_0/t_0 ratio ranged from 16.67 to 50 and τ ratio ranged from 0.5 to 1. The overall planning for the parametric study of RHS-RHS and CHS-RHS T-joints is summarized in Tables 5 and 6, respectively.

3.3.2. Specimens, modelling and material properties

The RHS and CHS members used in the parametric study covered a broad range of practical cross-sectional sizes. For brace members, the overall flange width (b_1) ranged from 30 to 500 mm, the overall web depth (h_1) ranged from 30 to 600 mm and thickness (t_1) ranged from 2.25 to 12.5 mm. For chord members, the overall flange width (b_0) ranged from 50 to 500 mm, the overall web depth (h_0) ranged from 40 to 500 mm and thickness (t_0) ranged from 3 to 10 mm. It should be noted that the upper and lower limits of the cross-sectional dimensions of selected RHS and CHS fall within the range of commercially available S900 and S960 steel grades tubes. Referring the production of S900 and S960 steel grades RHS [36,37], external corner radii (R_1 and R_0) were adopted as $2t$ for $t \leq 6$ mm, $2.5t$ for $6 < t \leq 10$ mm and $3t$ for $t > 10$ mm. These adopted values of external corner radii also fulfilled the requirements given in the prEN 10219-2 [34]. Subsequently, the internal corner radii (r_1 and r_0) for RHS brace and chord members were calculated as the difference of external corner radius and tube wall thickness (t). In order to avoid the overall buckling of brace member, the length of brace member (L_1) was kept equal to two times the maximum of b_1 and h_1 (i.e. $L_1=2\max[b_1, h_1]$) for RHS braces and two times the brace diameter d_1 (i.e. $L_1=2d_1$) for CHS braces, which was consistent with the test programme [1]. The mesh sizes ranged from 3 to 12 mm were used in the parametric study for different cross-sections. In general, the mesh sizes for RHS and CHS members were determined using the following expressions:

For RHS
$$\text{Mesh size} = \text{Roundup}\left\{\left(min\left[\frac{b}{30}, \frac{h}{30}\right], 0\right) \begin{matrix} \lessdot\ 3\ mm \\ \gtrdot\ 12\ mm \end{matrix}\right. \quad (1)$$

For CHS
$$\text{Mesh size} = \text{Roundup}\left\{\left(\frac{d}{30}, 0\right) \begin{matrix} \lessdot\ 3\ mm \\ \gtrdot\ 12\ mm \end{matrix}\right. \quad (2)$$

Further, the corner regions of all the brace and chord members were respectively divided into 6 and 10 elements. For both brace and chord members, one layer of solid C3D20 element was used along the thickness direction when $t \leq 6$ mm, whereas two layers of the solid C3D20 elements were used along the thickness direction when $t > 6$ mm. The mesh size for the weld was kept similar to the mesh size of the brace member, determined using Eq. (1) or (2), with a minimum value of 7 mm. The mesh size of the bearing plates was kept as 50 mm. For all hexahedral elements, the aspect ratio of the mesh was kept 1:1 (length : width). Similar to the validated FE models, corner regions of RHS members were extended up to $2t$ in the adjacent flat regions. For RHS-RHS and CHS-RHS T-joints with $\beta \leq 0.80$, FW was modelled all around the joint perimeter. For RHS-RHS and CHS-RHS T-joints with $\beta > 0.80$, FW was modelled along the chord transverse direction, whereas GW, without brace connecting end chamfer, was modelled along the chord longitudinal direction. The fillet weld leg size (w) was designed as $1.5t_{min}$ (where t_{min} is the minimum of brace and chord thickness) as per the recommendations given in the AWS D1.1/D1.1M [19], which was identical with the test programme [1].

For RHS members, flat and corner regions of the FE models were assigned the measured flat and corner region material properties of 150×150×6, respectively. However, for CHS members, the measured material property of 88.9×4 was used. The measured material properties of 150×150×6 and 88.9×4 were obtained from the tensile coupon tests conducted by Pandey and Young [1]. The measured material properties of the weld, obtained from all-weld metal tensile coupon tests [4], were assigned to the weld parts of the FE models. However, a bi-linear stress-strain curve with Young's modulus of 200 GPa and 0.2% proof stress of 1000 MPa was used for the bearing plates. The Poisson's ratio of steel materials was taken as 0.3 in this study. As detailed in Section 3.1.8 of this paper, the average material strength reductions for the WHAR of 3, 4 and 6 mm thicknesses were taken as 50%, 40% and 20%, respectively. Thus, using this data, a bi-linear material strength reduction model was proposed for other thicknesses used in the parametric study, as shown in Fig. 26. In the absence of material strength reduction data for thicknesses greater than 6 mm and also for conservative joint strength predictions, the WHAR material strength reduction was kept as 20% for $t > 6$ mm, in this study. Hence, for thicknesses except 3, 4 and 6 mm, the stress-strain curves for the WHAR were obtained by applying the corresponding strength reduction factor, obtained from Fig. 26 to the stress-strain curve obtained from the flat region of 150×150×6.

3.3.3. Chord length and chord imperfections

In order to investigate the effect of chord length (L_0) on the joint failure strengths of CFHSS tubular T-joints, the chord length was changed by changing the load distribution in the chord member. A total of 4 validated RHS-RHS T-joint FE models, i.e. T-50×100×4-150×150×6 (β=0.34, 2γ=25.3),

T-120×120×4-140×140×4 (β=0.86, 2γ=35.2), T-100×50×4-100×50×4 (β=1, h_0/t_0=12.7) and T-120×120×3-120×120×3 (β=1, h_0/t_0=38.8) were re-run by changing the load distribution ratio in the chord from 1 (vertical) : 0.5 (horizontal) to 1 (vertical) : 5 (horizontal), as shown in Fig. 27. A total of 28 simulations were performed and the obtained joint failure strengths, calculated using load and deformation criteria, are summarised in Table 7. The variations of joint failure strengths with chord length-to-chord width ratios (L_0/b_0) are shown in Fig. 28. From this comparison, it can be noticed that the variations of joint failure strengths for T-50×100×4-150×150×6 (β=0.34, 2γ=25.3) were negligible. However, the joint failure strengths of the other three T-joints (with large values of β ratio) sharply decreased with the increase of L_0/b_0 ratio. Nonetheless, the joint failure strengths of T-joints with large values of β ratio failed to converge with the increasing values L_0/b_0 ratios. Although, FE simulations can further be performed until there is no appreciable drop in the strengths of T-joints with increasing L_0/b_0 ratios, however, such practise would largely deviates from the objective of obtaining real joint failure strength and shifts towards the chord member strength under chord in-plane bending. Therefore, design recommendations for T-joints finally need to be based on a certain optimum chord length. This optimum chord length will not only prevent the occurrence of any surplus chord-in-plane bending moment, but at the same time, it will avoid the overlapping of stresses between the joint and chord end regions. The authors have performed an extensive literature review [1,16,27,38-51] of the notable research works available on hollow T-joints with RHS chords. Many of these experimental studies were CIDECT projects and their published results were used to validate the current chord face failure and chord side wall failure design rules given in the CIDECT [3]. The ratios of effective chord length (L_e) to the maximum of chord flange width and chord web depth (i.e. L_e /max[b_0, h_0]) from this literature review are summarised in Table 8. From this comparison, the average minimum value of L_e /max[b_0, h_0] ratio is 4.16. In order to propose a simple chord length formula and also for conservative joint strength prediction, the average minimum value of L_e /max[b_0, h_0] ratio was then rounded off on the upper side from 4.16 to 4.5. Furthermore, this chord length is equal to a simply supported span and must include half of the bearing plate width at each chord end. Thus, the generalised expression of the proposed chord length (L_0) is as follows:

Chord Length (L_0) = Simply supported span (L_e) + 2 half-width of end bearing plate (C) (3)

After observing the cross-sectional shapes of chord ends under concentrated end reactions for various FE simulations, a bearing plate of 90 mm width was found suitable when the max[b_0, h_0] was not more than 180 mm, which was consistent with the tests [1]. For cases where max[b_0, h_0] was more than 180 mm, the chord end bearing plate width was taken as 0.5 max[b_0, h_0]. Therefore, the proposed chord length formula, which was also used in this parametric study, for CFHSS tubular T-joints becomes:

$$L_0 = 4.5 \max[b_0, h_0] + C \quad \text{(in mm)} \tag{4}$$

where

$$C = \begin{cases} 90 & for \quad \max[b_0, h_0] \le 180 \\ 0.5 \max[b_0, h_0] & for \quad \max[b_0, h_0] > 180 \end{cases} \quad \text{(in mm)} \tag{5}$$

In this numerical investigation, the L_0/b_0 ratio ranged from 5 to 15, the L_0/h_0 ratio ranged from 5 to 15, and the $L_0/\max[b_0,h_0]$ ratio ranged from 5 to 5.4. Therefore, the chord length ratios (L_0/b_0, L_0/h_0 and $L_0/\max[b_0,h_0]$) adopted in this investigation are optimum for joint resistance computation and are between the practical ranges of chord lengths adopted in many studies [1,16,27,38-51] on tubular T-joints. Moreover, as mentioned in Section 3.1.9 of this paper, the effect of convex chord web bulge is significant on the joint failure strength of equal-width (β=1) tubular T-joints. Therefore, in this parametric study, a total convex bulge equal to 3% of nominal chord width (b_0) was introduced in the chord webs of all equal-width (β=1) tubular T-joints.

3.3.4. Failure modes

A total of 285 parametric results were generated, including 189 parametric results for RHS-RHS T-joints and 96 parametric results for CHS-RHS T-joints, as shown in Tables 9-14. In this parametric study, the joint failure strengths for all types of failure modes of RHS-RHS and CHS-RHS T-joints were obtained by using both load and deformation limit criteria. Thus, the joint failure strength was defined as the load corresponding to the first occurrence of the peak load or the load corresponding to the $0.03b_0$ deformation in the load vs chord face indentation curve, which was identical with the approach adopted in the tests [1]. In the parametric study, three types of failure modes were observed for RHS-RHS T-joints, namely chord face failure (for $0.30 \le \beta \le 0.75$), chord side wall failure (for β=1) and combined failure (for $0.80 \le \beta \le 0.90$). For CHS-RHS T-joints, two types of failure modes were observed, namely chord face failure (for $0.30 \le \beta \le 0.70$) and combined failure (for $0.73 \le \beta \le 0.90$).

In this study, for both RHS-RHS and CHS-RHS T-joints, a failure mode was described as chord face failure (F) when the joint failure strength of the T-joint was only controlled by its deformation limit, which is equal to 3% out-of-plane deformation of the overall chord connecting face width (b_0), i.e. $0.03b_0$. In the chord face failure (F) mode, the load-deformation curves for the majority of T-joints had shown no peak load. Due to the membrane action of the chord connecting face and strain hardening of the material, the load-deformation curves were continuously increasing with the increase of the applied load. For the remaining T-joints of chord face failure (F) mode, the attainment of peak loads and the corresponding post-ultimate load drops in the load-deformation curves were very gradual. These peak loads were attained at sufficiently large values of chord face indentations. The attainment of gradual peak load in such T-joints was due to the local buckling of brace members, with large η (= h_1/b_0) ratio, in their corresponding HAZ regions along the chord longitudinal direction. From this parametric study, it was also observed that for T-joints failed by chord face failure mode,

most of the deformation was contained in the flat region of the chord connecting face with the marginal participation of corresponding chord corner regions. In this study, the proposed upper limits of β values for the chord face failure modes of RHS-RHS and CHS-RHS T-joints are 0.75 and 0.70, respectively. As the welds were also modelled in the parametric FE analyses, therefore, these proposed limits of β values can also accommodate the inclusion of weld leg sizes in the chord face failure (F) mode of CFHSS T-joints. Similar to the current recommendations given in the EC3 [2] and CIDECT [3], the chord side wall failure mode in this study was also defined for equal-width (β=1) tubular T-joints, as the applied load was mostly resisted by the chord webs. The joint failure strengths of equal-width (β=1) tubular T-joints were mostly load controlled except for a few joints, where the joint failure strengths were obtained using $0.03b_0$ deformation limit criterion. It should be noted that for all equal-width (β=1) tubular T-joints, the chord face indentation values corresponding to the $0.03b_0$ deformation limit criterion and the peak load were very closed. Moreover, in this study, a combined failure mode is respectively introduced for RHS-RHS and CHS-RHS T-joints when $0.80 \leq \beta \leq 0.90$ and $0.73 \leq \beta \leq 0.90$. This failure mode was characterised by the combined deformations of chord flange, chord corner regions and chord webs, which was consistent with the corresponding observation noted in the test programme [1]. For the combined failure mode of this study, the joint failure strength was obtained as the load corresponding to the $0.03b_0$ deformation limit or the peak load, whichever occurred first in the corresponding load vs chord face indentation curve. For T-joints with $0.7 < \beta < 1$, the chord face indentation values corresponding to $0.03b_0$ deformation limit and peak load were quite close. Thus, unlike chord face failure mode, the joint failure strengths in combined failure mode were combinedly controlled by load and deformation limit criteria. The load-deformation curves have shown a clear peak load for all T-joints failed in combined failure mode. It should be noted that the joint failure strengths of RHS-RHS and CHS-RHS T-joints under combined failure mode included the effect of weld leg sizes, as the welds were modelled in all these T-joints. It is noteworthy to mention that no overall buckling of the brace member was observed in this parametric study.

3.3.5. Effects of critical geometric parameters on the behaviour of CFHSS T-joints

The parametric study in this paper was systematically planned, wherein efforts were made to check the influence of various governing geometrical parameters on the overall behaviour of RHS-RHS and CHS-RHS CFHSS T-joints. The load vs chord face indentation curves depicting the effects of various governing geometrical parameters on RHS-RHS and CHS-RHS T-joints failed in different failure modes are shown in Figs. 29-33. In this study, the geometric parameters which mainly affected the behaviour of RHS-RHS T-joints failed in chord face failure (F) mode were β, 2γ and η. The load vs chord face indentation curves presenting the effect of these parameters, one-by-one by duly keeping the other factors constant, are shown in Figs. 29(a)-29(c). Fig. 29(a) presents the variations

of load vs chord face indentation curves for β=0.30, 0.70 and 0.75 by duly keeping 2γ=30 and η=0.90, wherein it can be seen that the initial stiffness and joint strength increased with the increase of β ratio. The load vs chord face indentation curve at β=0.30 was monotonically increasing, however, the load vs chord face indentation curves at β=0.70 and 0.75 have shown clear peak loads with gradual post-ultimate load drops. It can also be noticed that, for this comparison, the loads corresponding to $0.03b_0$ deformation limit always occurred before their respective peak loads, thus, the joint strengths were clearly deformation controlled. With the increase of β ratio, brace side walls move towards chord corner regions, where the out-of-plane stiffness of the chord connecting face was relatively higher compared to its central region. Thus, it can be observed that, generally, the strength of CFHSS RHS-RHS T-joints increased with the increase of β ratio. Fig. 29(b) presents the variations of load vs chord face indentation curves of other 3 sets of RHS-RHS T-joints for 2γ=16.67, 30 and 50 with β=0.70 and η=0.90. It can be noticed from Fig. 29(b) that the initial stiffness and joint strength reduced as 2γ increased. With the increase of 2γ ratio, the tendency of load vs chord face indentation curve to possess peak load also reduced and it became eventually monotonically increasing for 2γ=50. With the increase of 2γ ratio, the chord connecting face became more slender, thus, out-of-plane stiffness of the chord connecting face significantly reduced. Consequently, the joint strength reduced and load-deformation curve changed to monotonically increasing. The rate of post-ultimate load drop also decreased as 2γ ratio increased. The strengths of T-joints, for this comparison, were deformation controlled, as loads corresponding to $0.03b_0$ deformation limit always occurred before their respective peak loads. Thus, it can be noticed that the potential use of HSS material couldn't be efficaciously utilised for joints with large values of 2γ ratio. The variations of load vs chord face indentation curves of RHS-RHS T-joints for η=0.60, 0.90 and 1.20 with β=0.70 and 2γ=30 are shown in Fig. 29(c). From Fig. 29(c), it is evident that the initial stiffness and joint strength increased with the increase of η ratio. The increase of η ratio for the same joint configuration means the increase of h_1, which in turn, allow the brace member to transfer loads on the wider area of chord connecting face, thereby increasing the brace-chord intersection region along the chord longitudinal direction. Thus, due to the increase in the brace-chord intersection region, and consequently, widespread deformation of the chord member, the strength of T-joint increased. The joint strengths for this comparison were also deformation controlled. It can be noticed that with the increase of η ratio and keeping other parameters constant, the tendency of load vs chord face indentation curves to possess peak load and subsequent post-ultimate load drop increased. One of the possible reasons for this behaviour could be the increase of the brace side wall slenderness (h_1/t_1), which could trigger local buckling in the post-ultimate region.

The governing geometric parameters which mainly affected the behaviour of RHS-RHS T-joints failed in combined failure (F+S) mode include β, h_0/t_0 and η. The variations of load vs chord face indentation curves with respect to β, h_0/t_0 and η are shown in Figs. 30(a)-30(c), respectively. On

observing Fig. 30(a), where β=0.80 and 0.90 for h_0/t_0=30 and η=0.90, it can be noted that the strength of T-joint significantly increased on increasing the β ratio in this high range. Further, it can be seen that the strength of T-joint with β=0.80 was deformation controlled, while the strength of T-joint with β=0.90 was controlled by its peak load. Therefore, for this failure mode, the strengths of T-joints controlled by both load and deformation criteria. In addition to joint strength, the initial stiffness of T-joints also increased as β ratio increased. On increasing the β ratio, load vs chord face indentation curve possessed more clear peak load followed by sharp post-ultimate load drop. For RHS-RHS T-joints failed in combined failure mode, Fig. 30(b) presents the variations of load vs chord face indentation curves for h_0/t_0=16.67, 30 and 50 by duly keeping β=0.90 and η=0.90. It can be seen from Fig. 30(b) that the initial stiffness and joint strength decreased with the increase of h_0/t_0 ratio. On increasing the h_0/t_0 ratio, the chord web slenderness increased which in turn increased the susceptibility of the chord webs towards buckling. Consequently, the initial stiffness and joint strength significantly decreased on increasing the h_0/t_0 ratio. The variations of load vs chord face indentation curves for η=0.60, 0.90 and 1.20 with β=0.90 and h_0/t_0=30 are shown in Fig. 30(c). From Fig. 30(c), it can be observed that the joint strength increased with the increase of η ratio, however, initial stiffnesses of T-joints were nearly the same. The increase in joint strength with increase in η ratio was possibly due to more widespread plastic deformation of the chord member, as explained earlier. For this comparison, the joint strengths were controlled by the load criterion.

The structural performance of RHS-RHS CFHSS T-joints failed in chord side wall failure (S) mode was mainly affected by h_0/t_0, η and τ. Figs. 31(a)-31(c) respectively present the variations of load vs chord face indentation curves with respect to h_0/t_0, η and τ. The variations of load vs chord face indentation curves for h_0/t_0=10, 20, 30, 40, 50 and 60 by keeping η=1 and τ=1 are shown in Fig. 31(a). From Fig. 31(a), it is evident that the peak load decreased with the increase of h_0/t_0 ratio. In the EC3 [2] and CIDECT [3], T-joint with chord side wall failure mode was assumed to be failed by the global buckling of its pinned ended chord webs of effective height equal to h_0-2t_0. However, in this study, simply supported CFHSS T-joints with β=1.0 were failed due to the local buckling of the upper half regions of the chord webs, which was consistent with the corresponding experimental [1] observation, as shown in Fig. 23. The variations of load vs chord face indentation curves for η=0.60, 0.90 and 1.20 with h_0/t_0=30 and τ=1 are shown in Fig. 31(b), where it can be seen that the joint strength increased with the increase of η ratio, which is consistent with the previous observations for load vs chord face indentation variations with respect to η. With the increase of η ratio, brace member can transfer load on the wider area of the chord side walls, thereby it can avoid early chord side wall failure which could occur for identical T-joints with small η ratio due to more concentrated loads. The load vs chord face indentation variations for τ=0.75, 1.0 and 1.25 with h_0/t_0=30 and η=1 are shown in Fig. 31(c). It can be seen that on increasing the τ ratio from 0.75 to 1.0, the joint strength increased considerably. However, a further increase in τ ratio from 1.0 to 1.25 resulted in nearly no

change in the initial stiffness and joint strength. Thus, for equal-width tubular T-joints, maximum joint strength could be attained by keeping brace and chord members equally strong (i.e. τ=1.0). For all these comparisons, the joint strengths were entirely controlled by the load criterion, as peak loads always occurred before their respective $0.03b_0$ deformation limit loads.

In this study, CHS-RHS T-joints which failed in chord face failure (F) mode and combined failure (F+S) mode were mainly influenced by β and 2γ ratios. With regard to CHS-RHS T-joints failed in chord face failure (F) mode, the variations of load vs chord face indentation curves with β and 2γ ratios are shown in Figs. 32(a) and 32(b), respectively. In order to observe the effect of β ratio, load vs chord face indentation curves were plotted for β=0.30, 0.50 and 0.70 by keeping 2γ=30. It is evident from Fig. 32(a) that the initial stiffness and joint strength increased with the increase of β ratio. However, all curves were monotonically increasing and the joint strengths were determined using $0.03b_0$ criterion. On the other hand, Fig. 32(b) presents the variations of load vs chord face indentation curves for 2γ=16.67, 30, 40 and 50 for β=0.70. Similar to RHS-RHS T-joints, the initial stiffness and joint strength reduced on increasing the 2γ ratio and curve with a peak load for 2γ=16.67 changed into a monotonically increasing curve for 2γ=50. For this comparison, the joint strengths were controlled by $0.03b_0$ deformation limit criterion. The variations of load vs chord face indentation curves for CHS-RHS T-joints failed in combined failure (F+S) mode with β and 2γ are shown in Figs. 33(a) and 33(b), respectively. From Fig. 33(a), which presents the influence of different values of β ratio (β=0.75, 0.80 and 0.90) for 2γ=30, it can be seen that the joint strength remarkably increased on increasing the β ratio in its high range, i.e. the joint strength was very sensitive with respect to β ratio for CFHSS CHS-RHS T-joints for large values of β ratio. The joint strengths are both load and deformation controlled for this comparison. Fig. 33(b) presents the variations of load vs chord face indentation curves of other 4 sets of CHS-RHS T-joints failed in combined failure mode for 2γ=16.67, 30, 40 and 50 for β=0.90. The initial stiffness and joint strength reduced as well as load vs chord face indentation curves became gradually flat on increasing the 2γ ratio.

4. Reliability analysis

In order to check the reliability of the existing and proposed design rules, reliability analyses were conducted as per the recommendations given in the AISI S100 [52]. According to AISI S100 [52], the reliability index (β_0) can be determined as follows:

$$\beta_0 = \frac{\ln(C_\phi M_m F_m P_m / \phi)}{\sqrt{V_M^2 + V_F^2 + C_P V_P^2 + V_Q^2}} \tag{6}$$

In Eq. (6), C_ϕ depends on the combination of dead load (DL) and live load (LL) and termed as calibration coefficient; C_P accounts for the effect of sample size and termed as correction factor; the mean values of the comparison and resistance factor are denoted by P_m and ϕ, respectively; the

average values of the fabrication and material factor are denoted by F_m and M_m, respectively; COVs of the fabrication and material factor are denoted by V_F and V_M, respectively; COVs of the load effects and comparison are denoted by V_Q and V_P, respectively. In the calculation of reliability index (β_0) using Eq. (6), the values M_m, F_m, V_M, V_F and V_Q were taken as 1.10, 1.0, 0.10, 0.10 and 0.21, respectively. For the comparison of design rules given in the EC3 [2], a load combination of 1.35DL+1.5LL was used as per the recommendations given in the EN [53]. However, for the comparison of design rules given in the CIDECT [3], a load combination of 1.2DL+1.6LL was used as per the recommendations given in the ASCE 7 [54]. The design rules were considered as probabilistically safe and reliable when the calculated value of the reliability index (β_0) was equal to or greater than 2.5.

5. Existing design provisions and comparison with joint strengths

5.1. General

The joint failure strengths (N_f) obtained from tests [1] and parametric study were compared with the nominal strengths ($N^*_{E,T}$, $N_{E,T}$, $N^*_{C,T}$ and $N_{C,T}$) calculated from the EC3 [2] and CIDECT [3], as shown in Tables 9-14 for different observed failure modes of RHS-RHS and CHS-RHS T-joints. The nominal strengths from both these specifications [2,3] were obtained by two methods, first, when the reduction factor was incorporated in the design rules, and second when the reduction factor was not incorporated in the design rules. The terms $N^*_{E,T}$ and $N_{E,T}$ respectively represent the nominal strengths obtained from the EC3 [2] for tubular T-joints by without and with incorporating the recommended reduction factor. Also, the terms $N^*_{C,T}$ and $N_{C,T}$ respectively represent the nominal strengths obtained from the CIDECT [3] for tubular T-joints by without and with incorporating the recommended reduction factor. The $N_f/N_{E,T}$ and $N_f/N_{C,T}$ ratios checked the applicability of the latest design rules. However, the $N_f/N^*_{E,T}$ and $N_f/N^*_{C,T}$ ratios checked the applicability of the design rules developed for mild steel tubular T-joints. The nominal strengths ($N^*_{E,T}$, $N_{E,T}$, $N^*_{C,T}$ and $N_{C,T}$) were obtained using the measured member dimensions and material properties, as reported in the test programme [1]. The nominal strength from the EC3 [2] was calculated using the yield strength of the tubular member, which was taken as 0.2% proof stress in this study. On the other hand, minimum of the yield strength and 80% of its corresponding ultimate strength was used to calculate the nominal strength from the CIDECT [3]. The nominal strengths ($N^*_{E,T}$, $N_{E,T}$, $N^*_{C,T}$ and $N_{C,T}$) for the comparison of parametric results were obtained using the nominal member dimensions and the flat region material properties of 150×150×6. The current chord stress function (Q_f) was developed for tubular joints made up of normal strength steels with yield strength less than or equal to 460 MPa. If the chord in-plane bending moment from test or FE (i.e. $M_{0,test}$ or $M_{0,FE}$) was used to calculate the chord stress parameter (n) for tubular T-joints made up of

S900 and S960 steels, the final obtained values of Q_f was too low and oftentimes became less than zero. Hence, for such cases, comparisons could not be made between the joint failure strengths obtained from the tests or FE (i.e. N_f) with nominal strengths obtained from the codes (i.e. $N^*_{E,T}$, $N_{E,T}$, $N^*_{C,T}$ and $N_{C,T}$). Therefore, in this numerical investigation, the nominal strength was obtained from the EC3 [2] and CIDECT [3] corresponding to identical T-joints with full chord support (i.e. no bending moment and no chord axial load; Q_f=1.0). This nominal strength was then used to calculate the $M_{0,Design}$, and thus, n and its belonging Q_f value. This Q_f value was then later multiplied with the nominal strength of T-joint with full chord support to obtain the reduced value of the nominal strength for simply supported T-joint (i.e. $N^*_{E,T}$, $N_{E,T}$, $N^*_{C,T}$ and $N_{C,T}$). This reduced value of nominal strength of simply supported T-joint (i.e. $N^*_{E,T}$, $N_{E,T}$, $N^*_{C,T}$ and $N_{C,T}$) was then used to compare with N_f. Therefore, a total of two iterations was performed, first, to obtain the nominal strength corresponding to identical T-joint with full chord support by assuming Q_f=1, and second, where the obtained nominal strength from the first iteration was used to calculate Q_f, and thus, the final reduced nominal strength of simply supported T-joint (i.e. $N^*_{E,T}$, $N_{E,T}$, $N^*_{C,T}$ and $N_{C,T}$) which was then used for its comparison with the corresponding test or FE joint failure strength (N_f). The same procedure of two iterations was performed to obtain the values of $N^*_{E,T}$, $N_{E,T}$, $N^*_{C,T}$ and $N_{C,T}$ for all T-joints covered in this investigation. In this study, the influence of normal stresses due to chord-in-plane bending on the nominal strength of T-joint was considered using the chord stress functions (k_n and Q_f) given in the EC3 [2] and CIDECT [3]. Furthermore, the chord side wall buckling strengths (f_b and f_k) were based on the buckling curve "c" of the EC3 [55].

5.2. EC3 [2] provisions

The design rules for chord face failure and chord side wall buckling modes, without and with incorporating the reduction factors, are as follows:

Chord face failure ($\beta \le 0.85$)

when the reduction factor is not incorporated:

$$N^*_{E,T} = \frac{k_n f_{y0} t_0^2}{(1-\beta)\sin\theta_1}\left(\frac{2\eta}{\sin\theta_1} + 4\sqrt{1-\beta}\right) / \gamma_{M5} \tag{7}$$

when the reduction factor is incorporated:

$$N_{E,T} = \zeta\left[\frac{k_n f_{y0} t_0^2}{(1-\beta)\sin\theta_1}\left(\frac{2\eta}{\sin\theta_1} + 4\sqrt{1-\beta}\right) / \gamma_{M5}\right] \tag{8}$$

Chord side wall buckling (β=1.0)

when the reduction factor is not incorporated:

$$N_{E,T}^{*} = \frac{k_n f_b t_0}{\sin\theta_1}\left(\frac{2h_1}{\sin\theta_1} + 10t_0\right)/\gamma_{M5} \tag{9}$$

when the reduction factor is incorporated:

$$N_{E,T} = \zeta\left[\frac{k_n f_b t_0}{\sin\theta_1}\left(\frac{2h_1}{\sin\theta_1} + 10t_0\right)/\gamma_{M5}\right] \tag{10}$$

5.3. CIDECT [3] provisions

The design rules for chord face plastification and chord side wall failure modes, without and with incorporating the reduction factors, are as follows:

Chord face plastification (β ≤ 0.85)

when the reduction factor is not incorporated:

$$N_{C,T}^{*} = Q_f \frac{f_{y0} t_0^2}{\sin\theta_1}\left(\frac{2\eta}{(1-\beta)\sin\theta_1} + \frac{4}{\sqrt{1-\beta}}\right) \tag{11}$$

when the reduction factor is incorporated:

$$N_{C,T} = \zeta\left[Q_f \frac{f_{y0} t_0^2}{\sin\theta_1}\left(\frac{2\eta}{(1-\beta)\sin\theta_1} + \frac{4}{\sqrt{1-\beta}}\right)\right] \tag{12}$$

Chord side wall failure (β=1.0)

when the reduction factor is not incorporated:

$$N_{C,T}^{*} = Q_f \frac{f_k t_0}{\sin\theta_1} b_w \tag{13}$$

when the reduction factor is incorporated:

$$N_{C,T} = \zeta\left[Q_f \frac{f_k t_0}{\sin\theta_1} b_w\right] \tag{14}$$

5.4. Comparison with joint strengths

A total of 309 data, including 24 test data [1] and 285 numerical data of this study, were used for the comparisons, as shown in Tables 9-14. These comparisons helped in checking the feasibility of previous and latest design provisions given in the EC3 [2] and CIDECT [3] for CFHSS tubular T-joints of S900 and S960 steel grades. The comparisons are broadly divided as per the observed failure modes of RHS-RHS and CHS-RHS T-joints. In Tables 9-14, the fields marked with '*' corresponded to the cases where the values of the chord stress factor (n) were very large such that the chord stress functions (k_n and Q_f) approached to zero or even became negative. It should be noted that such cases

were excluded from the calculations of the corresponding mean (P_m), COV (V_p) and reliability index (β_0). The comparisons for the chord face failure mode (F) of RHS-RHS T-joints are shown in Table 9 and include a total of 88 test and numerical data. The mean values of ratios $N_f/N_{E,T}^*$, $N_f/N_{E,T}$, $N_f/N_{C,T}^*$ and $N_f/N_{C,T}$ are 0.92, 1.10, 1.20 and 1.29, respectively. The corresponding COVs are 0.309, 0.304, 0.385 and 0.364, respectively. Using a resistance factor (ϕ) of 0.80, the corresponding values of reliability index (β_0) are 1.54, 1.98, 1.97 and 2.21, respectively. The comparisons for the combined failure mode (F+S) of RHS-RHS T-joints are shown in Table 10 and include a total of 59 test and numerical data. The mean values of ratios $N_f/N_{E,T}^*$, $N_f/N_{E,T}$, $N_f/N_{C,T}^*$ and $N_f/N_{C,T}$ are 1.15, 1.33, 1.47 and 1.60, respectively. The corresponding COVs are 0.293, 0.234, 0.219 and 0.221, respectively. Using a resistance factor (ϕ) of 0.70, the corresponding values of reliability index (β_0) are 2.47, 3.19, 3.70 and 3.94, respectively. The comparisons for the chord side wall failure mode (S) of RHS-RHS T-joints are shown in Tables 11 and 12 and include a total of 58 test and numerical data. The mean values of ratios $N_f/N_{E,T}^*$, $N_f/N_{E,T}$, $N_f/N_{C,T}^*$ and $N_f/N_{C,T}$ are 4.94, 5.93, 5.76 and 6.29, respectively. The corresponding COVs are 0.750, 0.793, 0.639 and 0.653, respectively. Using a resistance factor (ϕ) of 0.70, the corresponding values of reliability index (β_0) are 2.99, 3.06, 3.70 and 3.75, respectively. The comparisons for the chord face failure mode (F) of CHS-RHS T-joints are shown in Table 13 and include a total of 49 test and numerical data. The mean values of ratios $N_f/N_{E,T}^*$, $N_f/N_{E,T}$, $N_f/N_{C,T}^*$ and $N_f/N_{C,T}$ are 0.69, 0.85, 0.87 and 0.96, respectively. The corresponding COVs are 0.319, 0.324, 0.352 and 0.347, respectively. Using a resistance factor (ϕ) of 0.85, the corresponding values of reliability index (β_0) are 0.64, 1.13, 1.23 and 1.44, respectively. The comparisons for the combined failure mode (F+S) of CHS-RHS T-joints are shown in Table 14 and include a total of 55 test and numerical data. The mean values of ratios $N_f/N_{E,T}^*$, $N_f/N_{E,T}$, $N_f/N_{C,T}^*$ and $N_f/N_{C,T}$ are 1.08, 1.31, 1.39 and 1.50, respectively. The corresponding COVs are 0.239, 0.245, 0.242 and 0.238, respectively. Using a resistance factor (ϕ) of 0.80, the corresponding values of reliability index (β_0) are 2.21, 2.71, 3.01 and 3.25, respectively. Therefore, from these comparisons, it can generally be concluded that the design rules of T-joints given in the EC3 [2] and CIDECT [3] are not directly suitable for the design of CFHSS tubular T-joints of S900 and S960 steels and their modifications are needed.

On the other hand, upon strictly limiting the validity ranges as per the recommendations given in the EC3 [2] and CIDECT [3], it is found that the current design rules given in the EC3 [2] and CIDECT [3] ($N_{E,T}$ and $N_{C,T}$) are generally conservative for RHS-RHS T-joints failed in chord face failure (F) mode, but $N_{E,T}$ and $N_{C,T}$ are quite unconservative for small values of β ratio ($\beta \leq 0.57$), particularly when small values of β ratio accompanied with medium to large values of 2γ ratio ($2\gamma \geq 25$) and small to medium values of η ratio ($\eta \leq 0.83$). Similarly, on limiting the comparisons within the validity ranges given in the EC3 [2] and CIDECT [3], it is found that the current design rules given in the EC3 [2] and CIDECT [3] ($N_{E,T}$ and $N_{C,T}$) are quite conservative and very conservative

for RHS-RHS T-joints failed in combined failure (F+S) and chord side wall failure (S) modes, respectively. Furthermore, on extending such comparisons for CHS-RHS T-joints, it is found that the current design rules given in the EC3 [2] and CIDECT [3] ($N_{E,T}$ and $N_{C,T}$) are generally slightly conservative for specimens failed in chord face failure (F) mode, but $N_{E,T}$ and $N_{C,T}$ are quite unconservative for small values of β ratio ($\beta \leq 0.50$), particularly when small values of β ratio accompanied with medium to large values of 2γ ratio ($2\gamma \geq 30$) and small values of η ratio ($\eta \leq 0.50$). In addition, the current design rules given in the EC3 [2] and CIDECT [3] ($N_{E,T}$ and $N_{C,T}$) are overall quite conservative for CHS-RHS T-joints failed in combined failure (F+S) mode.

Figs. 34-38 presented the variations of test and numerical joint failure strengths (N_f) and their corresponding nominal strengths ($N^*_{E,T}$, $N_{E,T}$, $N^*_{C,T}$ and $N_{C,T}$) calculated from the EC3 [2] and CIDECT [3]. In Figs. 34(a)-34(d), the data below the unit-slope (i.e. slope=1) line mainly represent T-joints with small values of β ratio (i.e. β=0.30), where the tendency of data to become low with respect to the unit-slope line increased with the increase of 2γ ratio and decrease of η ratio. For such T-joints, of low β and large 2γ ratios, yielding of the chord connecting regions might not had occurred at the failure loads. On the other hand, EC3 [2] and CIDECT [3] predictions were corresponding to the yielding of the chord connecting regions. Consequently, for such cases, nominal strengths obtained from the EC3 [2] and CIDECT [3] were higher than the test and numerical joint failure strengths. Hence, the comparison data fall below the unit-slope line. With the increase of 2γ ratio, the yielding tendency of the chord connecting region, at the failure load, also sharply decreased, and thus, the comparison data for such cases fall more in the downward direction of the unit-slope line. In Figs. 35(a)-35(d), the data above the unit-slope (i.e. slope=1) line represents all T-joints with β=0.90 and some T-joints having β=0.80 with low values of 2γ and h_0/t_0 ratios. For T-joints with large values of β ratio ($0.80 \leq \beta < 1.0$), the side walls of brace members were positioned near the chord corner regions. The out-of-plane stiffness of the chord corner regions was relatively large compared to the out-of-plane stiffness of the corresponding chord central region. Therefore, the strengths of T-joints generally increased with the increase of β ratio. On the other hand, EC3 [2] and CIDECT [3] predictions at β=0.80 were corresponding to the yielding of the chord connecting regions, while at β=0.90, nominal strengths from the EC3 [2] and CIDECT [3] were obtained by performing linear interpolation between chord face failure and chord side wall failure modes. The increase in joint strength in the high range of β ratio, particularly for β=0.90, was quite large compared to the corresponding increase in the nominal strength obtained from the EC3 [2] and CIDECT [3]. Consequently, for such cases, the comparison data fall above the unit-slope line.

5.5. Discussion of results

5.5.1. Chord face failure (F)

The existing design rule for the chord face failure (F) mode of T-joint is based on a lower bound simplified yield line model. The design recommendations for T- and X-joints in the EC3 [2] and CIDECT [3] were originally made for mild steel joints with ductile behaviour. The yield line model was developed ignoring the effects of membrane action, strain hardening of the material and weld leg size, i.e. the model assumed small deformations just sufficient to cause material yielding. However, the model showed a convincing validation for T-joints with steel grades up to S355 [56]. The stress-strain behaviour of S900 and S960 steel grades significantly deviates from the mild steel (steel grades up to S355). The prolonged elasticity, relatively gradual yielding, absence of yield plateau, different extent of strain hardening and low ultimate-to-yield strength ratio could change the response of HSS tubular joints, specially in the deformation and propagation of chord face yield line patterns and development of chord face membrane actions, compared to their mild steel counterparts. For small to medium values of β ratio (i.e. $\beta \leq 0.75$), normal strength steel T-joints are expected to undergo relatively larger chord connecting face deformation compared to corresponding HSS T-joints. For HSS T-joints with small to medium values of β ratio (i.e. $\beta \leq 0.75$), and specially for large values of 2γ ratio, the current $3\%b_0$ deformation limit seems not sufficient to develop plastic hinges in the chord connecting face. Therefore, the strength of HSS material from the inelastic region to yield strength could not be effectively utilised due to the existing $3\%b_0$ deformation limit criterion, and thus, the current simplified yield line model which takes into the account of only material yield strength becomes unconservative. For the same β ratio, due to high out-of-plane stiffness of the chord connecting face, T-joints with small values of 2γ ratio have demonstrated relatively larger joint strengths compared to T-joints with large values of 2γ ratio. In order to cover a wide range of structural applications, the 2γ ratio in the current parametric study was varied from 16.67 to 50. Therefore, the mean values (P_m) of comparisons for the chord face failure (F) mode of RHS-RHS and CHS-RHS T-joints reflected the results obtained for a wide 2γ range.

5.5.2. Chord side wall failure (S)

The existing design rule for chord side wall failure (S) mode of T-joint is based on a simplified combined web bearing and buckling analytical model. The findings from the tests [1] and parametric study proved that the existing joint resistance expression becomes increasingly conservative with the increase of chord side wall slenderness ratio (h_0/t_0). The reason for this trend is due to the assumption of chord webs as a pin-ended column of effective length equal to h_0-$2t_0$. The authors believe that the behaviour of T-joints failed in chord side wall failure mode is neither a pure column buckling nor a pure plate buckling, but rather a complex phenomenon involving combined column and plate buckling behaviour depending on the chord side wall slenderness ratio (h_0/t_0). This behaviour is quite sensitive towards the interaction of normal bending stresses in the chord due to chord in-plane bending with the existing stresses in the chord webs due to the applied brace axial load. In terms of

overall joint behaviour, it also depends on η ($=h_1/b_0$) ratio; τ ($=t_1/t_0$) ratio; and restraints offered by the chord flanges and corresponding strain hardening of the material.

5.5.3. Combined failure (F+S)

When a T-joint failed by involving the characteristics of both chord face failure (F) mode and chord side wall failure (S) mode, it is referred to as combined failure (F+S) mode in this study. The joint strength in the current EC3 [2] and CIDECT [3] specifications, for $0.85 < \beta < 1$, is obtained by performing a linear interpolation between the strength predictions at β=0.85 and β=1. The strength predictions in the current EC3 [2] and CIDECT [3] specifications for equal-width (β=1) T-joints are already very conservative and scattered. Also, in general, the strength of T-joints increases with the increase of β ratio. Therefore, the overall comparisons of RHS-RHS and CHS-RHS T-joints failed in combined failure mode are quite conservative and scattered.

5.6. Evaluation of existing chord stress function

The effect of chord stress on the static joint resistance of a tubular joint is incorporated with the help of a chord stress function, which is designated by Q_f in the CIDECT [3] and k_n in the EC3 [2]. In order to keep the format of chord stress function consistent between various CHS and RHS joints, the chord stress function in its new format was proposed by Wardenier et al. [57], which was then later adopted in the latest edition of the CIDECT [3]. However, the current chord stress function (Q_f) for RHS T- and X-joints was based on the numerical studies of Yu [42], which was conducted on tubular joints made up of normal strength steel grades. Hence, it is imperative to examine the applicability of the current chord stress function (Q_f) function for CFHSS tubular T-joints made up of S900 and S960 steel grades. Therefore, in this study, an attempt has been made to calculate Q_f from the FE analysis (i.e. $Q_{f,FE}$) and compared with the Q_f calculated from the CIDECT [3] (i.e. $Q_{f,CIDECT}$). The Q_f from the FE analysis (i.e. $Q_{f,FE}$) was determined by comparing the joint failure strength of simply supported T-joint (i.e. N_f) with the compression capacity of identical T-joint with full chord support (i.e. $N_{f,TF}$). Hence, by comparing the ratio of $N_f/N_{f,TF}$, the effect of chord in-plane bending moment on the static joint resistance of CFHSS tubular T-joint of S900 and S960 steel grades can be determined. On the other hand, Q_f from the CIDECT [3] (i.e. $Q_{f,CIDECT}$) was calculated by also first considering T-joint with full chord support, i.e. calculating the nominal strength from the CIDECT [3] ($N_{C,T}$) by assuming Q_f=1. It should be noted that, in order to calculate $N_{C,T}$, the tubular member dimensions and material properties were kept similar to its respective FE model. This nominal strength ($N_{C,T}$) was then further used in the second iteration to compute the chord stress factor (n) for the corresponding chord in-plane bending moment, and thus, $Q_{f,CIDECT}$. Finally, in order to check the applicability of the current chord stress function (Q_f) function for CFHSS tubular T-

joints made up of S900 and S960 steels, the $Q_{f,FE}$ was then compared with the $Q_{f,CIDECT}$, i.e. $Q_{f,FE}/Q_{f,CIDECT}$. If the ratio of $Q_{f,FE}/Q_{f,CIDECT}$ was more than unity, then the current chord stress function given in the CIDECT [3] was considered as conservative, whereas it was considered as unconservative if the ratio of $Q_{f,FE}/Q_{f,CIDECT}$ was less than unity.

In order to check the applicability of the current chord stress function (Q_f) given in the CIDECT [3] for all RHS-RHS and CHS-RHS T-joints of this investigation, all 189 RHS-RHS and 96 CHS-RHS T-joints were again numerically simulated in the ABAQUS [10] by changing the boundary conditions of the chord members from simply supported to full chord supported [58]. Upon successful convergence of these FE models of T-joints with full chord support, joint failure strengths of these joints ($N_{f,TF}$) [58] were then determined using the same principle as used for simply supported T-joints, i.e. the strength corresponding to the first occurrence of peak load or $0.03b_0$ deformation limit load. The numerical results for the comparison of $Q_{f,FE}$ vs $Q_{f,CIDECT}$ for RHS-RHS and CHS-RHS T-joints and their corresponding observed failure modes are graphically shown in Figs. 39-43 with respect to different β values. It is worth noting that those cases were ignored for these comparisons where either chord stress factor (n) was more than unity or $Q_{f,FE}$ ($N_f/N_{f,TF}$) was more than unity. For RHS-RHS T-joints failed in chord face failure (F) mode, the comparison results are shown in Fig. 39 for β=0.30, 0.70 and 0.75. It can be seen from Fig. 39 that for each β series, some T-joints have $Q_{f,FE}$ less than $Q_{f,CIDECT}$, i.e. the current chord stress function given in the CIDECT [3] is not safe for these T-joints. For RHS-RHS T-joints failed in combined failure (F+S) mode, the comparison results are shown in Fig. 40 for β=0.80 and 0.90. It can be noticed from Fig. 40 that the current chord stress function given in the CIDECT [3] could not predict the lower bound results for CFHSS T-joints and for nearly half of the cases, $Q_{f,FE}$ was less than $Q_{f,CIDECT}$. For RHS-RHS T-joints failed in chord side wall failure (S) mode, the comparison results are shown in Fig. 41. It can be observed from Fig. 41 that for the majority of equal-width CFHSS T-joints, the current chord stress function given in the CIDECT [3] is quite unconservative. Looking the overall trend of $Q_{f,FE}$ and $Q_{f,CIDECT}$ comparison with chord stress factor (n) for RHS-RHS T-joints, it can generally be noticed that the current chord stress function given in the CIDECT [3] becomes increasingly unconservative with the increase of β ratio. The comparisons of $Q_{f,FE}$ and $Q_{f,CIDECT}$ results with chord stress factor (n) of CHS-RHS T-joints failed in chord face failure (F) mode are shown in Fig. 42 for β=0.30, 0.50 and 0.70. From Fig. 42, it is evident that for many CHS-RHS T-joints with β=0.50 and 0.70, the current chord stress function given in the CIDECT [3] was unconservative. On the other hand, for CHS-RHS T-joints failed in combined failure (F+S) mode, the comparisons of $Q_{f,FE}$ and $Q_{f,CIDECT}$ results with chord stress factor (n) are shown in Fig. 43 for β=0.75, 0.80 and 0.90. The comparison showed that the existing chord stress function given in the CIDECT [3] is not safe for many CHS-RHS CFHSS T-joints failed in combined failure mode.

Finally, from all these comparisons, it can be concluded that the current chord stress function

given in the CIDECT [3] cannot be directly used for RHS-RHS and CHS-RHS CFHSS simply supported T-joints of S900 and S960 steel grades, where, generally, it becomes increasingly unconservative with the increase of β ratio. In part (b) of Figs. 39-43, the data which fall below the unit-slope line represent the cases where the current chord stress function given in the CIDECT [3] was found unsafe for the CFHSS T-joints covered in this study. For large values of β ratio, the strengths of simply supported CFHSS T-joints (N_f) were considerably smaller than the compression capacities of identical CFHSS T-joint with full chord support ($N_{f,TF}$). Consequently, the values of $Q_{f,FE}$ ($N_f/N_{f,TF}$) ratio sharply decreased. Unlike T-joints with small values of β ratio, the effect of change in boundary condition on the joint strength was quite significant for T-joints with large values of β ratio. On the other hand, the current chord stress function given in the CIDECT [3] (Q_f) was developed by performing statistical regression analyses on the data of T-joints made up of normal strength steel grades by duly excluding those cases where the values of chord stress factor (n) was equal to or more than 0.90 [57]. Thus, the current chord stress function given in the CIDECT [3] (Q_f) needs modification before it can be safely used for cold-formed tubular T-joints of S900 and S960 steel grades.

Figs. 44-48 present the comparison between the joint failure strengths of simply supported T-joints (N_f) and compression capacities of identical T-joints with full chord support ($N_{f,TF}$) [58]. The joint failure strengths of both these types of joints were determined using both load and $0.03b_0$ deformation limit criteria, whichever occurred earlier in their respective load vs chord face indentation curves. From Figs. 44-48, it is evident that for the majority of RHS-RHS and CHS-RHS CFHSS T-joints, the joint failure strengths of full chord supported T-joints ($N_{f,TF}$) were greater than their corresponding simply supported T-joints (N_f). For simply supported T-joints with large values of β ratio ($0.80 \leq \beta \leq 1.0$), the normal stresses developed in the chord members due to chord in-plane bending significantly reduced the strengths of the chord members, and thus, the overall joint strengths of such T-joints were sharply decreased. However, the detrimental effect of chord in-plane bending was absent for T-joints with full chord support, therefore, full chord supported T-joints possessed generally high joint strengths compared to their identical simply supported counterparts.

6. Proposed design rules and comparison with joint strengths

6.1. General

The appropriate procedure to propose design resistance expressions of hollow section joints is as follows:

- Obtain the best-fit equation from the regression analysis of experimental and/or numerical data which give rise to its mean strength equation. It should be noted that the experimental and/or numerical data should be based on the measured properties.

- Determine the nominal strength (or characteristic strength) equation from the mean strength equation considering mean values, scattering of experimental and/or numerical data, fabrication tolerances and variation in material strengths.
- Determine the design strength equation from the nominal strength equation by including a partial safety factor depending on the failure mode and code.

In this study, the experimental [1] and numerical joint strengths are based on the measured properties, therefore, the best-fit equation obtained from the regression analysis corresponds to the mean strength equation. Further, while developing the design proposal, mean of the comparison, scatter of the comparison and joint factor were duly considered. As T-joints in this study had shown sufficient deformation, thus, in this study, the joint factor (γ_m) was taken as 1.0 for all the observed failure modes. The new proposed design rules, in this study, are semi-empirical in nature, therefore, the strength equation obtained after duly considering the mean, COV and joint factor lead to its corresponding characteristic strength equation. Finally, in order to obtain the design strength equation from its characteristic strength equation, a resistance factor (ϕ) was introduced for each design proposal of RHS-RHS and CHS-RHS CFHSS T-joints. Compared to a pure analytical approach, a semi-empirical approach could be a more appropriate option for the design of HSS tubular joints, as it combines the backgrounds of analytical approach with the observations of experimental and numerical findings. In an attempt to extend the validity limits of the governing parameters in the proposed design rules, their limits, in this study, exceeds their corresponding limits mentioned in the current EC3 [2] and CIDECT [3] specifications. The effects of weld leg size, chord stress and WHAR are included in the proposed design equations. In the absence of any experimental evidence on the effect of chord stress on the joint failure strengths of CFHSS tubular T-joints of S900 and S960 steel grades, the chord stress function is not explicitly mentioned in the proposed design rules. However, the experimental and numerical joint strengths have already included the adverse effect of normal stresses in the chord member due to chord in-plane bending.

In addition to the proposed semi-empirical design rules, the authors have also proposed simplified design rules (where the proposed nominal strength is denoted by N_{spn}) by employing correction factors on the latest design rules of T-joints given in the EC3 [2,59]. For each simplified proposed design rule, the correction factors include the effects of WHAR and other governing geometric parameters affecting the behaviour of CFHSS T-joints failed in that particular mode. As the effect of WHAR relates to the reduction of material strength in the WHAR, which in turn depends on the thickness of the tubular member. Therefore, the simplified correction factor for WHAR, in this study, was expressed in terms of a linear function of the chord member thickness (t_0). In order to observe the direct impact of WHAR on the joint failure strengths of simply supported T-joints, and thus, to propose correction factor for the WHAR effect, FE simulations using ABAQUS [10] were performed on all identical simply supported T-joint FE models by ignoring their WHAR material

properties. The joint failure strengths of FE T-joints obtained without incorporating the WHAR were compared with the joint failure strengths of FE T-joints with WHAR incorporated in order to propose the WHAR correction factor. With regard to other governing geometric parameters, simplified linear correction factors were proposed. It is worth noting that for both types of proposed design rules, the corresponding design strength (N_d) can be obtained from the proposed nominal strengths (N_{pn} and N_{spn}) by multiplying the proposed nominal strengths (N_{pn} and N_{spn}) with their respective resistance factors (ϕ), i.e. $N_d = \phi(N_{pn})$ and $N_d = \phi(N_{spn})$.

6.2. Influence of various governing parameters for their inclusion in the proposed semi-empirical design rules

The design rules proposed in the following sub-sections for RHS-RHS and CHS-RHS T-joints of S900 and S960 steels and their corresponding observed failure modes were based on comprehensive, reliable and meticulous experimental and numerical evidence. The parametric study was performed in a systematic way, wherein each critical parameter was varied for at least three times by duly keeping the other parameters constant. The existing design rules for the static resistances of T-joints in the EC3 [2] and CIDECT [3] are based on simplified analytical models, wherein some important geometrical parameters were neglected in order to keep the design rules simple, conservative and designer friendly. For example, this study showed the importance of 2γ parameter for chord face failure mode, which is neglected in the current design equation for simplicity. The behaviour of tubular joints of HSS grades is complicated and depends on many factors, including strength reductions in WHAR, applicability of chord stress function for HSS grades and so on. Further, at this point of time, there is no other investigation available on cold-formed T-joints of S900 and S960 TMCP steels. Therefore, due to all these reasons, the authors have adopted a semi-empirical approach, wherein before developing the semi-empirical design equations, the basic backgrounds of existing simplified analytical models and the overall trend of critical parameters were duly considered. For example, considering the yielding of the chord connecting face, and thus, adopting its plastic moment capacity per unit length ($f_{yo}t_0^2/4$) for the proposed chord face failure design rule. On the other hand, the background of the proposed chord side wall failure design rule is entirely based on the current simplified web bearing and buckling analytical model.

Figs. 49-53 present the variations of the values of $N_f/N_{E,T}$ ratio (where N_f is the joint failure strengths of simply supported T-joints obtained from the FE parametric study, while $N_{E,T}$ is the nominal strength of identical T-joint obtained from the EC3 [2,59] by including the reduction factor) with various governing geometrical parameters which mainly influence the behaviour of RHS-RHS and CHS-RHS CFHSS T-joints failed in different observed failure modes. For RHS-RHS T-joints failed in chord face failure (F) mode, the variations of the values of $N_f/N_{E,T}$ ratio are presented in Fig. 49 with respect to 2γ for different values of β, η and h_0/t_0 ratios. It can be noticed from Fig. 49 that

the values of $N_f/N_{E,T}$ ratio decreased with the increase of 2γ for β=0.30 to 0.75, η=0.30 to 1.20 and h_0/t_0=16.67 to 50. On the other hand, for a particular 2γ value and on increasing the values of β and η ratios, the values of $N_f/N_{E,T}$ ratio increased by a significant amount. The values of $N_f/N_{E,T}$ ratio marginally decreased with the increase of h_0/t_0 ratio, thus, its contribution has been neglected in the proposed design equation for RHS-RHS T-joints failed in chord face failure (F) mode. The variations of the values of $N_f/N_{E,T}$ ratio for RHS-RHS T-joints failed in combined failure (F+S) mode with respect to h_0/t_0 for different values of β, 2γ and η ratios are shown in Fig. 50. For T-joints with β=0.80, the values of $N_f/N_{E,T}$ ratio decreased for 2γ=16.67 with the increase of h_0/t_0 ratio, whereas for the same value of h_0/t_0 ratio, the values of $N_f/N_{E,T}$ ratio reduced with the increase of 2γ ratio. On the other hand, for β=0.90, the values of $N_f/N_{E,T}$ ratio increased with the increase of h_0/t_0 and 2γ ratios. In addition, an unclear trend is observed for the variations of the values of $N_f/N_{E,T}$ ratio on increasing the η ratio. Thus, the proposed design equation for RHS-RHS T-joints failed in combined failure (F+S) mode accordingly included the influences of all these parameters. For equal-width RHS-RHS T-joints failed in chord side wall failure (S) mode, the variations of the values of $N_f/N_{E,T}$ ratio for different values of h_0/t_0, η, 2γ and τ ratios are shown in Fig. 51. It is evident from Fig. 51 that the values of $N_f/N_{E,T}$ ratio increased with the increase of h_0/t_0 ratio and decreased with the increase of η ratio. Whereas, the values of $N_f/N_{E,T}$ ratio first increased with the increase of 2γ and τ ratios, followed by the decrease of the values of $N_f/N_{E,T}$ ratio at higher values of 2γ and τ ratios. Hence, accordingly, the influence of these critical parameters was included in the proposed design equation of chord side wall failure mode of RHS-RHS T-joints. With regard to CHS-RHS T-joints failed in chord face failure (F) and combined failure (F+S) modes, the variations of the values of $N_f/N_{E,T}$ ratio with respect to 2γ ratio for different values of β, τ and h_0/t_0 ratios are presented in Figs. 52 and 53, respectively. It is clear from Figs. 52 and 53 that the overall trend of the values of $N_f/N_{E,T}$ ratio generally increased with the increase of β ratio and decreased with the increase of 2γ ratio. On the other hand, τ and h_0/t_0 ratios had small influences on the variations of the values of $N_f/N_{E,T}$ ratio, except for β=0.90.

6.3. RHS-RHS T-joints

6.3.1. Chord face failure ($0.30 \leq \beta \leq 0.75$)

The observations of experimental [1] and numerical studies confirmed that chord face failure (F) mode of RHS-RHS T-joints occurred when $0.30 \leq \beta \leq 0.75$. In this study, the findings of experimental [1] and numerical studies concluded a significant effect of 2γ ratio on the joint strength. Keeping the β and τ ratios unchanged, the values of $N_f/N_{E,T}$ ratios decreased with the increase of 2γ ratios. After duly considering the mean and scatter of comparison, a new semi-empirical equation is proposed, to predict the nominal strength (or characteristic strength) of CFHSS RHS-RHS T-joints of S900 and S960 steel grades failed in chord face failure (F) mode, as follows:

$$N_{pn} = f_{y0} t_0^2 \left(\frac{30\beta + 4.5\eta - 6.6}{0.5 + 0.03(2\gamma)} \right) \quad (15a)$$

The corresponding design strength (N_d) can be obtained by employing a resistance factor (ϕ) of 0.80 on Eq. (15a). This proposed design rule is valid for $0.30 \le \beta \le 0.75$, $16.6 \le 2\gamma \le 50$, $16.7 \le h_0/t_0 \le 50$, $0.3 \le \eta \le 1.2$ and $0.67 \le \tau \le 1.27$. In Eq. (15a), the term $f_{y0} t_0^2$ partially represents the plastic moment capacity of the chord connecting face per unit length. The comparison of joint strengths with proposed nominal strengths yielded a mean value of 1.0 with the corresponding COV of 0.145, as shown in Table 9. Using a resistance factor (ϕ) of 0.80, the calculated value of β_0 is 2.51. The comparison of current and proposed design rules for chord face failure mode of RHS-RHS T-joints is graphically shown in Fig. 54. Therefore, it can be concluded that the proposed design equation is relatively more accurate, less scatter and reliable.

The simplified proposed nominal strength (N_{spn}) for cold-formed RHS-RHS T-joints of S900 and S960 steel grades failed in chord face failure (F) mode, by duly considering the effects of WHAR and affecting governing geometrical parameters, is as follows:

$$N_{spn} = \left[\frac{(0.01 t_0 + 0.85)(1.5\beta + 0.6)}{(0.03(2\gamma) + 0.4)} \right] N_{E,T} \quad (15b)$$

The corresponding design strength (N_d) can be obtained by employing a resistance factor (ϕ) of 0.80 on Eq. (15b). The $N_{E,T}$ can be obtained using Eq. (8), where Eq. (8) represents the nominal chord face failure strength of T-joint and calculated in accordance with the EC3 [2,59]. As shown in Table 9, the mean and COV of the comparison between joint failure strengths and simplified proposed nominal strengths are 1.04 and 0.167, respectively. Using a resistance factor (ϕ) of 0.80, the calculated value of β_0 is 2.54.

6.3.2. Combined failure ($0.80 \le \beta \le 0.90$)

In the current EC3 [2] and CIDECT [3] specifications, a linear interpolation is recommended between chord face failure ($\beta \le 0.85$) and chord side wall failure (β=1), and there is no specific design rule to consider the combined failure mode (F+S). The description of the combined failure mode (F+S) is explained in Section 3.3.4 of this paper. The outcomes of experimental [1] and numerical studies, showed that the combined failure (F+S) mode for RHS-RHS T-joints occurred when $0.80 \le \beta \le 0.90$. The comparisons showed that the existing design rule of the EC3 [2] and CIDECT [3] are quite conservative and scattered for CFHSS RHS-RHS T-joints failed in combined failure mode. Thus, by duly accounting the mean and scatter of comparisons, a new semi-empirical equation is proposed, to predict the nominal strength (or characteristic strength) of CFHSS RHS-RHS T-joints of S900 and S960 steel grades failed in combined failure (F+S) mode, as follows:

$$N_{pn} = f_{y0} t_0^2 \left(\frac{55\beta + 4.5\eta - 33}{0.75 + 0.0075(2\gamma)} \right) \quad (16a)$$

The design strength (N_d) corresponding to Eq. (16a) can be obtained by employing a resistance factor (ϕ) of 0.70 on Eq. (16a). This proposed design rule is valid for $16.6 \leq 2\gamma \leq 50$, $12.7 \leq h_0/t_0 \leq 50$, $0.6 \leq \eta \leq 1.2$ and $0.52 \leq \tau \leq 1$. As shown in Table 10, the mean and corresponding COV of the comparison of joint strengths with proposed nominal strengths are 1.0 and 0.218, respectively. The respective calculated value of β_0 is 2.59, using a resistance factor (ϕ) of 0.70. The comparison of current and proposed design rules for combined failure mode of RHS-RHS T-joints is graphically shown in Fig. 55. Hence, it can be seen that the proposed design equation is relatively more accurate, less scatter and reliable.

The simplified proposed nominal strength (N_{spn}) for cold-formed RHS-RHS T-joints of S900 and S960 steel grades failed in combined failure (F+S) mode, by duly considering the effects of WHAR and affecting governing geometrical parameters, is as follows:

$$N_{spn} = \left[\frac{(0.02t_0 + 0.8)(5\beta - 2.5)}{(0.01(2\gamma) + 1)} \right] N_{E,T} \quad (16b)$$

The corresponding design strength (N_d) can be obtained by employing a resistance factor (ϕ) of 0.75 on Eq. (16b). When $\beta \leq 0.85$, the $N_{E,T}$ can be obtained using Eq. (8), whereas when $0.85 < \beta < 1.0$, the $N_{E,T}$ can be obtained using Eqs. (8) and (10), where Eq. (10) represents the nominal chord side wall buckling strength of T-joint and calculated in accordance with the EC3 [2,59]. As shown in Table 10, the mean and COV of the comparison between joint failure strengths and simplified proposed nominal strengths are 1.05 and 0.211, respectively. Using a resistance factor (ϕ) of 0.75, the calculated value of β_0 is 2.57.

6.3.3. Chord side wall failure (β=1.0)

Similar to the recommendations given in the current EC3 [2] and CIDECT [3], chord side wall failure (S) mode was proposed in this study for equal-width (β=1) RHS-RHS T-joints. The findings proved a remarkable effect of chord side wall slenderness ratio (h_0/t_0) on the joint strengths. The values of $N_f/N_{E,T}$ ratio abruptly increased with the increase of h_0/t_0 ratio. On the other hand, the values of $N_f/N_{E,T}$ ratio gradually decreased with the increase of η ratio. The comparisons showed that the existing design rule given in the EC3 [2] and CIDECT [3] are very conservative and very scattered for CFHSS RHS-RHS T-joints failed in chord side wall failure mode, as shown in Table 11. Therefore, by incorporating the effects of the mean and scatter of comparisons, a new semi-empirical equation is proposed, to predict the nominal strength (or characteristic strength) of CFHSS RHS-RHS T-joints of S900 and S960 steel grades failed in chord side wall failure (S) mode, as follows:

$$N_{pn} = \frac{f_k\left(2b_w t_0\right)}{\left(1.5\eta + 1\right)}\left(\frac{1.83 - 0.05\left(2\gamma\right) + 1.2\tau}{588\left(\frac{h_0}{t_0}\right)^{-2.17}}\right) \tag{17a}$$

The design strength (N_d) corresponding to the nominal strength shown in Eq. (17a) can be obtained by using a resistance factor (ϕ) of 0.70. This proposed design rule is valid for $16.6 \leq 2\gamma \leq 50$, $10 \leq h_0/t_0 \leq 60$, $0.5 \leq \eta \leq 1.2$ and $0.75 \leq \tau \leq 1.25$. In Eq. (17a), the term f_k is the chord side wall buckling stress determined using the buckling curve 'a' of EC3 [55]. Table 12 presents a comparison of mean, COV and reliability index corresponding to different buckling curves given in the EC3 [55] for this failure mode. Overall, it can be noticed that the buckling curve 'a' is more appropriate over other buckling curves. As the boundary condition of the chord webs is somewhere between pin-end and fixed-end conditions, thus, the effective length factor of 0.85 was adopted in this study. In this failure mode, the flat region of the chord web (i.e. h_0-$2R_0$) was considered as a semi-fixed column. Therefore, the effective length of the semi-fixed column becomes equal to 0.85 (h_0-$2R_0$). However, the effective width of the semi-fixed column was kept similar to the recommendations given in the current specifications [2,3], i.e. b_w=h_1+$5t_0$. The comparison of the tests [1] and numerical data with proposed nominal strengths is shown in Table 11, wherein the respective mean and COV of the comparison are 1.02 and 0.219. Using a resistance factor (ϕ) of 0.70, the calculated value of β_0 is 2.63. The comparison of current and proposed design rules for chord side wall failure mode of RHS-RHS T-joints is graphically shown in Fig. 56. Hence, it can be concluded that the proposed design equation is relatively more accurate, less scatter and reliable.

The simplified proposed nominal strength (N_{spn}) for cold-formed RHS-RHS T-joints of S900 and S960 steel grades failed in chord side wall failure (S) mode, by duly considering the effects of WHAR and affecting governing geometrical parameters, is as follows:

$$N_{spn} = \left[\frac{\left(0.03t_0 + 0.6\right)\left(0.3\frac{h_0}{t_0} - 2\right)}{1.5\eta}\right] N_{E,T} \tag{17b}$$

The corresponding design strength (N_d) can be obtained by employing a resistance factor (ϕ) of 0.50 on Eq. (17b). The $N_{E,T}$ can be obtained using Eq. (10). As shown in Table 11, the mean and COV of the comparison between joint failure strengths and simplified proposed nominal strengths are 1.02 and 0.374, respectively. Using a resistance factor (ϕ) of 0.50, the calculated value of β_0 is 2.66.

It is noteworthy to mention that when the β ratio of CFHSS RHS-RHS T-joint falls between 0.75 to 0.80, i.e. $0.75 < \beta < 0.80$, the corresponding proposed design strength has to be obtained by

performing a linear interpolation between Eqs. 15(a)-16(a) and 15(b)-16(b). Moreover, when the β ratio of CFHSS RHS-RHS T-joint falls between 0.90 to 1, i.e. $0.90 < \beta < 1$, the corresponding proposed design strength has to be obtained by performing a linear interpolation between Eqs. 16(a)-17(a) and 16(b)-17(b).

6.4. CHS-RHS T-joints

6.4.1. Chord face failure ($0.30 \le \beta \le 0.70$)

In this study, the chord face failure (F) mode of CHS-RHS T-joints occurred when $0.30 \le \beta \le 0.70$. It should be noted that no particular design rules are available for CHS-RHS T-joints in the current EC3 [2] and CIDECT [3] specifications. The findings of this investigation have shown a significant effect of 2γ ratio on the CHS-RHS T-joint strengths. The values of $N_f/N_{E,T}$ ratio decreased with the increase of 2γ ratio. By taking account of the mean and scatter of the experimental and numerical comparisons, a new semi-empirical equation is proposed, to predict the nominal strength (or characteristic strength) of CFHSS CHS-RHS T-joints of S900 and S960 steel grades failed in chord face failure (F) mode. The proposed nominal strength equation is shown below:

$$N_{pn} = f_{y0} t_0^2 \left(\frac{1.2 e^{3.1\beta}}{0.6 + 0.025(2\gamma)} \right) \tag{18a}$$

The corresponding design strength (N_d) can be obtained by employing a resistance factor (ϕ) of 0.85 on Eq. (18a). This proposed design rule is valid for $16.6 \le 2\gamma \le 50$, $16.7 \le h_0/t_0 \le 50$ and $0.5 \le \tau \le 1$. In Eq. (18a), the term $f_{y0} t_0^2$ partially represents the plastic moment capacity of the chord connecting face per unit length. The comparison of joint strengths with proposed nominal strength yields a mean value of 1.02 with the corresponding COV of 0.093, as shown in Table 13. Using a resistance factor (ϕ) of 0.85, the calculated value of β_0 is 2.58. The comparison of current and proposed design rules for chord face failure mode of CHS-RHS T-joints is graphically shown in Fig. 57. Therefore, it can be concluded that the proposed design equation is relatively more accurate, less scatter and reliable.

The simplified proposed nominal strength (N_{spn}) for cold-formed CHS-RHS T-joints of S900 and S960 steel grades failed in chord face failure (F) mode, by duly considering the effects of WHAR and affecting governing geometrical parameters, is as follows:

$$N_{spn} = \left[\frac{(0.01 t_0 + 0.83)(2.5\beta + 0.5)}{(0.07(2\gamma) - 0.3)} \right] N_{E,T} \tag{18b}$$

The corresponding design strength (N_d) can be obtained by employing a resistance factor (ϕ) of 0.65 on Eq. (18b). The $N_{E,T}$ can be obtained using Eq. (8). As shown in Table 13, the mean and COV of the comparison between joint failure strengths and simplified proposed nominal strengths

are 1.04 and 0.277, respectively. Using a resistance factor (ϕ) of 0.65, the calculated values of β_0 is 2.58.

6.4.2. Combined failure ($0.73 \leq \beta \leq 0.90$)

The findings of experimental [1] and numerical studies concluded that the combined failure (F+S) mode was found in CHS-RHS T-joints when $0.73 \leq \beta \leq 0.90$. From the comparisons, it can be noticed that the 2γ ratio has an important effect, wherein the values of $N_f/N_{E,T}$ ratio decreased with the increase of 2γ ratio. As mentioned before that there are no specific design rules for CHS-RHS T-joints in the current EC3 [2] and CIDECT [3] specifications. The existing procedure of calculating the design strengths of CHS-RHS T-joints in the EC3 [2] and CIDECT [3], using the design rules of T-joints with RHS chord, proved to be very conservative and scattered for CFHSS CHS-RHS T-joints failed in combined failure mode. Hence, by appropriately taking into account the mean and scatter of the comparisons, a new semi-empirical equation is proposed, to predict the nominal strength (or characteristic strength) of CFHSS CHS-RHS T-joints of S900 and S960 steel grades failed in combined failure (F+S) mode, as follows:

$$N_{pn} = f_{y0} t_0^2 \left(\frac{57\beta - 30}{0.8 + 0.013(2\gamma)} \right) \tag{19a}$$

The design strength (N_d) corresponding to the nominal strength shown in Eq. (19a) can be obtained by using a resistance factor (ϕ) of 0.80. This proposed design rule is valid for $16.6 \leq 2\gamma \leq 50$, $15.2 \leq h_0/t_0 \leq 50$ and $0.66 \leq \tau \leq 1$. The comparison of tests [1] and numerical data with proposed nominal strengths is shown in Table 14, wherein the respective mean and COV of the comparison are 0.99 and 0.128. Using a resistance factor (ϕ) of 0.80, the calculated value of β_0 is 2.56. The comparison of current and proposed design rules for combined failure mode of CHS-RHS T-joints is graphically shown in Fig. 58. Therefore, it can be concluded that the proposed design equation is relatively more accurate, less scatter and reliable.

The simplified proposed nominal strength (N_{spn}) for cold-formed CHS-RHS T-joints of S900 and S960 steel grades failed in combined failure (F+S) mode, by duly considering the effects of WHAR and affecting governing geometrical parameters, is as follows:

$$N_{spn} = \left[\frac{(0.01t_0 + 0.8)(6.7\beta - 3.5)}{(0.03(2\gamma) + 0.4)} \right] N_{E,T} \tag{19b}$$

The corresponding design strength (N_d) can be obtained by employing a resistance factor (ϕ) of 0.75 on Eq. (19b). When $\beta \leq 0.85$, the $N_{E,T}$ can be obtained using Eq. (8), whereas when $0.85 < \beta < 1.0$, the $N_{E,T}$ can be obtained using Eqs. (8) and (10). As shown in Table 14, the mean and COV of the comparison between joint failure strengths and simplified proposed nominal strengths are 1.10

and 0.216, respectively. Using a resistance factor (ϕ) of 0.75, the calculated values of β_0 is 2.67. It is important to note that when the β ratio of CFHSS CHS-RHS T-joint falls between 0.70 to 0.73, i.e. $0.70 < \beta < 0.73$, the corresponding proposed design strengths have to be obtained by performing a linear interpolation between Eqs. 18(a)-19(a) and 18(b)-19(b).

7. Conclusions

This paper presents a detailed finite element analysis of cold-formed high strength steel tubular T-joints made up of S900 and S960 thermo-mechanically controlled process steels. The brace members were made up of square, rectangular and circular hollow sections, whereas the chord members were made up of square and rectangular hollow sections. Finite element models were developed and verified against the tests conducted by Pandey and Young [1], showing the capability of replicating the joint strengths, failure modes and load-deformation histories. Subsequently, an extensive parametric study comprising of 285 finite element analyses was performed by duly covering a wide range of governing geometrical parameters. The validity ranges of governing parameters in this study exceeded the current validity ranges given in the EC3 [2] and CIDECT [3]. The experimental [1] and numerical joint strengths were compared with the nominal strengths calculated from the EC3 [2] and CIDECT [3]. The key findings of this investigation are as follows:

- The use of second-order solid elements for welds and tubular members helped in obtaining realistic joint behaviour and strength. The ignorance of welds in FE models underestimated the joint strengths by 6 to 32%.
- Cold-formed high strength steel tubular members produced using the thermo-mechanically controlled process are sensitive towards welding and need careful attention to avoid excessive softening of the fusion and heat affected zones. The inclusion of material properties of weld heat affected regions (WHAR) has a significant effect on the joint behaviour and helped in achieving the actual joint failure strengths of CFHSS T-joints.
- Three types of failure modes were observed namely chord face failure, chord side wall failure and combined failure. The strengths of T-joints failed in chord face failure were purely deformation controlled, however, the strengths of T-joints failed in chord side wall failure and combined failure were both load and deformation controlled.
- The applicability of current chord stress function given in the CIDECT [3] was also evaluated for T-joints of S900 and S960 steel grades. In this study, the chord stress function generally becomes increasingly unconservative with the increase of β ratio.
- Existing design rules given in the EC3 [2] and CIDECT [3] are not directly suitable for T-joints of S900 and S960 steel grades with validity ranges of governing parameters exceeding the limits specified in these specifications.

- The experimental and numerical evidence found a significant effect of 2γ ratio on the joint strength, wherein, in general, the joint strength decreased with the increase of 2γ ratio. On the other hand, the degree of over-conservatism of the EC3 [2] and CIDECT [3] predictions for chord side wall failure increased with the increase of h_0/t_0 ratio.
- Using two approaches, i.e. semi-empirical and by applying correction factors on the latest EC3 [2,59] equations, design rules are proposed for cold-formed tubular T-joints of RHS and CHS braces and RHS chords of S900 and S960 steel grades.
- A new equation was proposed to design the chord length of T-joint, where the simply supported chord span was kept equal to 4.5 times the maximum cross-sectional width or depth. Accordingly, in this study, the chord length-to-chord width and chord length-to-chord depth ratios ranged from 5 to 15.
- The buckling curve 'a' of the EC3 [55] was found more appropriate in the determination of chord side wall buckling stress for cold-formed high strength steel tubular T-joints made up of S900 and S960 steel grades.

Acknowledgements

The research work described in this paper was supported by a grant from the Research Grants Council of the Hong Kong Special Administrative Region, China (Project No. 17210218). It is also partially funded by the Chinese National Engineering Research Centre for Steel Construction (Hong Kong Branch) at the Hong Kong Polytechnic University which is funded by the Innovation and Technology Fund administrated by the Innovation and Technology Commission of the Commissioner of the Government of Hong Kong SAR.

References

[1] Pandey M, Young B. Tests of cold-formed high strength steel tubular T-joints. Thin-Walled Struct 2019;143:106200.
[2] EN 1993-1-8. Eurocode 3: Design of steel structures–Part 1-8: Design of joints. European Committee for Standardization (CEN), Brussels, Belgium; 2005.
[3] Packer JA, Wardenier J, Zhao XL, van der Vegte GJ, Kurobane Y. Design guide for rectangular hollow section (RHS) joints under predominantly static loading. Cologne, Germany: CIDECT, Verlag TUV Rheinland; 2009.
[4] Pandey M, Young B. Compression capacities of cold-formed high strength steel tubular T-joints. J Constr Steel Res 2019;162:105650.
[5] Pandey M and Young B. Structural performance of cold-formed high strength steel tubular X-Joints under brace axial compression. Engineering Structures, 2020; 208:109768.
[6] Li HT, Young B. Experimental Investigation of Concrete-Filled High-Strength Steel Tubular X Joints. J. Struct. Eng. 2018;144(10): 04018178.
[7] Lan XY, Chan TM, Young B. Structural behaviour and design of high strength steel RHS X-joints. Eng Struct 2019;200:109494.
[8] Feldmann M, Schillo N, Schaffrath S, Virdi K, Björk T, Tuominen N, et al. Rules on high strength steel. Luxembourg: Publications Office of the European Union; 2016.
[9] Havula J, Garifullin M, Heinisuo M, Mela K, Pajunen S. Moment-rotation behavior of welded tubular high strength steel T joint. Eng Struct 2018;172:523–37.
[10] Abaqus/Standard. Version 6.17. USA: K. a. S. Hibbit; 2017.
[11] van der Vegte GJ, Wardenier J, Puthli RS. FE analysis for welded hollow-section joints and bolted joints. Proceedings of the Institution of Civil Engineers-Structures and Buildings 2010;163(6):427-437.
[12] Choo YS, Qian XD, Wardenier J. Effects of boundary conditions and chord stresses on static strength of thick-walled CHS K-joints. J Constr Steel Res 2006;62(4):316-328.
[13] Cao JJ, Packer JA, Kosteski N. Design guidelines for longitudinal plate to HSS connections. J. Struct. Eng. 1998;124(7):784-791.
[14] Kosteski N, Packer JA. Longitudinal plate and through plate-to-hollow structural section welded connections. J. Struct. Eng. 2003;129(4):478-486.
[15] Pang HLJ, Lee CW. Three-dimensional finite element analysis of a tubular T-joint under combined axial and bending loading. International journal of fatigue 1995;17(5):313-320.
[16] Crockett P. Finite element analysis of welded tubular connections. PhD Thesis, University of Nottingham, 1994.
[17] Gardner L, Nethercot DA. Numerical modeling of stainless steel structural components—A consistent approach. J. Struct. Eng. 2004;130(10):1586-1601.
[18] Ma J. Behaviour and design of cold-formed high strength steel tubular members. HKU Theses Online (HKUTO), 2016.
[19] AWS D1.1/D1.1M. Structural Welding Code – Steel. American Welding Society (AWS), Miami, USA, 2015.
[20] Reimer RB, Litton RW, Babcock, JH. Finite Element Analysis of Complex, Welded Tubular Joints. In Offshore Technology Conference. Offshore Technology Conference, 1979.
[21] Bhuyan GS, Munaswamy K, Arockiasamy M. Through Thickness and Surface Stress Distribution of Welded Tubular T Joints using the FE Method. Canadian Journal of Civil Engineering, 1986:Vol 13.
[22] van der Vegte GJ, de Koning CHM, Puthli RS and Wardenier J. Static Behaviour of Multiplanar Welded Joints in Circular Hollow Sections. Stevin report, Delft University 1991.

[23] de Koning CHM, Liu DK, Puthli RS, Wardenier J. Static Behaviour of Multiplanar Connections in Rectangular Hollow Sections. Stevin report, Delft University, 1992.
[24] Feng R, Young B. Design of cold-formed stainless steel tubular T- and X-joints. J Constr Steel Res 2011;67:421-436.
[25] Packer JA. A theoretical analysis of welded steel joints in rectangular hollow sections. PhD Thesis, University of Nottingham, 1978.
[26] Davies G, Morita K. Three Dimensional Cross joints under Combined Axial Branch Loading. Proceedings of the Fourth International Symposium, Delft, Netherlands, 1991.
[27] Yu Y, Wardenier J. Influence of the types of welds on the static strength of RHS T-and X-joints loaded in compression. In Proceedings of the Sixth International Symposium on Tubular Structures. Lucedale, MS, USA: Tubular Structures, 597-605, 1994.
[28] Stroetmann R, Kastner T, Halsig A, Mayr P. Mechanical properties and a new design approach for welded joints at high strength steels. Hong Kong:Engineering Research and Practice for Steel Construction; 2018:79–90.
[29] Dilthey U. Schweißtechnische Fertigungsverfahren 2 – Verhalten der Werkstoffe beim Schweißen. Auflage, Berlin, Heidelberg, New York: Springer-Verlag, 2006 (in German).
[30] Javidan F, Heidarpour A, Zhao XL, Hutchinson CR, Minkkinen J. Effect of weld on the mechanical properties of high strength and ultra-high strength steel tubes in fabricated hybrid sections. Eng Struct 2016;118:16–27.
[31] Amraei M., Ahola A., Afkhami S., Bjork T., Heidarpour A. and Zhao X.L. .Effects of heat input on the mechanical properties of butt-welded high and ultra-high strength steels, Engineering Structures, 2019, 198, 109460.
[32] Amraei M., Afkhami S., Javaheri V., Larkiola J., Skriko T., Bjork T. and Zhao X.L. .Mechanical properties and microstructural evaluation of the heat-affected zone in ultra-high strength steels, Thin-Walled Structures, 2020, 157, 107072.
[33] Pandey M, Young B. Static Strengths of Cold-formed High Strength Steel Tubular Non-90˚ X-Joints. Engineering Structures, Elsevier (under review).
[34] prEN 10219-2. Cold formed welded structural hollow sections of non-alloy and fine grain steels-Part 2: Tolerances, dimensions and sectional properties. European Committee for Standardization (CEN), Brussels, Belgium; 2006.
[35] Garifullin M, Bronzova MK, Heinisuo M, Mela K, Pajunen S. Cold-formed RHS T joints with initial geometrical imperfections. Magazine of Civil Engineering 2018,82(6).
[36] SSAB. Strenx Tube 900 MH. Data Sheet 2042, Sweden, 2017.
[37] SSAB. Strenx Tube 960 MH. Data Sheet 2043, Sweden, 2017.
[38] Kato B, Nishiyama I. The static strength of RR-joints with large b/B ratio. CIDECT Prog. 5Y. Dept. of Arch., Faculty of Eng., Univ. of Tokyo, 1979.
[39] Wardenier J, Stark JWB. The static strength of welded lattice girder joints in structural hollow sections: Parts 1-10. CIDECT Final Report 5Q-78/4, Delft University of Technology, Delft, The Netherlands, 1978.
[40] Redwood RG. The behaviour of joints between rectangular hollow structural members. Civil Engineering and Public Works Review, Canada, 1463-1469, 1965.
[41] Korol RM, Mirza FA. Finite element analysis of RHS T-joints. J. Struct. Eng. 1982;108:2081-2098.
[42] Yu Y. The static strength of uniplanar and multiplanar connections in rectangular hollow sections. Ph.D. Thesis, Delft University Press, Delft, The Netherlands, 1997.
[43] Lu LH, Winkel GD de, Yu Y, Wardenier J. Deformation limit for the ultimate strength of hollow section joints. Proceedings 6th International Symposium on Tubular Structures, Melbourne, Australia,

Tubular Structures VI, Balkema, Rotterdam, The Netherlands, 341-347, 1994.
[44] Wardenier J. Investigation on Vierendeel joints - Determination of M-Φ and P-δ characteristics and the fatigue behaviour. Stevin Report 6-72-11, 1972.
[45] Wardenier J, Koning CHM. Static tensile tests on T-joints in structural hollow sections. Stevin Report 6-74-7, 1975.
[46] Davies G, Crockett P. The strength of welded T-DT joints in rectangular and circular hollow section under variable axial loads. J Constr Steel Res 1996;37(1):1-31.
[47] Zhao XL, Hancock GJ. T-joints in rectangular hollow sections subject to combined actions. J. Struct. Eng. 1991;117(8):2258-2277.
[48] Bae KW, Park KS, Choi YH, Moon TS, Stiemer SF. Behavior of branch-rotated T joints with cold-formed square hollow sections. Canadian Journal of Civil Engineering, 2006;33(7):827-836.
[49] Aguilera J, Shaat A, Fam A. Strengthening T-joints of rectangular hollow steel sections against web buckling under brace axial compression using through-wall bolts. Thin-Walled Structures, 2012:56:71-78.
[50] Sharaf T, Fam A. Finite element analysis of beam-column T-joints of rectangular hollow steel sections strengthened using through-wall bolts. Thin-Walled Structures, 2013;64:31-40.
[51] Chang H, Xia J, Zhang F, Chang H. Compression behaviour of doubler-plate reinforced square hollow section T-joints. Adv. Steel Constr. Inter. J, 2014;10(3):289-309.
[52] AISI S100. North American Specification for the design of cold-formed steel structural members. American Iron and Steel Institute (AISI), Washington, D.C., USA, 2016.
[53] EN 1990. Eurocode: Basis of structural design. European Committee for Standardization (CEN), Brussels, Belgium, 2002.
[54] ASCE/SEI 7. Minimum Design Loads for Buildings and Other Structures. American Society of Civil Engineers (ASCE), New York, USA, 2016.
[55] EN 1993-1-1, Eurocode 3: Design of Steel Structures–Part 1-1: General Rules and Rules for Buildings, European Committee for Standardization (CEN), Brussels, Belgium, 2005.
[56] Wardenier J. Hollow Section Joints. Delft University Press, Delft, 1982.
[57] Wardenier J, van der Vegte GJ, Liu DK. Chord stress function for rectangular hollow section X and T joints. Proceedings of the Sixteenth International Offshore and Polar Engineering Conference (ISOPE) 2007;3363:3370.
[58] Pandey M, Chung KF, Young B. Numerical Investigation and Design of Fully Chord Supported Tubular T-Joints, Engineering Structures, Elsevier (under review).
[59] EN 1993-1-12. Eurocode 3: Design of Steel Structures – Part 1-12: Additional Rules for the Extension of EN 1993 Up to Steel Grades S700. European Committee for Standardization (CEN), Brussels, Belgium, 2007.

Notation

b_1	Brace flange width
b_0	Chord flange width
$b_{0,max}$	Maximum chord cross-sectional width
b_w	Effective width of the semi-fixed chord web column
C	Width of end bearing plate
C_ϕ	Calibration coefficient
C_P	Correction factor to consider test sample size
d_1	Brace diameter
f_{y0}	Design yield strength of the chord member
f_k and f_b	Chord side wall buckling strength
F_m	Mean value for fabrication factor
h_1	Brace web height
h_0	Chord web height
$h_{0,max}$	Maximum chord cross-sectional web height
h_0/t_0	Chord side wall slenderness
k_n	Chord stress function as per EC3
L_0	Chord length
L_1	Brace length
L_e	Simply supported chord length
M_m	Mean value for material factor
n	Chord stress factor
N	Applied load (experimental and/or numerical)
N_d	Design strength
N_{FE}	Numerical strength
N_f	Joint failure strength (experimental and/or numerical)
$N_{f,TF}$	Compression capacity of fully chord supported T-joint (experimental and/or numerical)
$N^*_{E,T}$	Nominal strength of T-joint calculated from EC3 without including the reduction factor
$N_{E,T}$	Nominal strength of T-joint calculated from EC3 with reduction factor included
$N^*_{C,T}$	Nominal strength of T-joint calculated from CIDECT without including the reduction factor
$N_{C,T}$	Nominal strength of T-joint calculated from CIDECT with reduction factor included
N_{pn}	Proposed nominal strength (or proposed characteristic strength)
N_{spn}	Simplified proposed nominal strength (or simplified proposed characteristic strength)
P_m	Mean value of the comparison
Q_f or Q_{CIDECT}	Chord stress function as per CIDECT
Q_{FE}	Chord stress function calculated from FE
r_1	Internal radius of brace member corner region
r_0	Internal radius of chord member corner region
R_1	External radius of brace member corner region
R_0	External radius of chord member corner region
S_{rl}	Linear strength reduction
t	Tubular wall thickness
t_1	Brace thickness
t_0	Chord thickness

t_w	Effective throat thickness of fillet weld
u	Chord face indentation
v	Chord side wall deformation
V_M	COV for material factor
V_F	COV for fabrication factor
V_P	COV of the comparison
V_Q	COV for load effects
w	Fillet weld leg size
w'	Weld measurement for PJP flare bevel groove weld for equal-width T-joints
w_r	Weld reinforcement for PJP flare bevel groove weld for equal-width T-joints
z	Axial shortening of T-joint
β	Brace width-to-chord width ratio
β_0	Reliability index
2γ	Chord width-to-chord thickness ratio
γ_{M5}	Partial safety factor for tubular joints as per EC3
ζ	Reduction factor for HSS material
η	Brace web height-to-chord flange width ratio
θ_1	Included angle between brace and chord members
τ	Brace-to-chord thickness ratio
ϕ	Resistance factor
CHS	Circular hollow sections
CHS-RHS	Circular hollow section brace-to-Square and rectangular hollow section chord
CFHSS	Cold-formed high strength steel
COV	Coefficients of variation
DL	Dead load
F	Chord face failure mode
FE	Finite element
F+S	Combined failure mode
FW	Fillet weld
FZ	Fusion zone
GW	Partial joint penetration flare bevel groove weld
HAZ	Heat affected zone
HSS	High strength steel
LL	Live load
RHS	Square and rectangular hollow sections
RHS-RHS	Square and rectangular hollow section brace-to-Square and rectangular hollow section chord
S	Chord side wall failure mode
TMCP	Thermomechanical control process
WHAR	Weld heat affected region

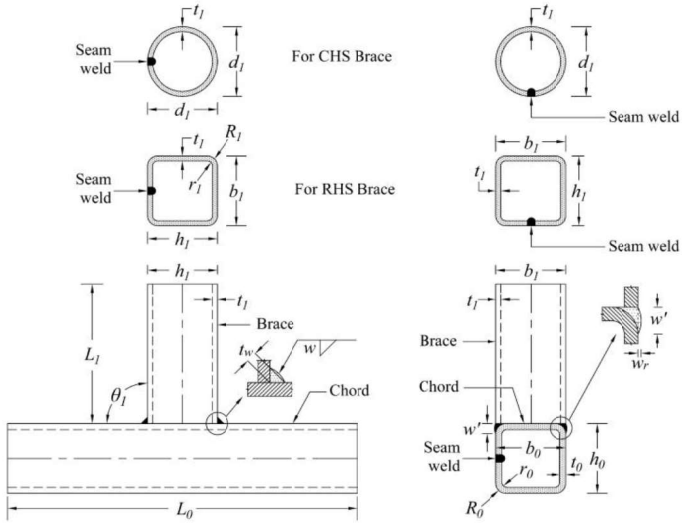

Fig. 1. Definition of symbols

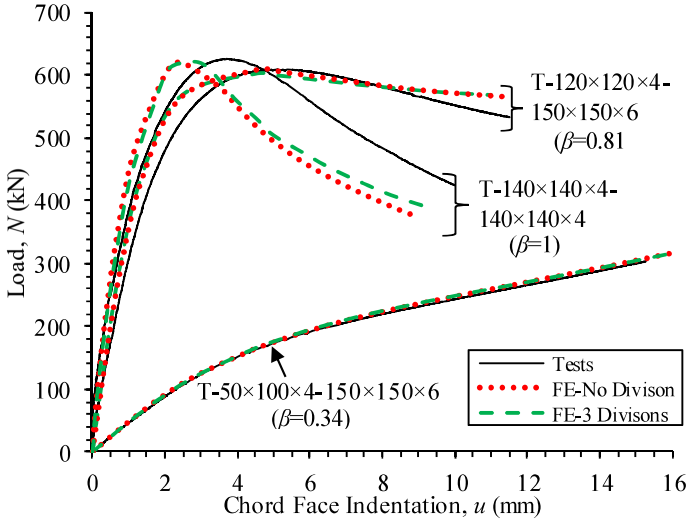

Fig. 2. Through-thickness division effects on RHS-RHS T-joints

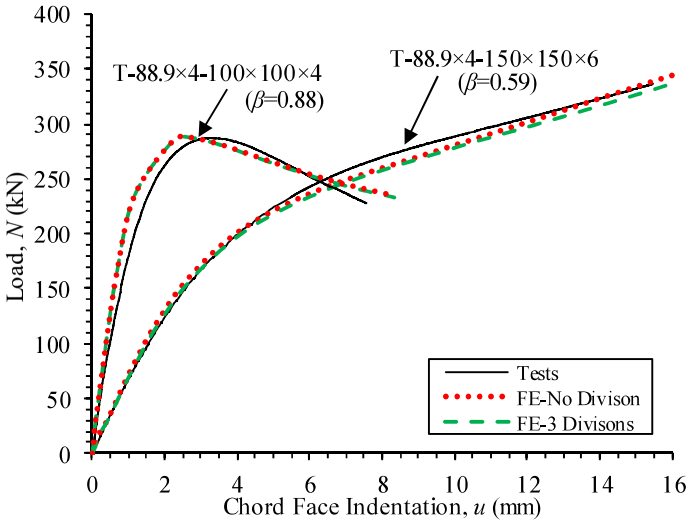

Fig. 3. Through-thickness division effects on CHS-RHS T-joints

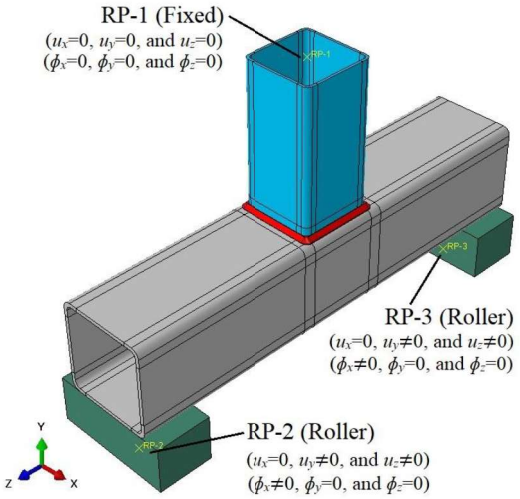

Fig. 4. Boundary conditions assigned in FE model

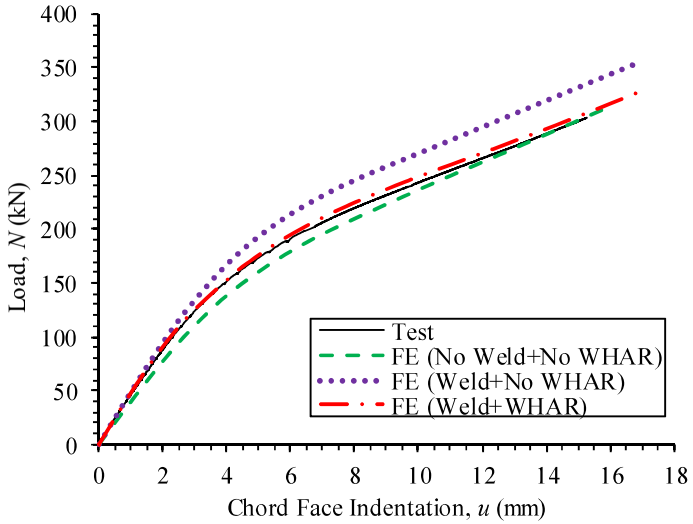

Fig. 5. Weld and WHAR effects on RHS-RHS T-joints failed in 'F' mode

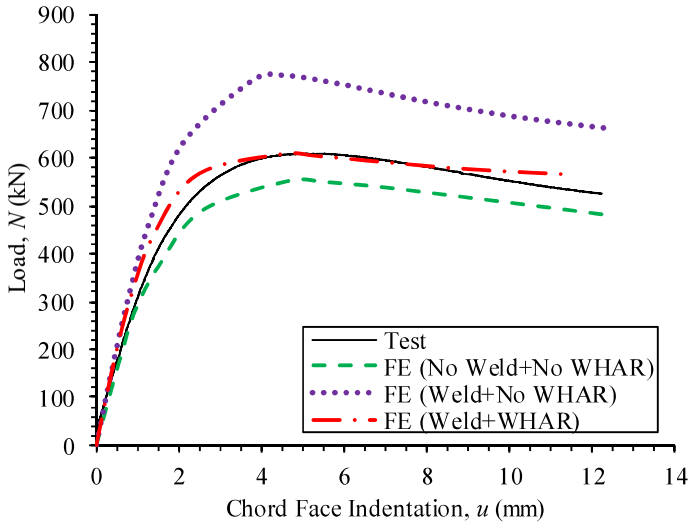

Fig. 6. Weld and WHAR effects on RHS-RHS T-joints failed in 'F+S' mode

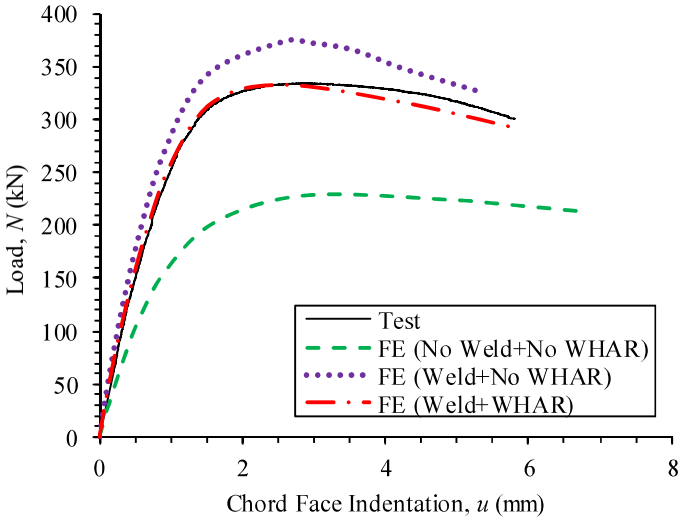

Fig. 7. Weld and WHAR effects on RHS-RHS T-joints failed in 'S' mode

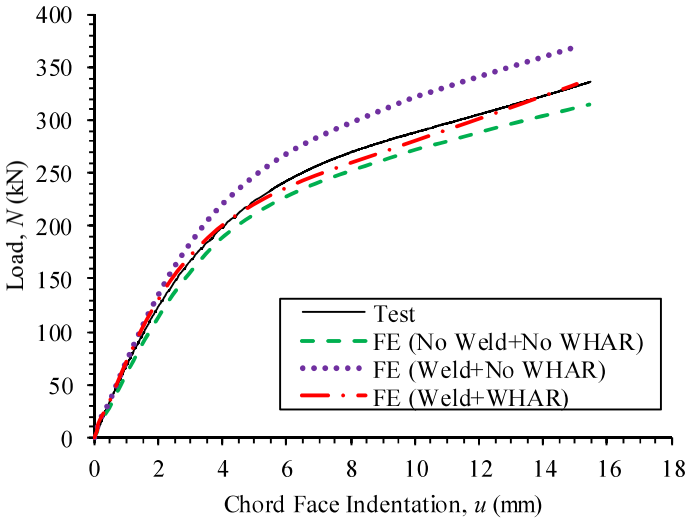

Fig. 8. Weld and WHAR effect on CHS-RHS T-joints failed in 'F' mode

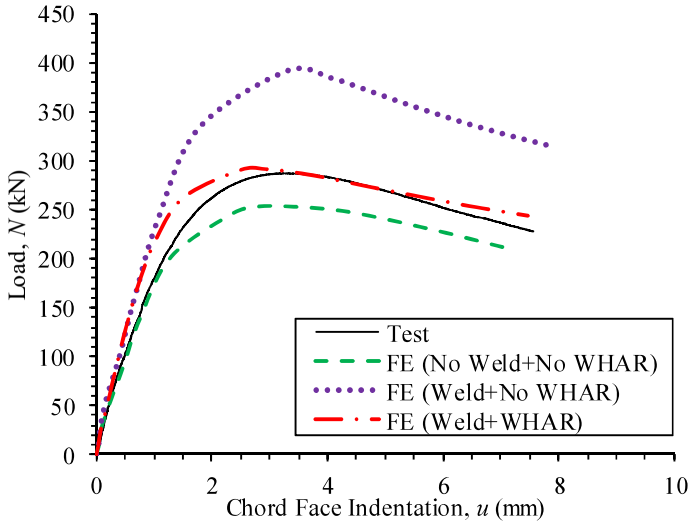

Fig. 9. Weld and WHAR effect on CHS-RHS T-joints failed in 'F+S' mode

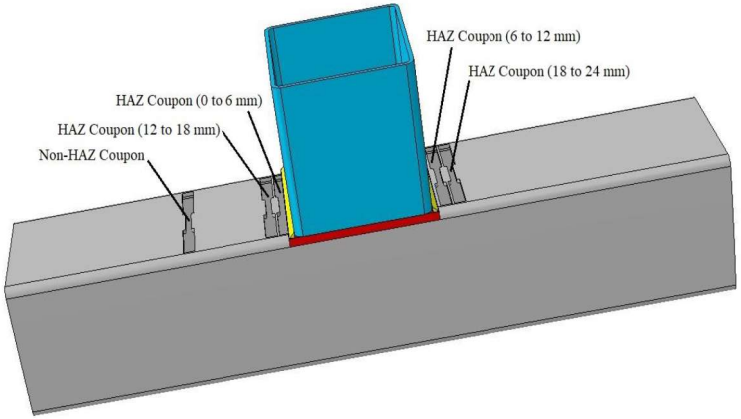

Fig. 10. Extracted locations of HAZ and non-HAZ tensile coupons [33]

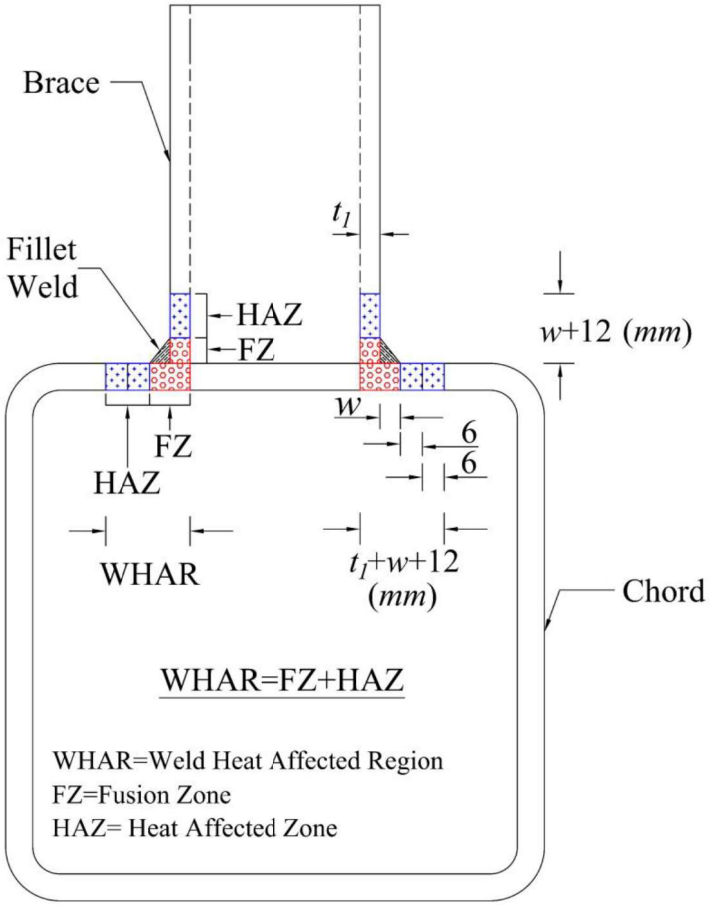

Fig. 11. Definitions of WHAR, FZ and HAZ

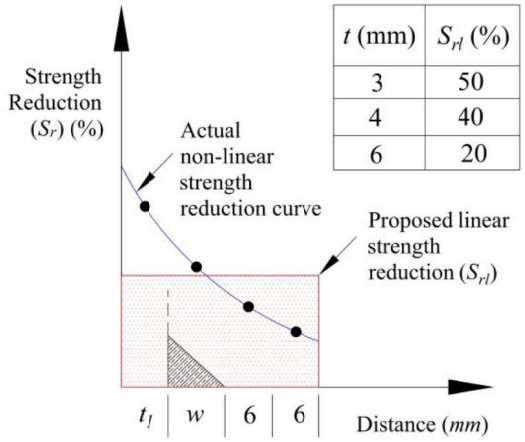

t (mm)	S_{rl} (%)
3	50
4	40
6	20

Fig. 12. Linear strength reduction model for WHAR

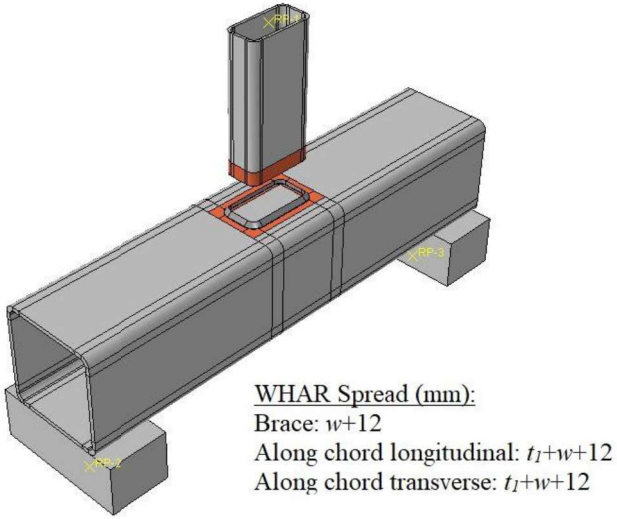

Fig. 13. Spread of WHAR for T-joints ($\beta \leq 0.75$)

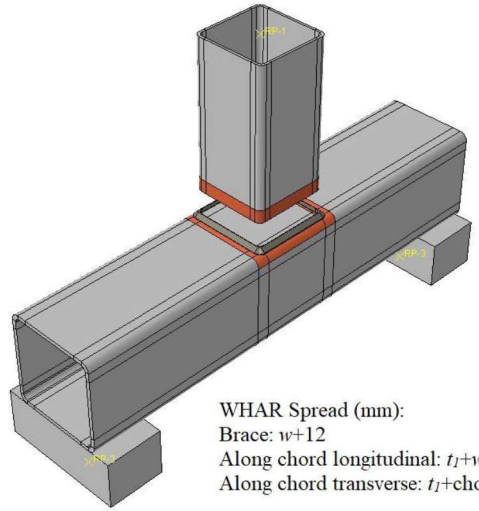

Fig. 14. Spread of WHAR for T-joints ($0.75<\beta<1$)

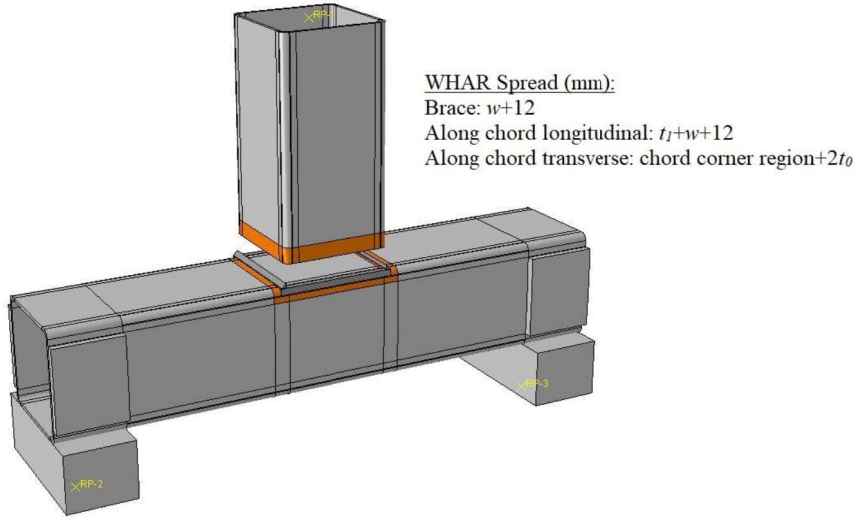

Fig. 15. Spread of WHAR for T-joints (β=1.0)

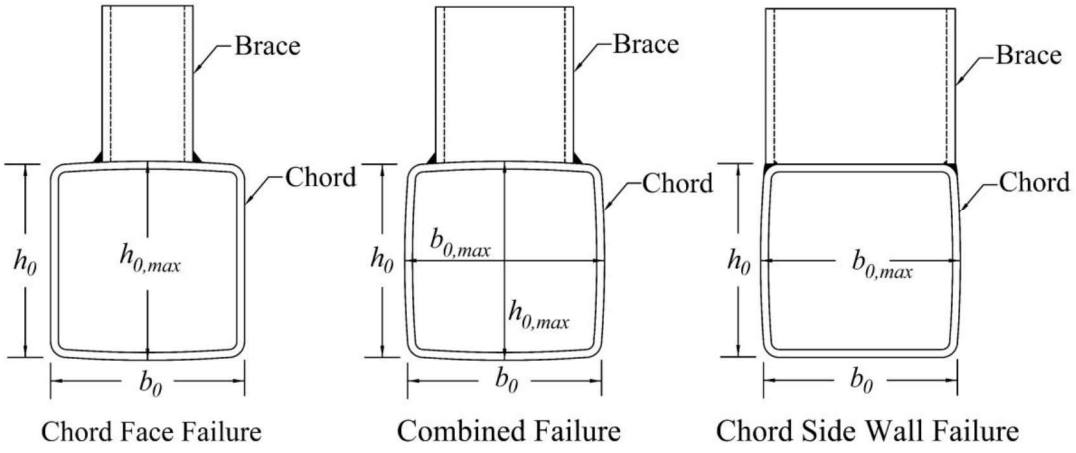

Fig. 16. Governing convex bulges for different failure modes

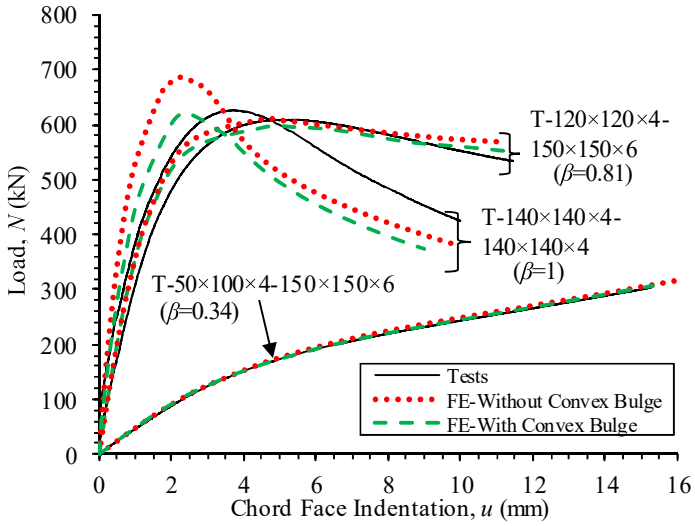

Fig. 17. Effect of convex bulges on RHS-RHS T-joints

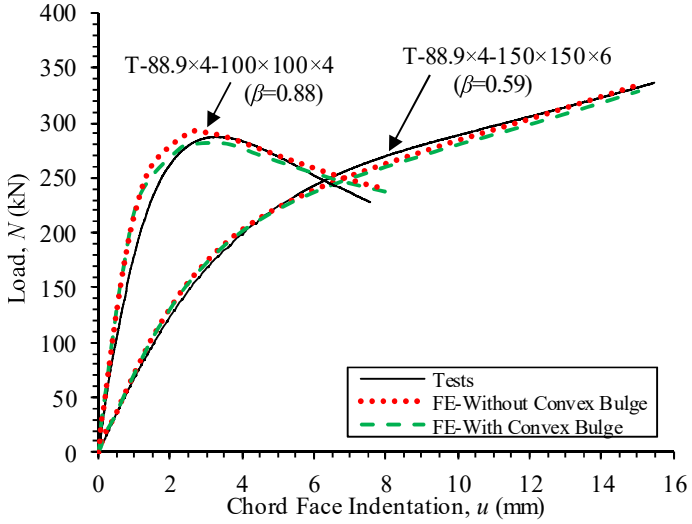

Fig. 18. Effect of convex bulges on CHS-RHS T-joints

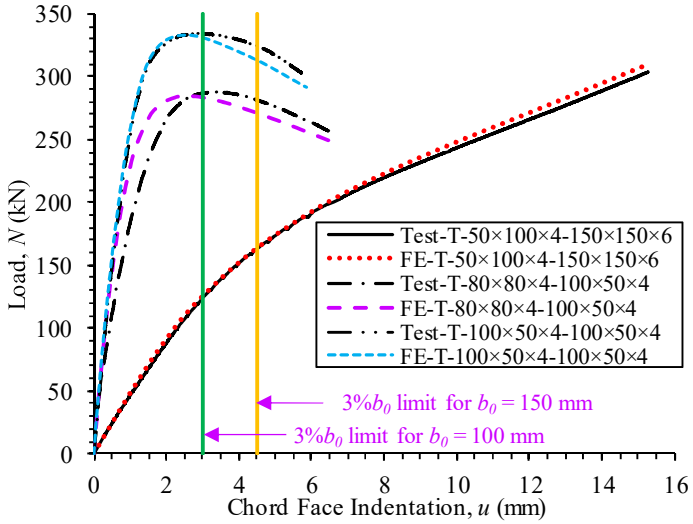

a. Load vs chord face indentation curves

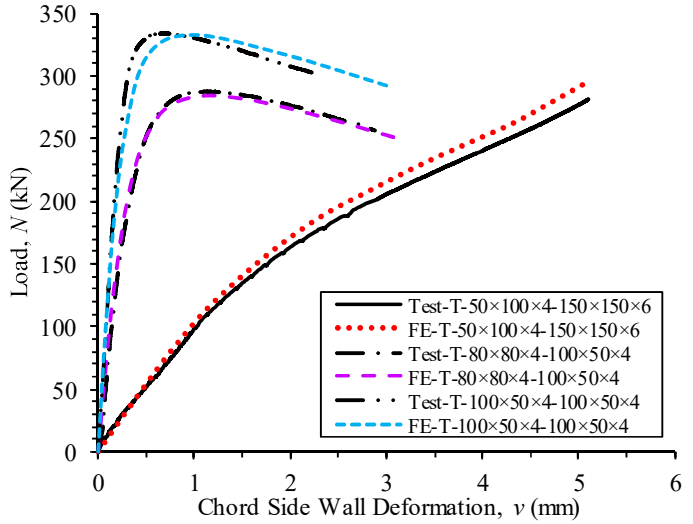

b. Load vs chord side wall deformation curves

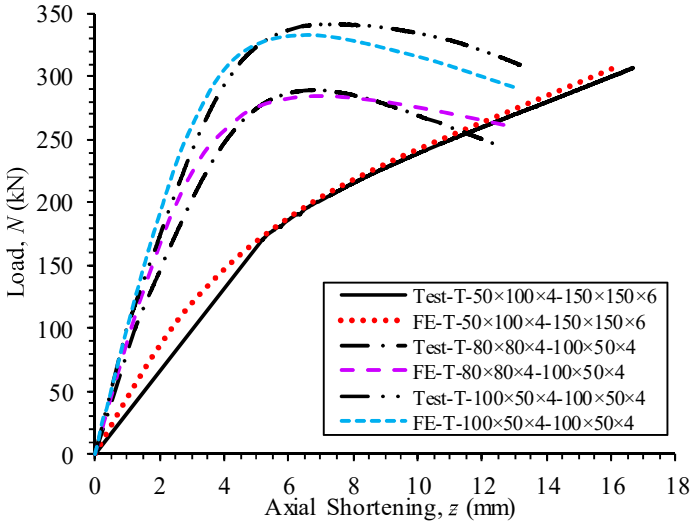

c. Load vs axial shortening curves

Fig. 19. Comparison of test and FE load-deformation curves for RHS-RHS T-joints

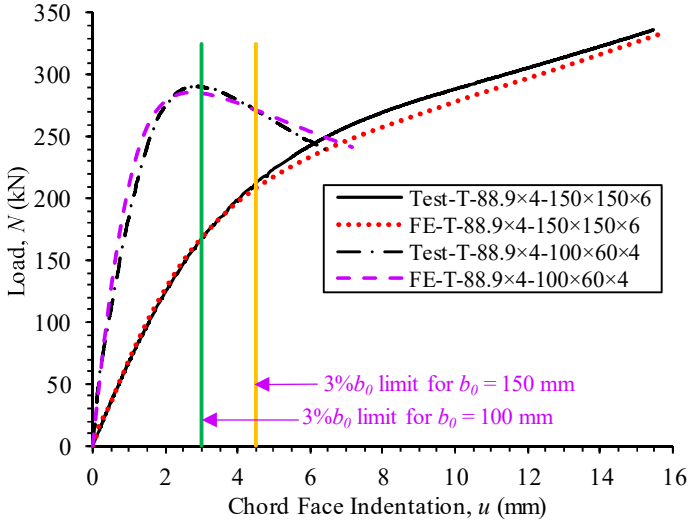

a. Load vs chord face indentation curves

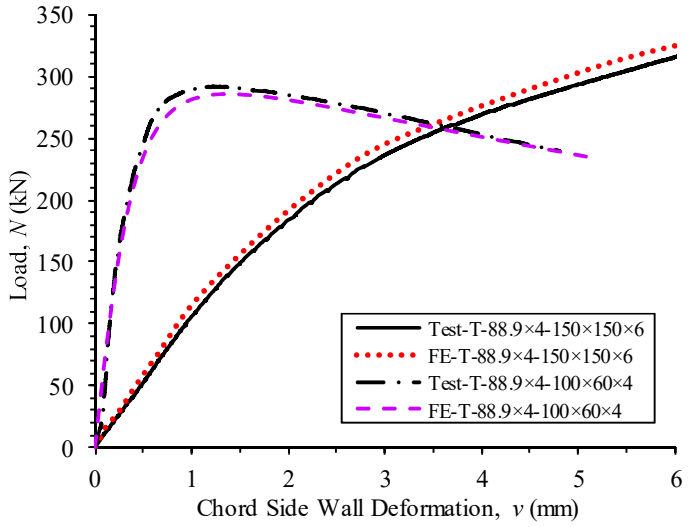

b. Load vs chord side wall deformation curves

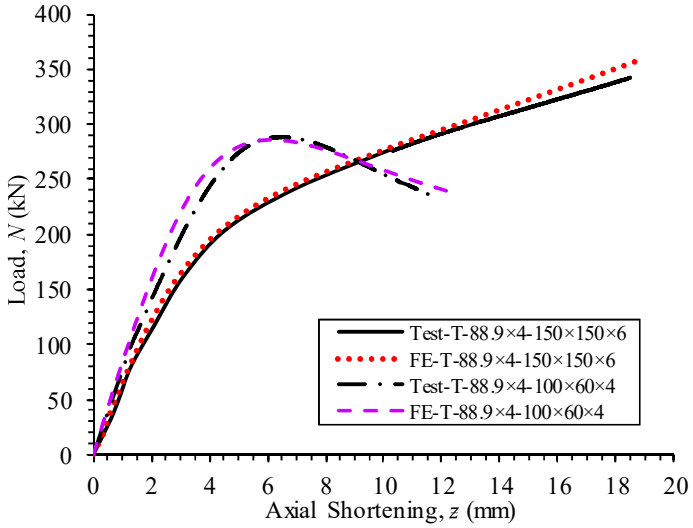

c. Load vs axial shortening curves

Fig. 20. Comparison of test and FE load-deformation curves for CHS-RHS T-joints

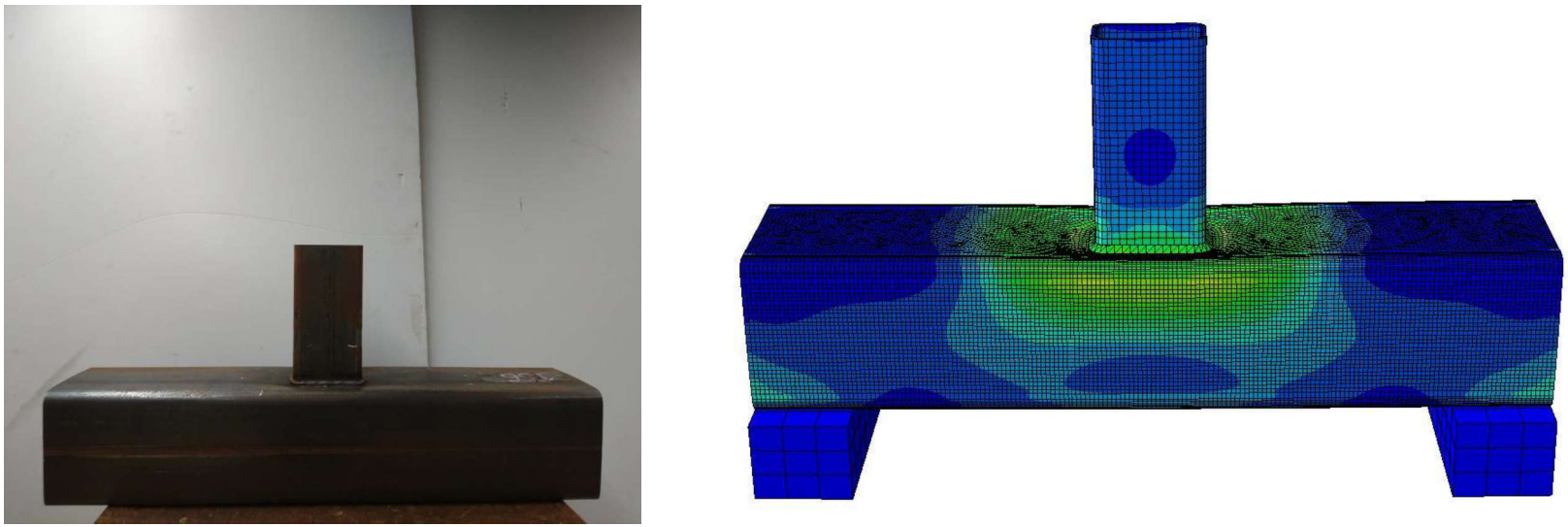

Fig. 21. Chord face failure mode (F) comparison between test and FE RHS-RHS T-joint

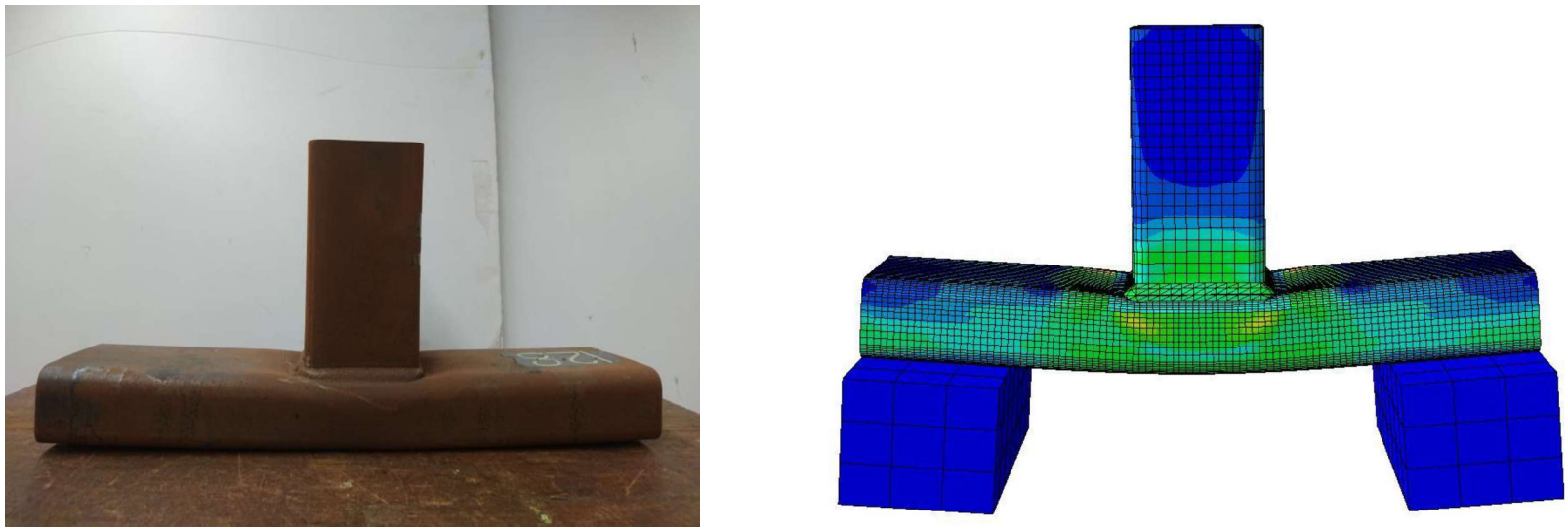

Fig. 22. Combined failure mode (F+S) comparison between test and FE RHS-RHS T-joint

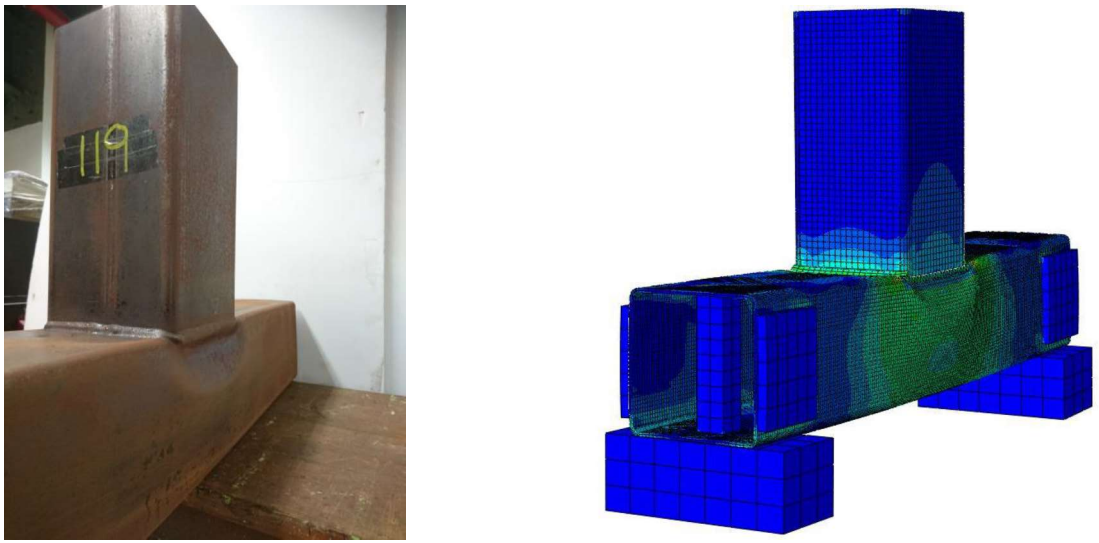

Fig. 23. Chord side wall failure mode (S) comparison between test and FE RHS-RHS T-joint

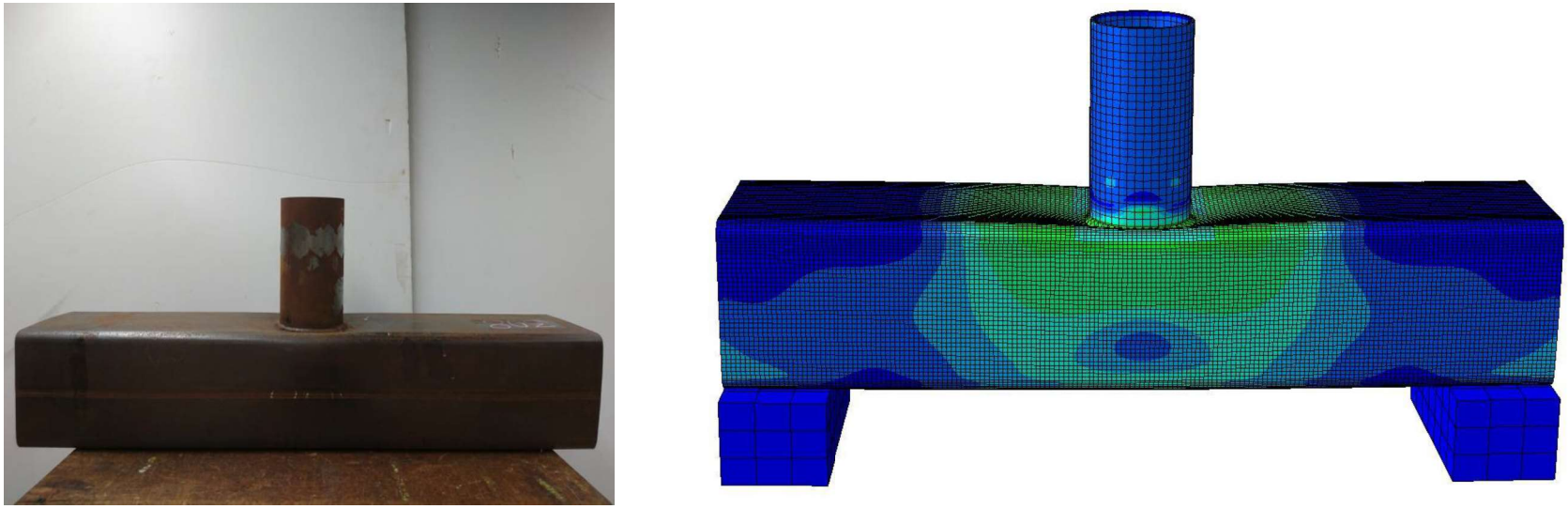

Fig. 24. Chord face failure mode (F) comparison between test and FE CHS-RHS T-joint

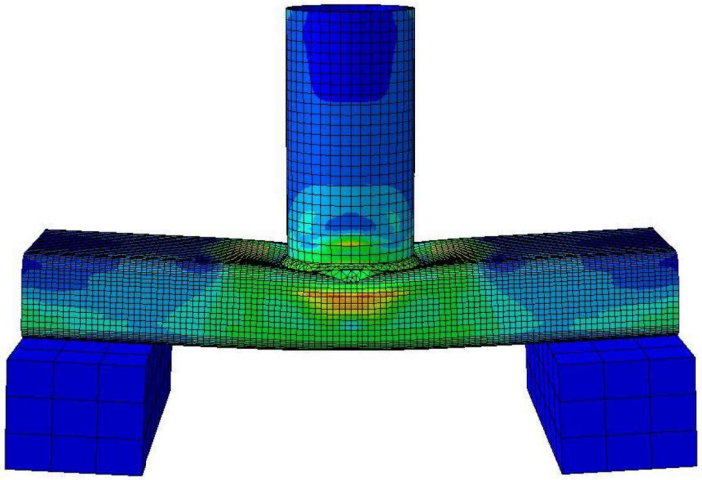

Fig. 25. Combined failure mode (F+S) comparison between test and FE CHS-RHS T-joint

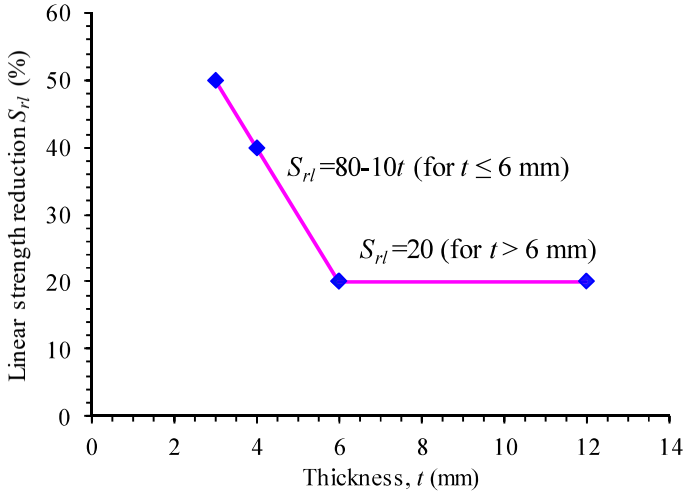

Fig. 26. Linear strength reduction in WHAR for different wall thicknesses

V	1	1	1	1	1	1	1
H	0.5	1	1.5	2	3	4	5

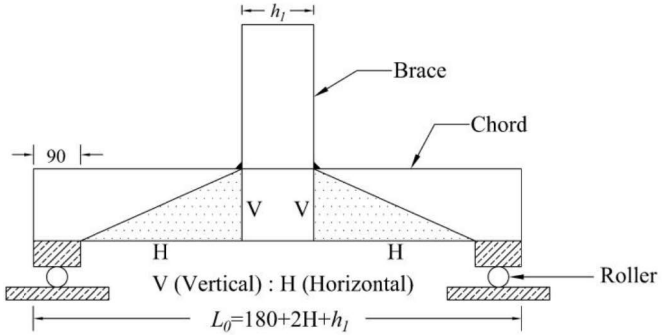

Fig. 27. Change of chord length using different load distributions

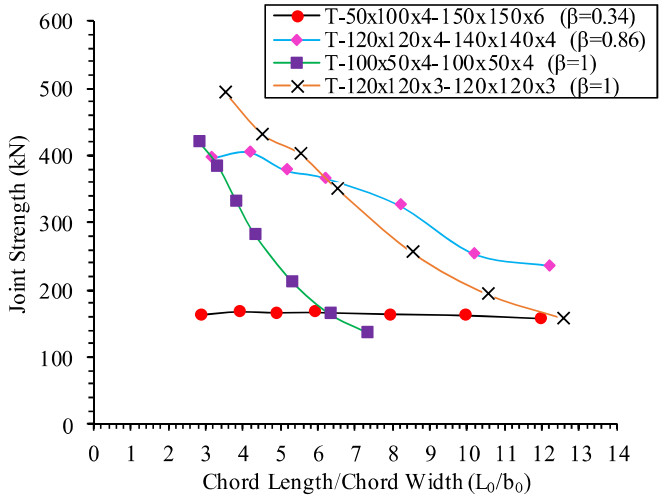

Fig. 28. Variation of joint strengths with L_0/b_0 ratios

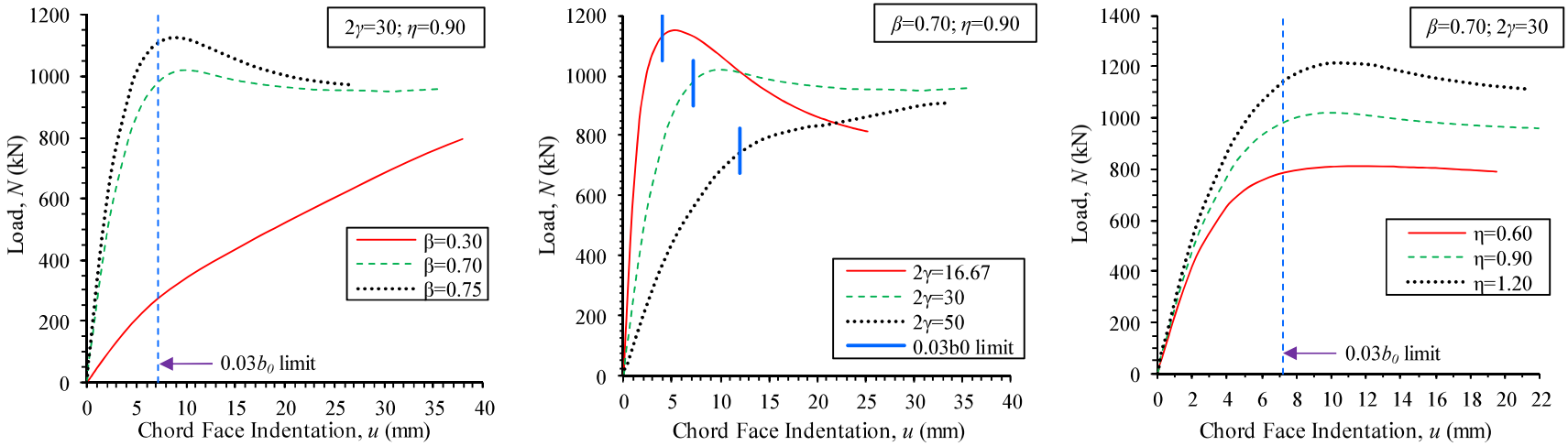

(a) Effect of β ratio (b) Effect of 2γ ratio (c) Effect of η ratio

Fig. 29. Effects of governing parameters on the load-deformation behaviour of RHS-RHS T-joints failed in chord face failure mode

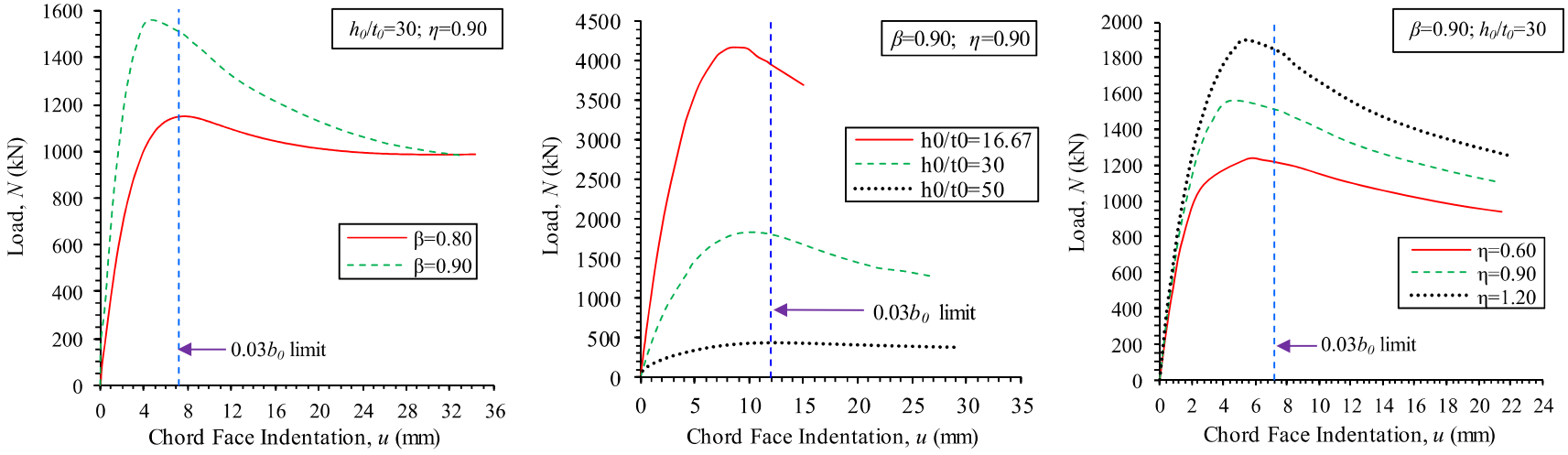

(a) Effect of β ratio (b) Effect of h_0/t_0 ratio (c) Effect of η ratio

Fig. 30. Effects of governing parameters on the load-deformation behaviour of RHS-RHS T-joints failed in combined failure mode

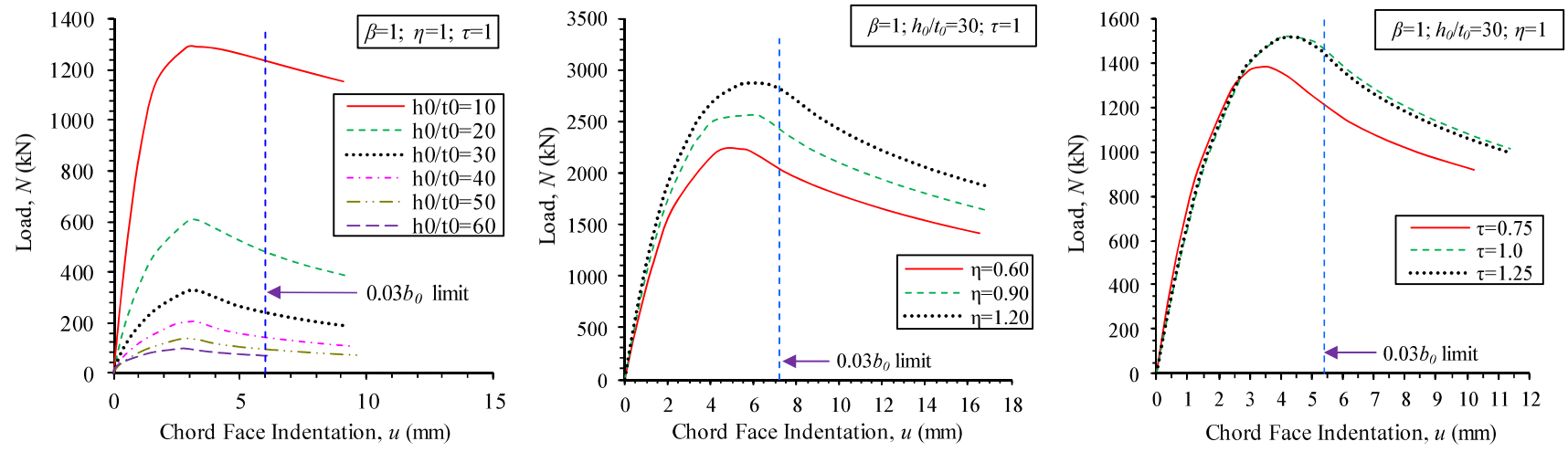

(a) Effect of h_0/t_0 ratio (b) Effect of η ratio (c) Effect of τ ratio

Fig. 31. Effects of governing parameters on the load-deformation behaviour of RHS-RHS T-joints failed in chord side wall failure mode

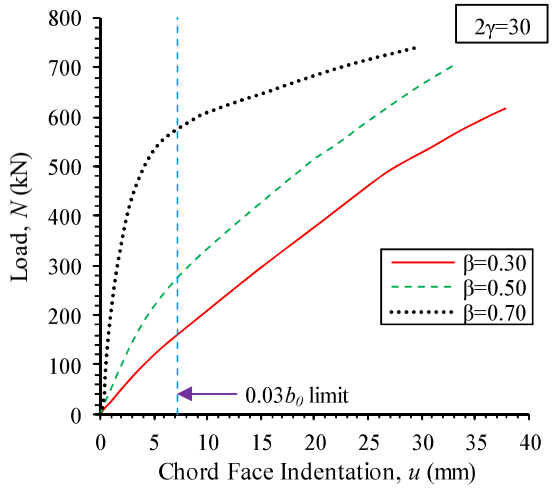

(a) Effect of β ratio

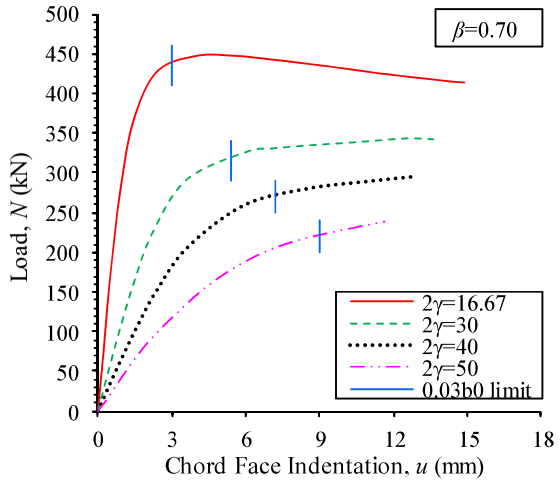

(b) Effect of 2γ ratio

Fig. 32. Effects of governing parameters on the load-deformation behaviour of CHS-RHS T-joints failed in chord face failure mode

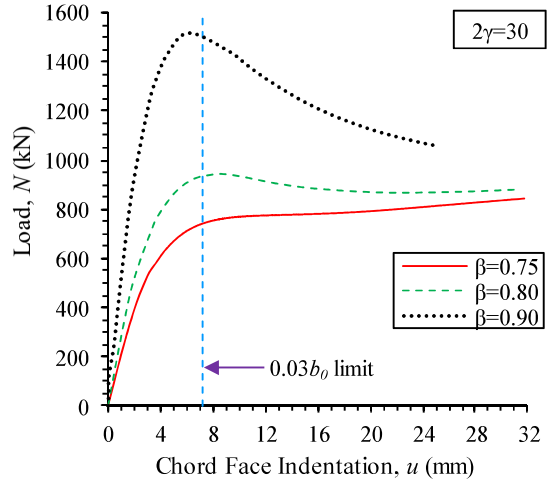

(a) Effect of β ratio

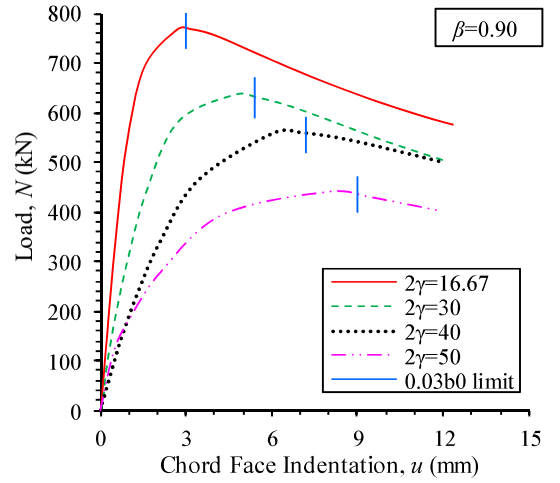

(b) Effect of 2γ ratio

Fig. 33. Effects of governing parameters on the load-deformation behaviour of CHS-RHS T-joints failed in combined failure mode

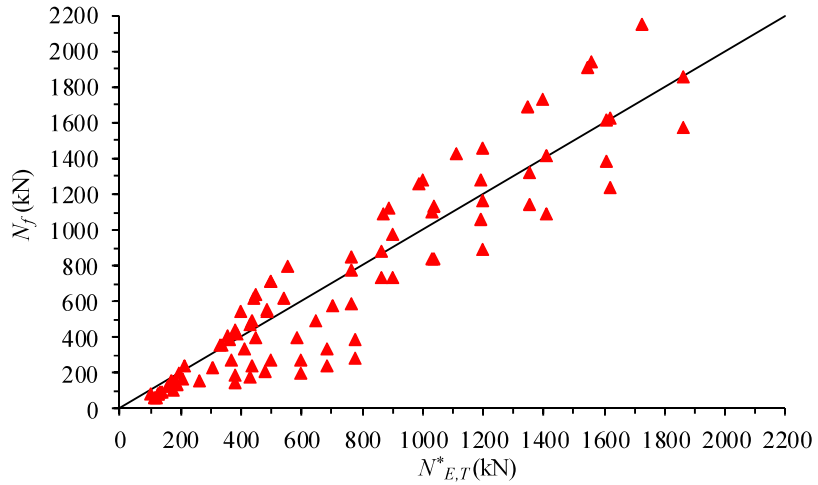

(a) N_f vs $N^*_{E,T}$

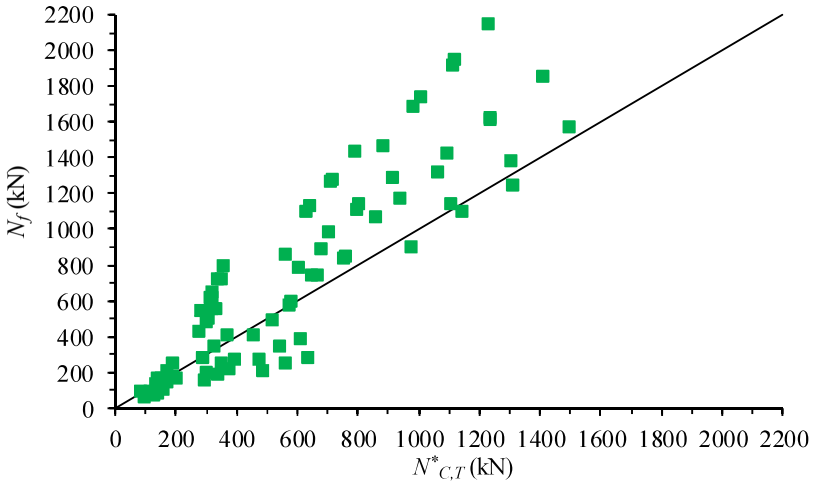

(c) N_f vs $N^*_{C,T}$

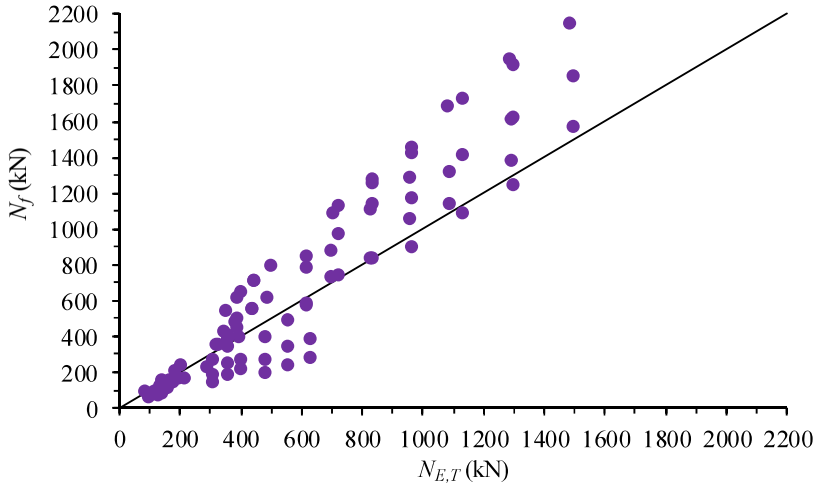

(b) N_f vs $N_{E,T}$

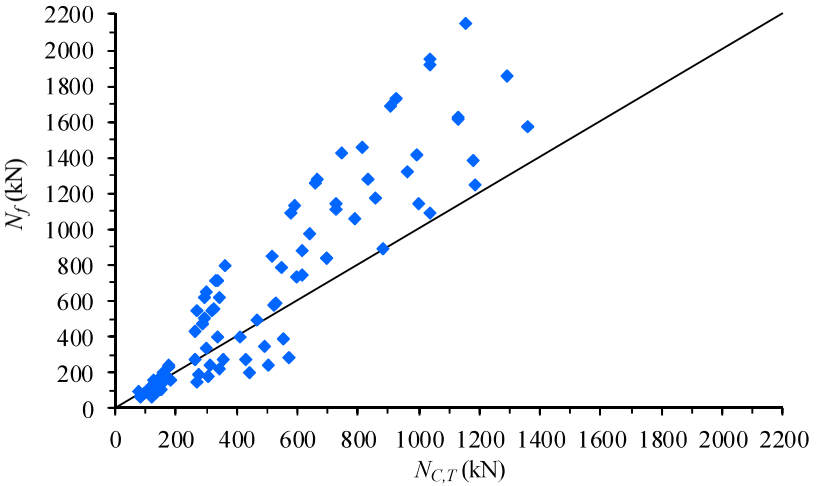

(d) N_f vs $N_{C,T}$

Fig. 34. Variations of test and FE T-joint strengths with nominal strengths for RHS-RHS T-joints failed in chord face failure mode

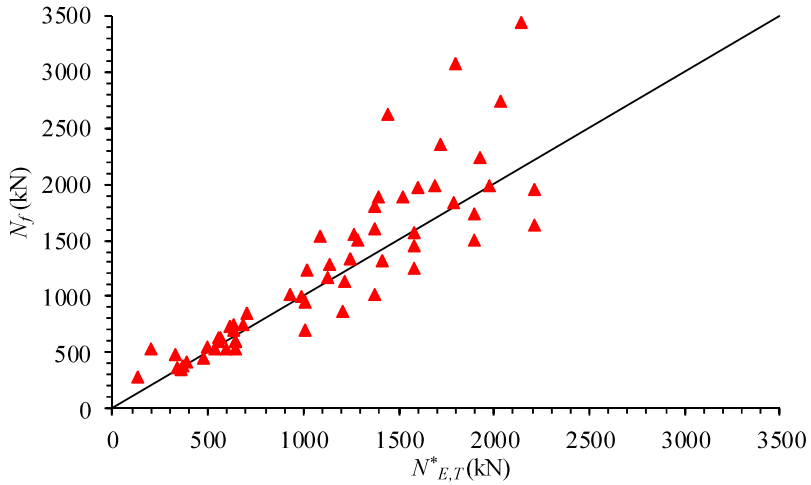

(a) N_f vs $N^*_{E,T}$

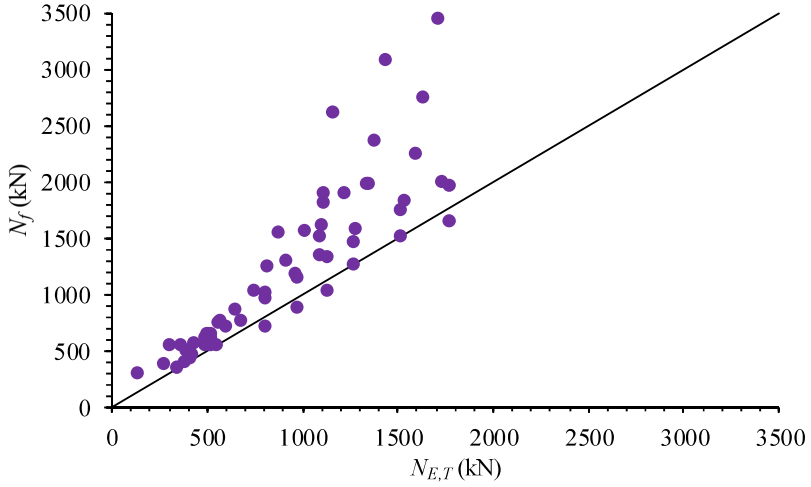

(b) N_f vs $N_{E,T}$

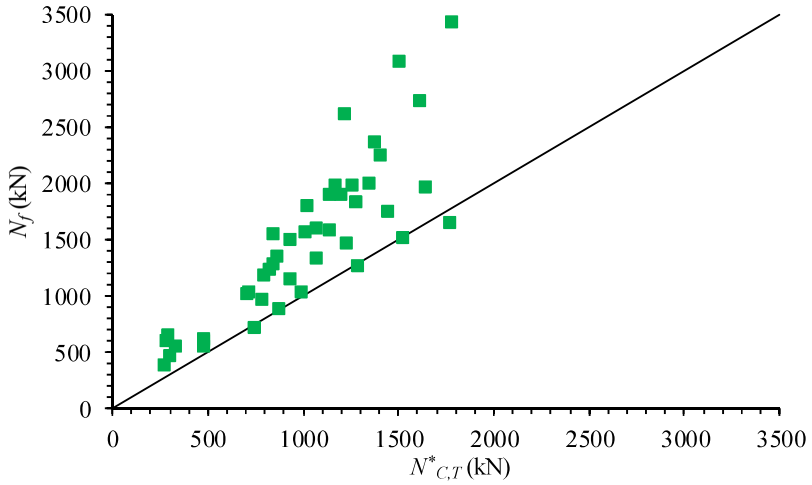

(c) N_f vs $N^*_{C,T}$

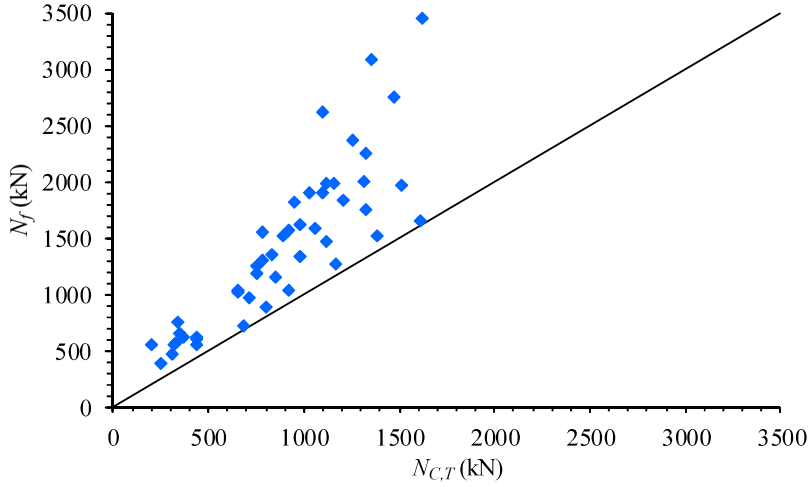

(d) N_f vs $N_{C,T}$

Fig. 35. Variations of test and FE T-joint strengths with nominal strengths for RHS-RHS T-joints failed in combined failure mode

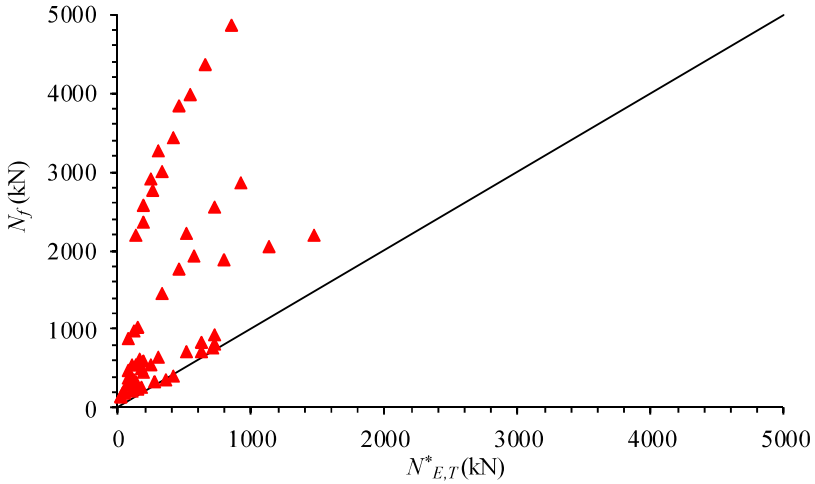

(a) N_f vs $N^*_{E,T}$

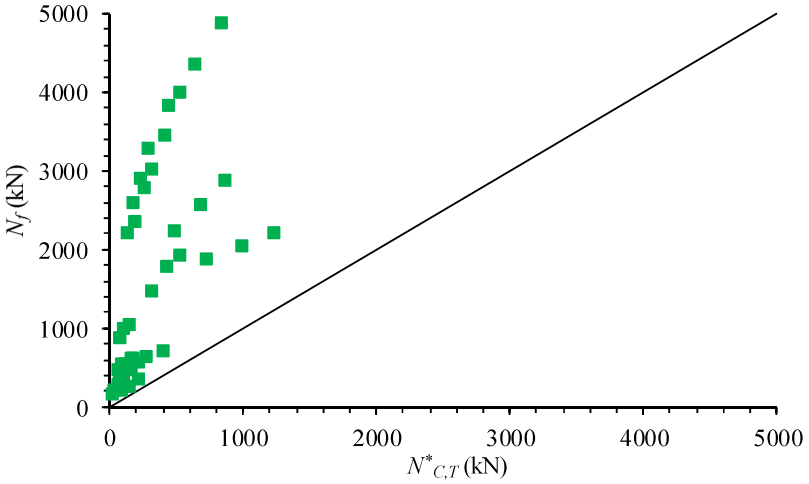

(c) N_f vs $N^*_{C,T}$

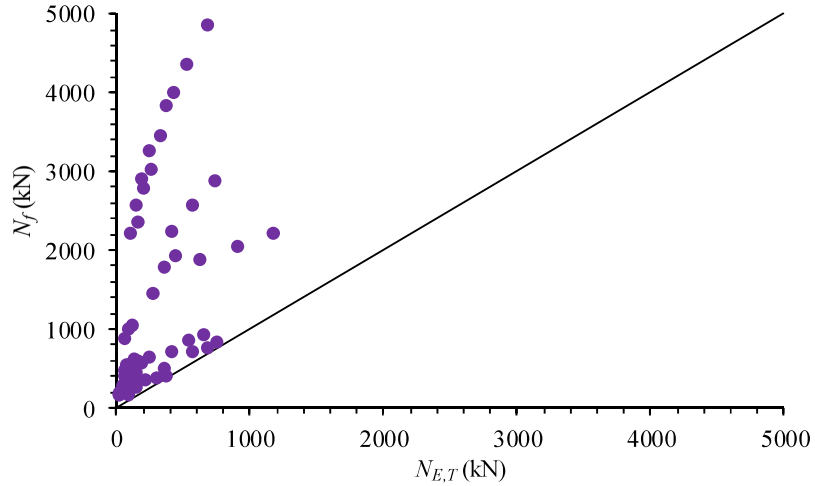

(b) N_f vs $N_{E,T}$

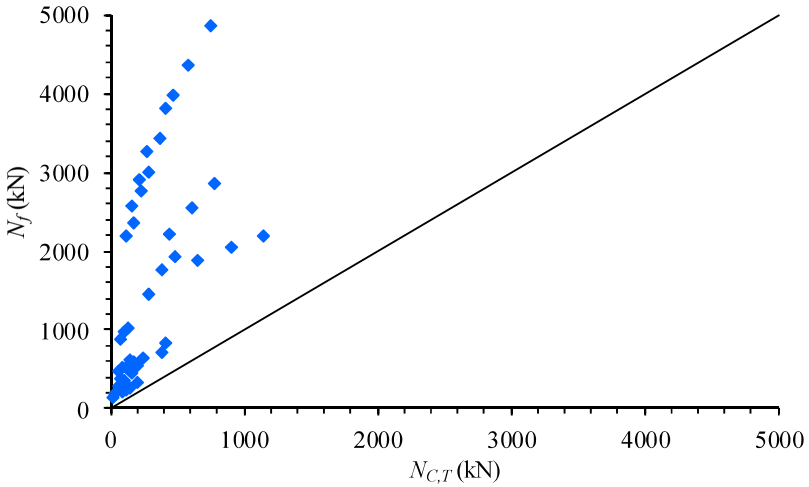

(d) N_f vs $N_{C,T}$

Fig. 36. Variations of test and FE T-joint strengths with nominal strengths for RHS-RHS T-joints failed in chord side wall failure mode

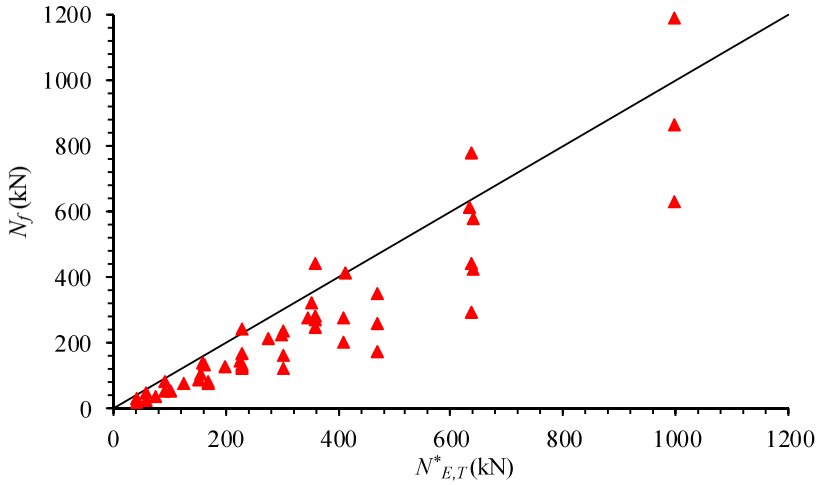

(a) N_f vs $N^*_{E,T}$

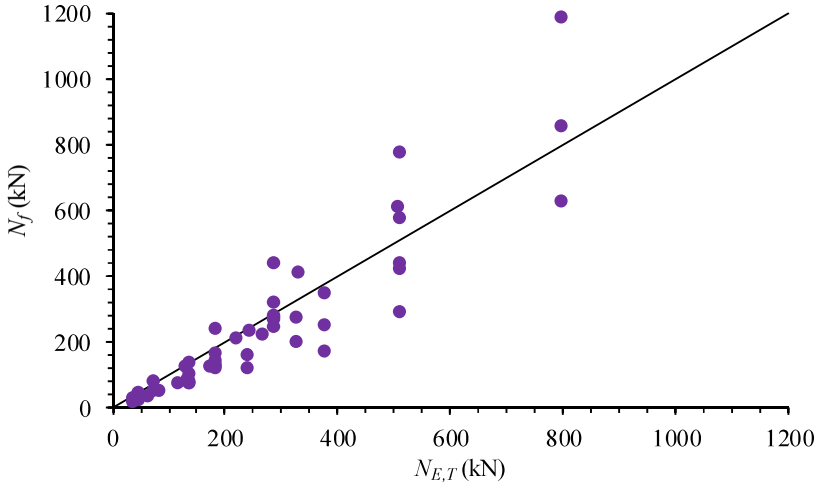

(b) N_f vs $N_{E,T}$

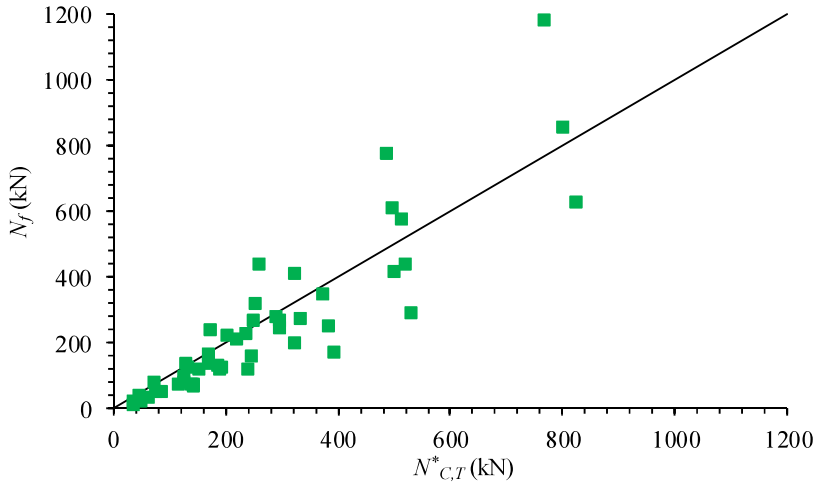

(c) N_f vs $N^*_{C,T}$

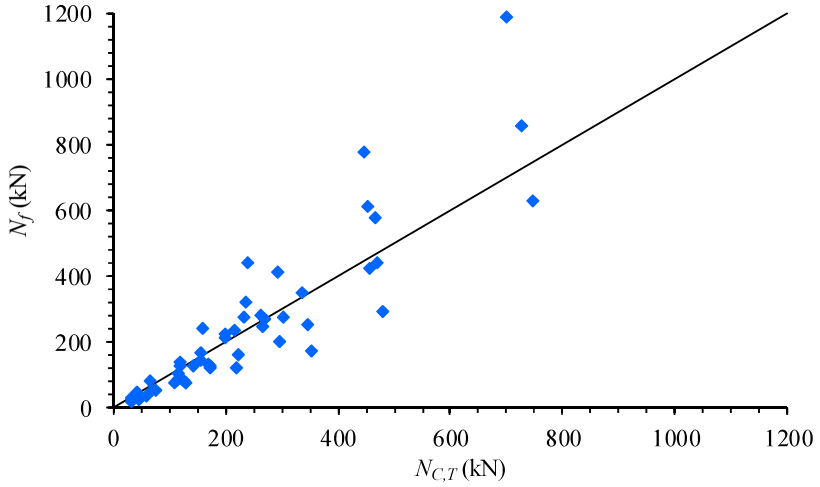

(d) N_f vs $N_{C,T}$

Fig. 37. Variations of test and FE T-joint strengths with nominal strengths for CHS-RHS T-joints failed in chord face failure mode

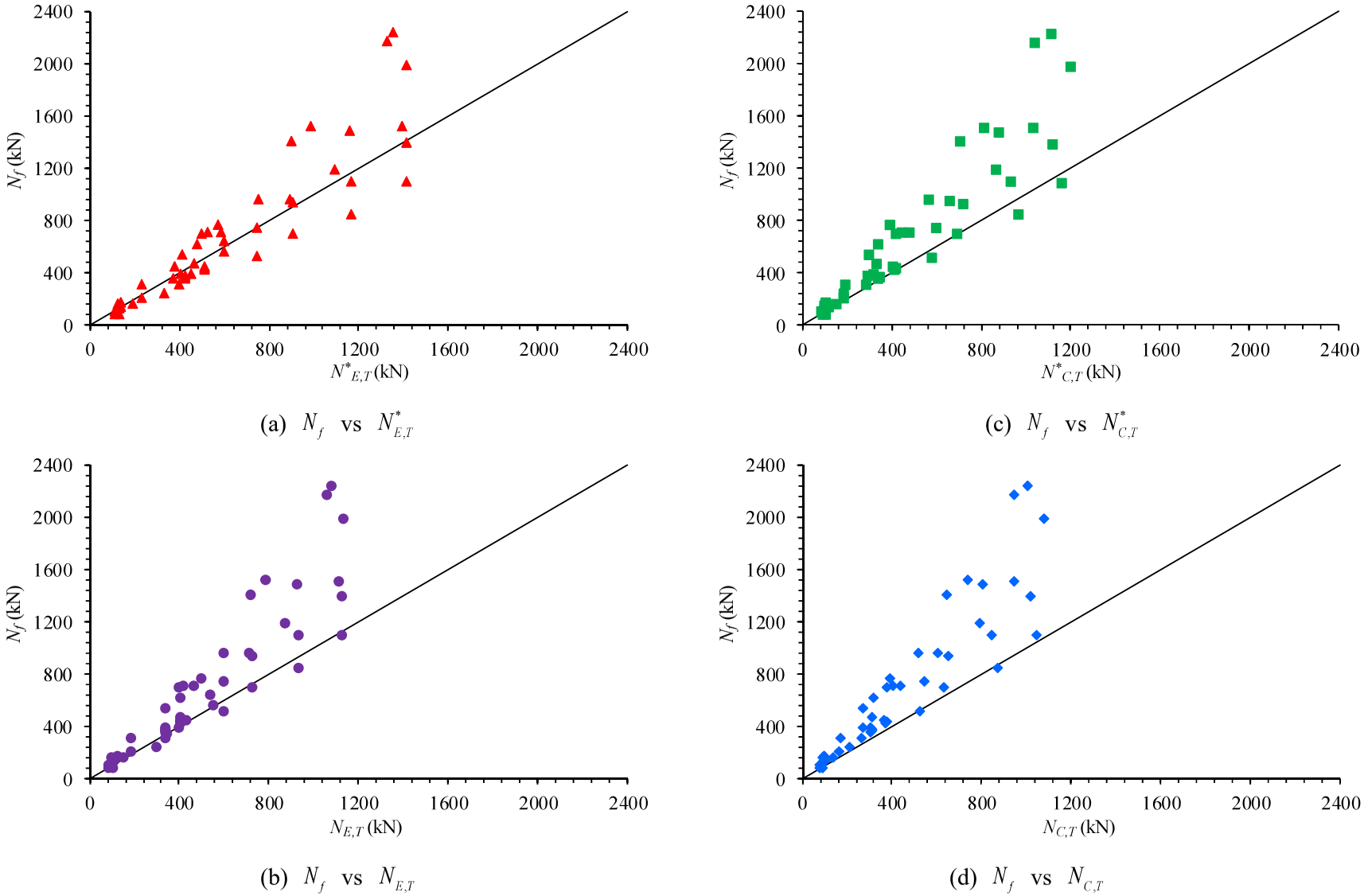

(a) N_f vs $N^*_{E,T}$

(c) N_f vs $N^*_{C,T}$

(b) N_f vs $N_{E,T}$

(d) N_f vs $N_{C,T}$

Fig. 38. Variations of test and FE T-joint strengths with nominal strengths for CHS-RHS T-joints failed in combined failure mode

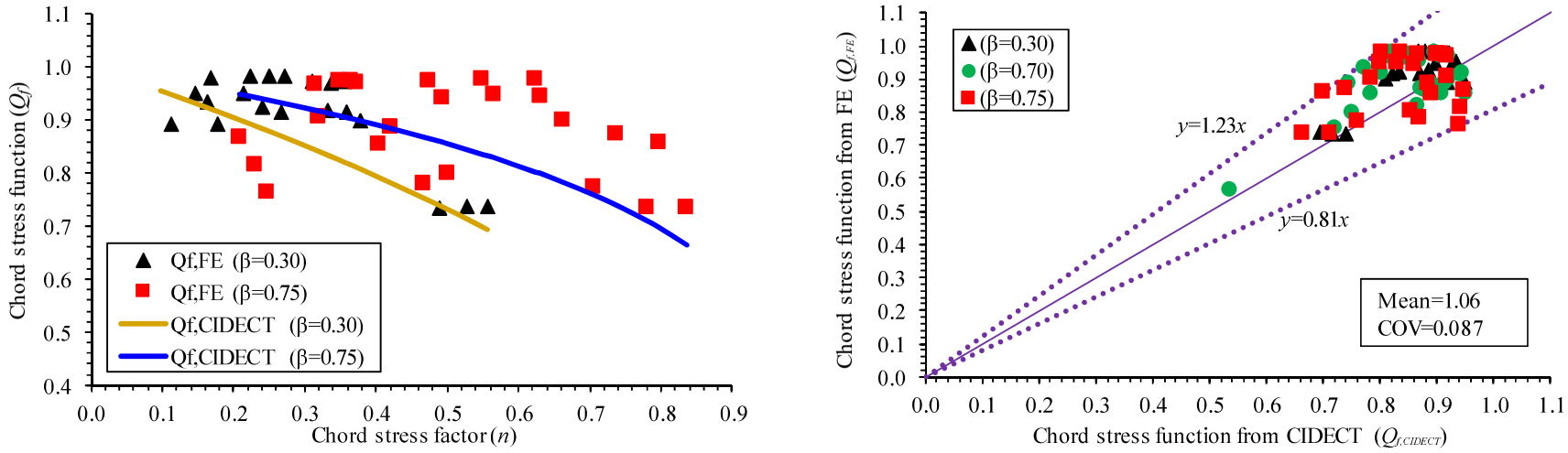

(a) Q_f vs n (b) $Q_{f,FE}$ vs $Q_{f,CIDECT}$

Fig. 39. Comparisons between $Q_{f,FE}$ and $Q_{f,CIDECT}$ for RHS-RHS T-joints failed in chord face failure mode

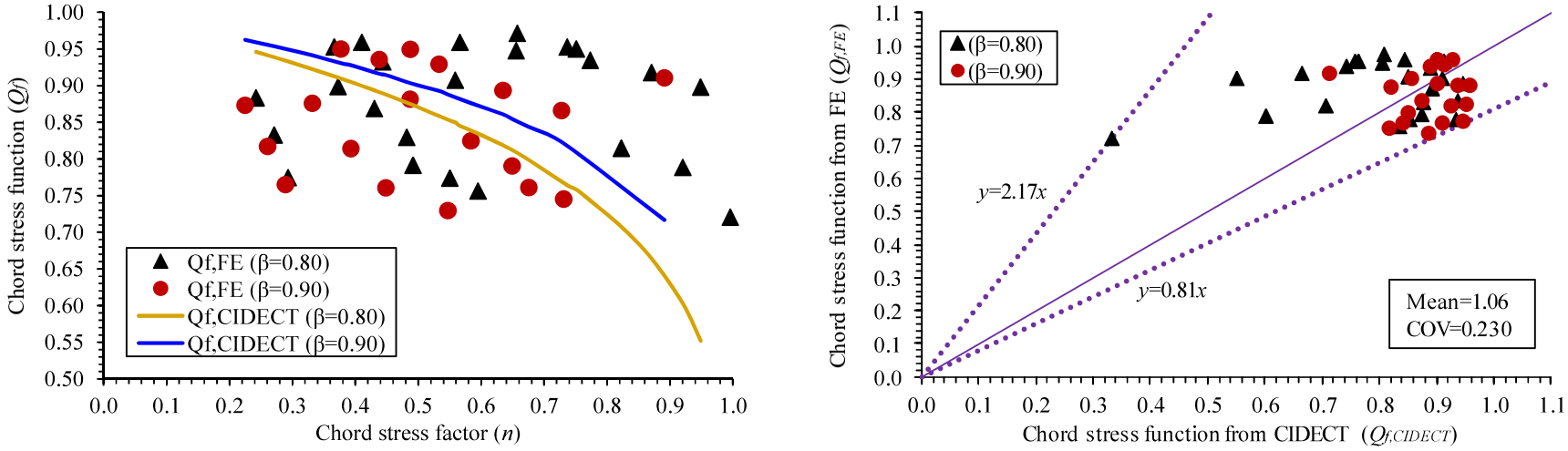

(a) Q_f vs n (b) $Q_{f,FE}$ vs $Q_{f,CIDECT}$

Fig. 40. Comparisons between $Q_{f,FE}$ and $Q_{f,CIDECT}$ for RHS-RHS T-joints failed in combined failure mode

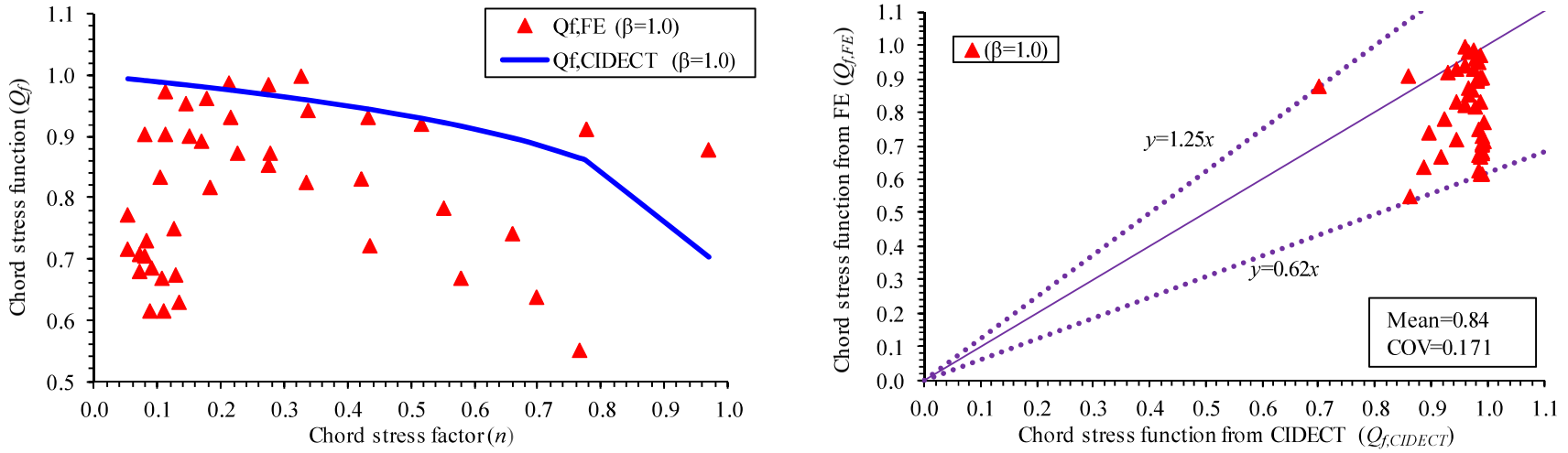

(a) Q_f vs n (b) $Q_{f,FE}$ vs $Q_{f,CIDECT}$

Fig. 41. Comparisons between $Q_{f,FE}$ and $Q_{f,CIDECT}$ for RHS-RHS T-joints failed in chord side wall failure mode

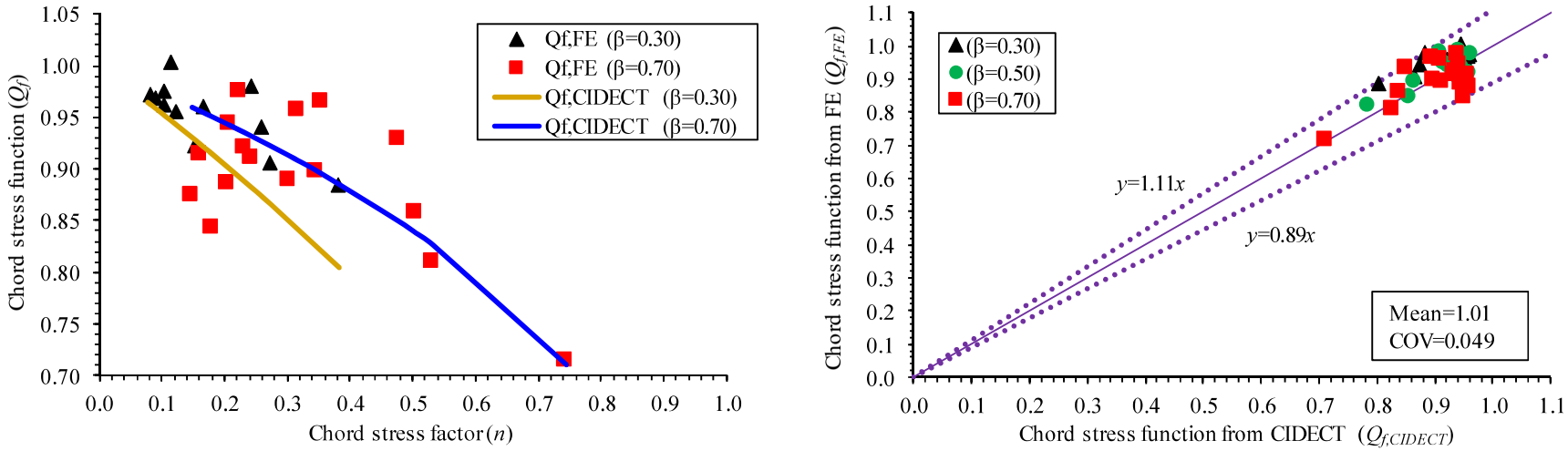

(a) Q_f vs n (b) $Q_{f,FE}$ vs $Q_{f,CIDECT}$

Fig. 42. Comparisons between $Q_{f,FE}$ and $Q_{f,CIDECT}$ for CHS-RHS T-joints failed in chord face failure mode

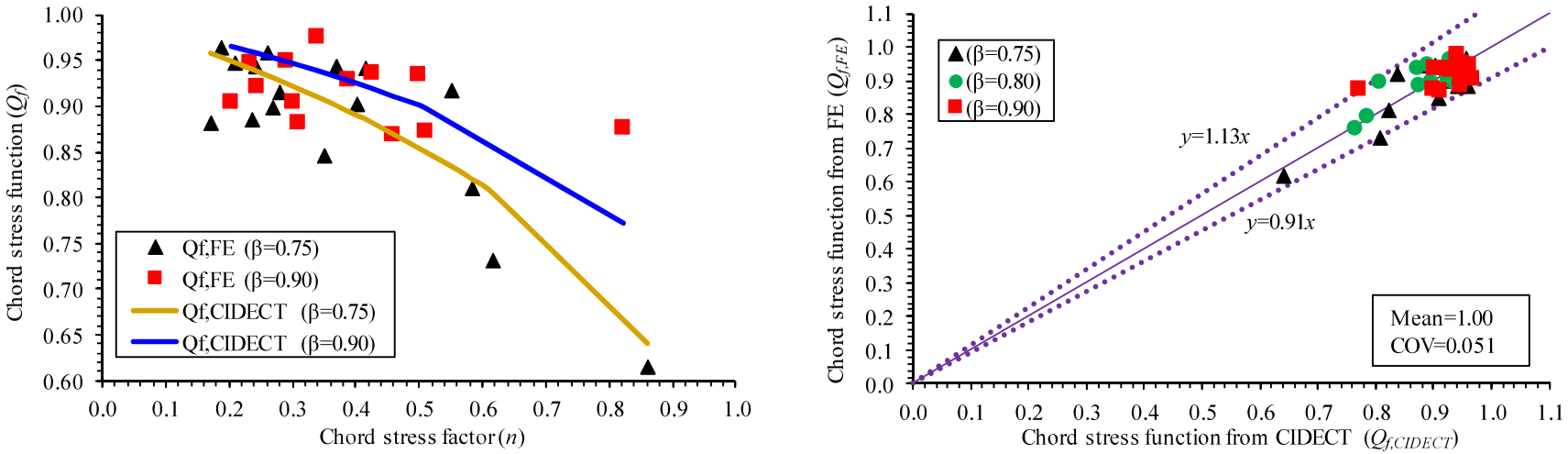

(a) Q_f vs n (b) $Q_{f,FE}$ vs $Q_{f,CIDECT}$

Fig. 43. Comparisons between $Q_{f,FE}$ and $Q_{f,CIDECT}$ for CHS-RHS T-joints failed in combined failure mode

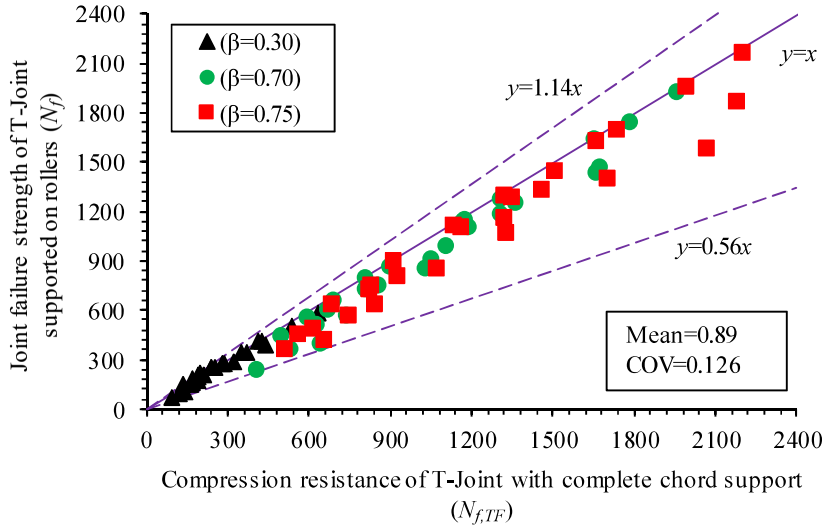

Fig. 44. Comparisons between N_f and $N_{f,TF}$ for RHS-RHS T-joints failed in chord face failure mode

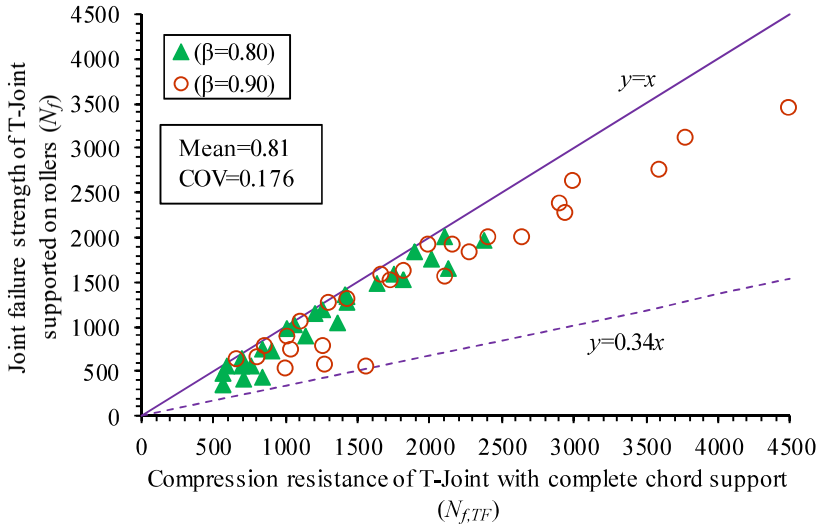

Fig. 45. Comparisons between N_f and $N_{f,TF}$ for RHS-RHS T-joints failed in combined failure mode

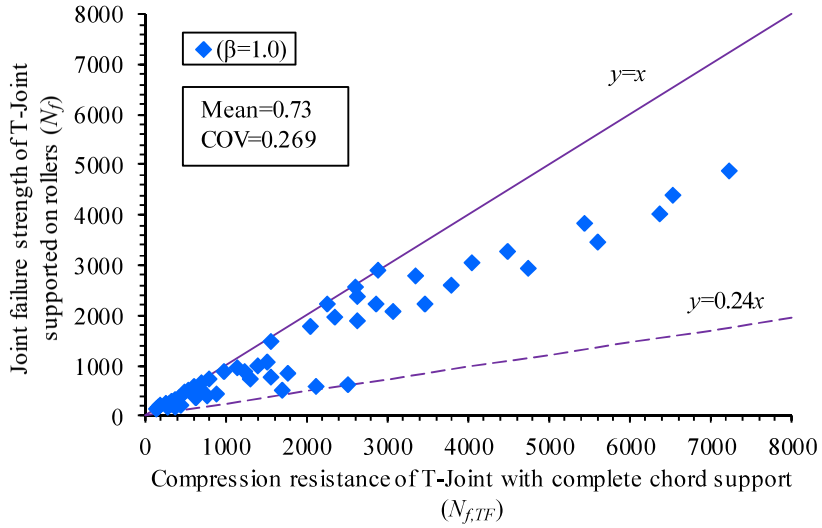

Fig. 46. Comparisons between N_f and $N_{f,TF}$ for RHS-RHS T-joints failed in chord side wall failure mode

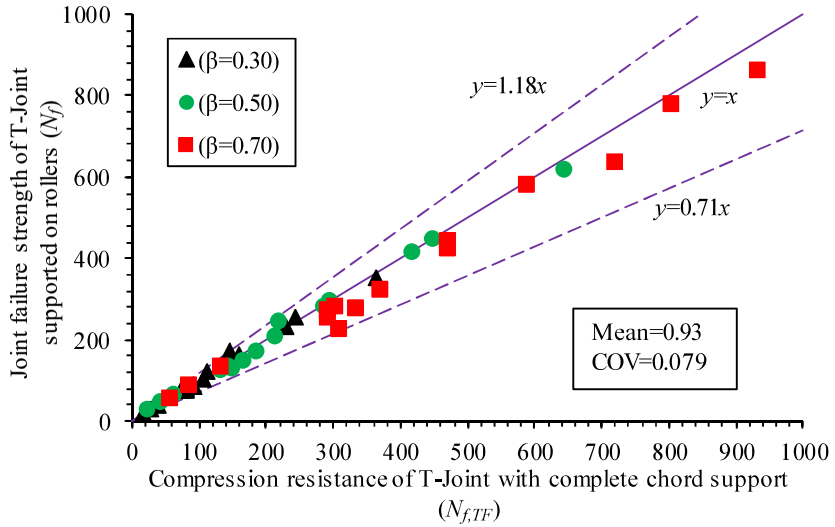

Fig. 47. Comparisons between N_f and $N_{f,TF}$ for CHS-RHS T-joints failed in chord face failure mode

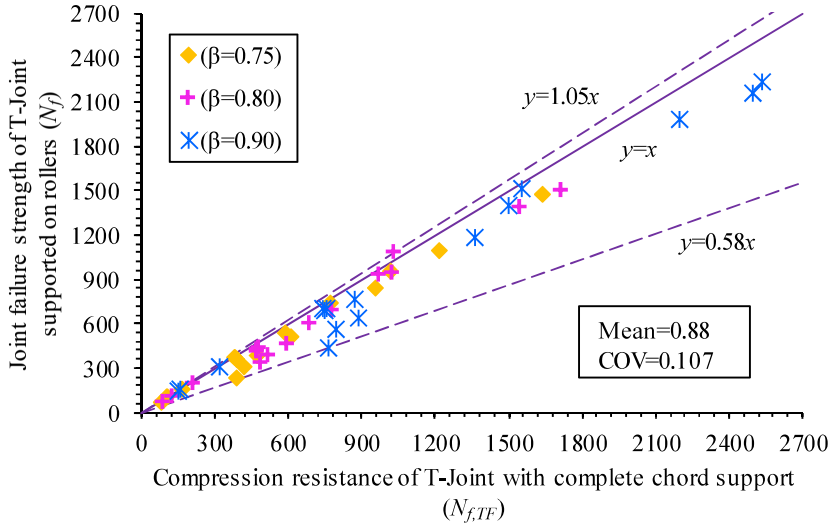

Fig. 48. Comparisons between N_f and $N_{f,TF}$ for CHS-RHS T-joints failed in combined failure mode

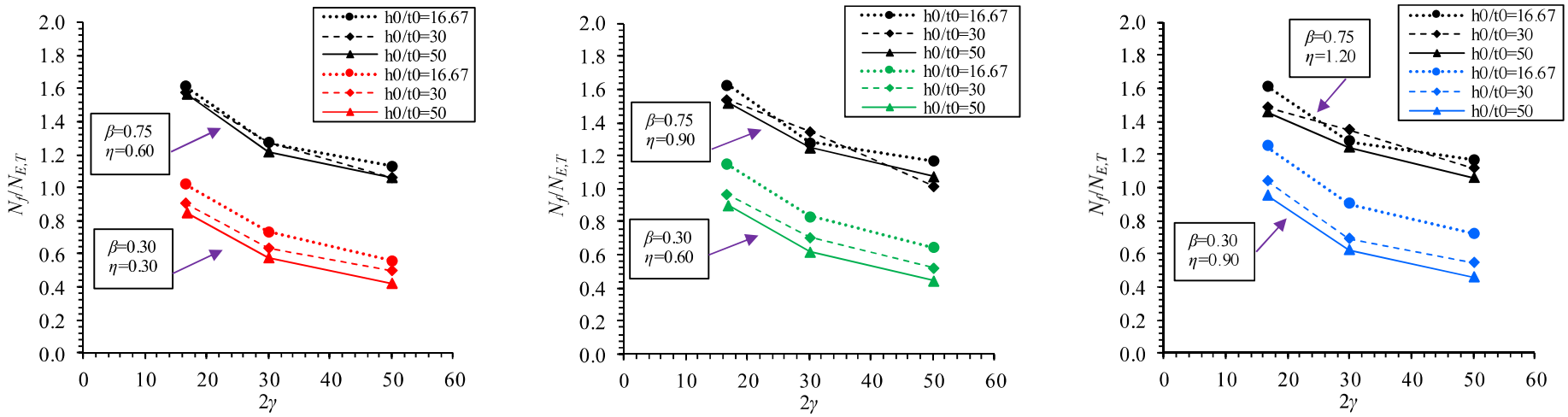

Fig. 49. Influence of governing parameters for the design proposal of RHS-RHS T-joints failed in chord face failure mode

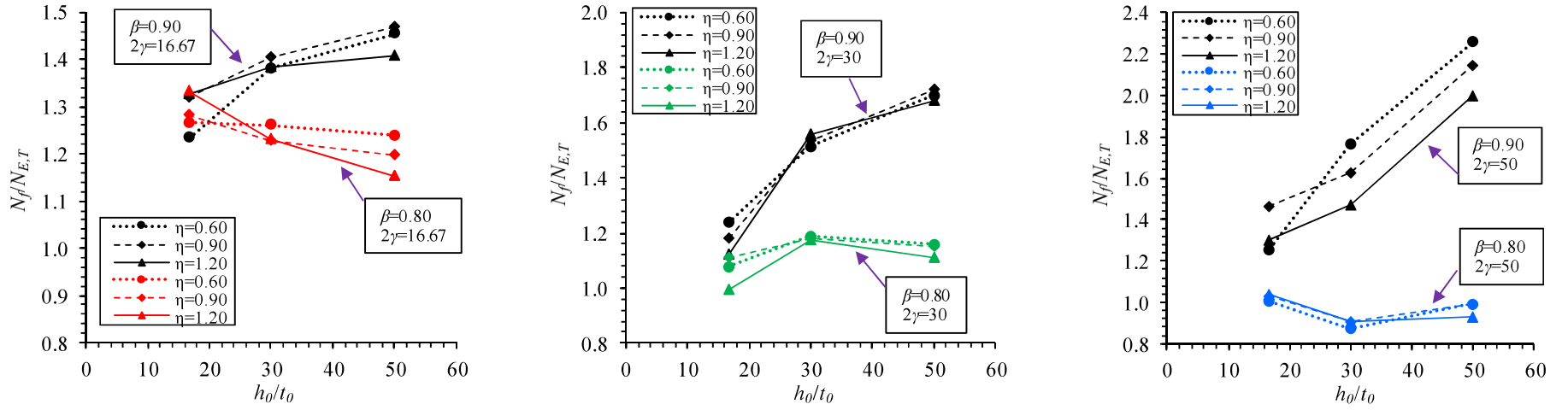

Fig. 50. Influence of governing parameters for the design proposal of RHS-RHS T-joints failed in combined failure mode

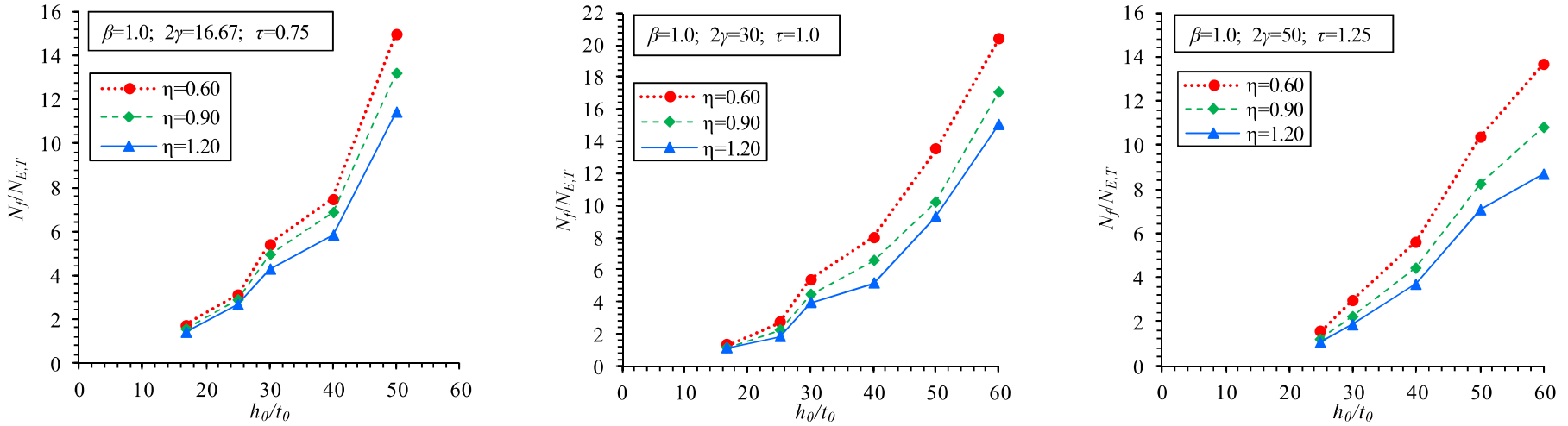

Fig. 51. Influence of governing parameters for the design proposal of RHS-RHS T-joints failed in chord side wall failure mode

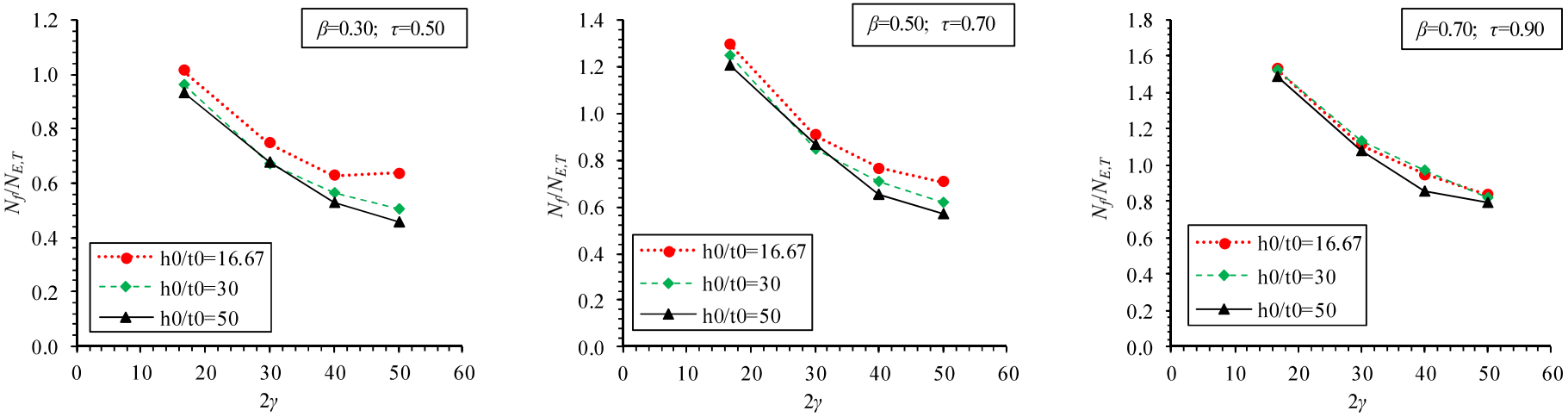

Fig. 52. Influence of governing parameters for the design proposal of CHS-RHS T-joints failed in chord face failure mode

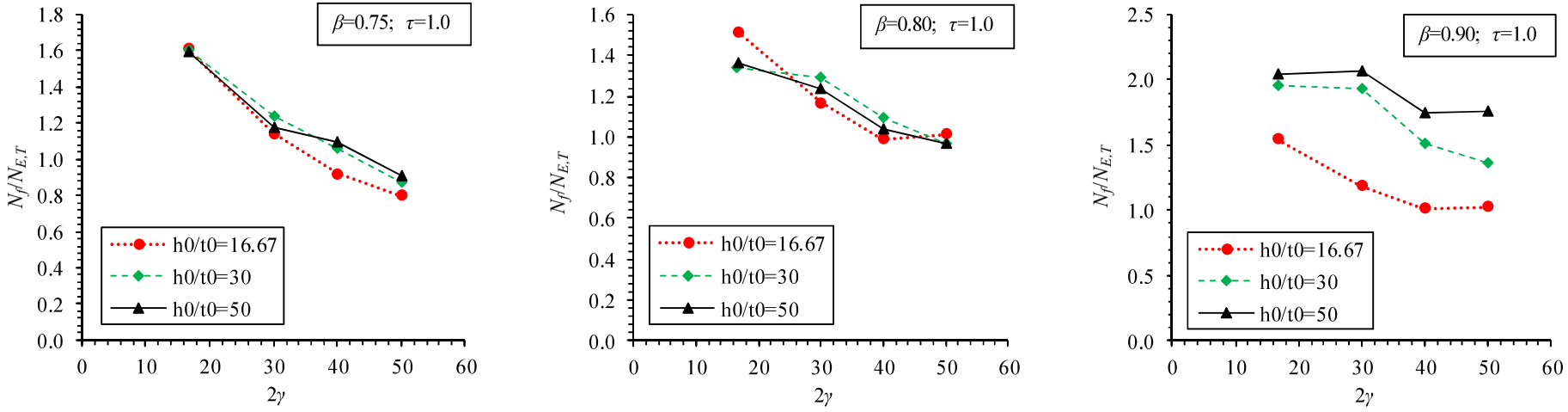

Fig. 53. Influence of governing parameters for the design proposal of CHS-RHS T-joints failed in combined failure mode

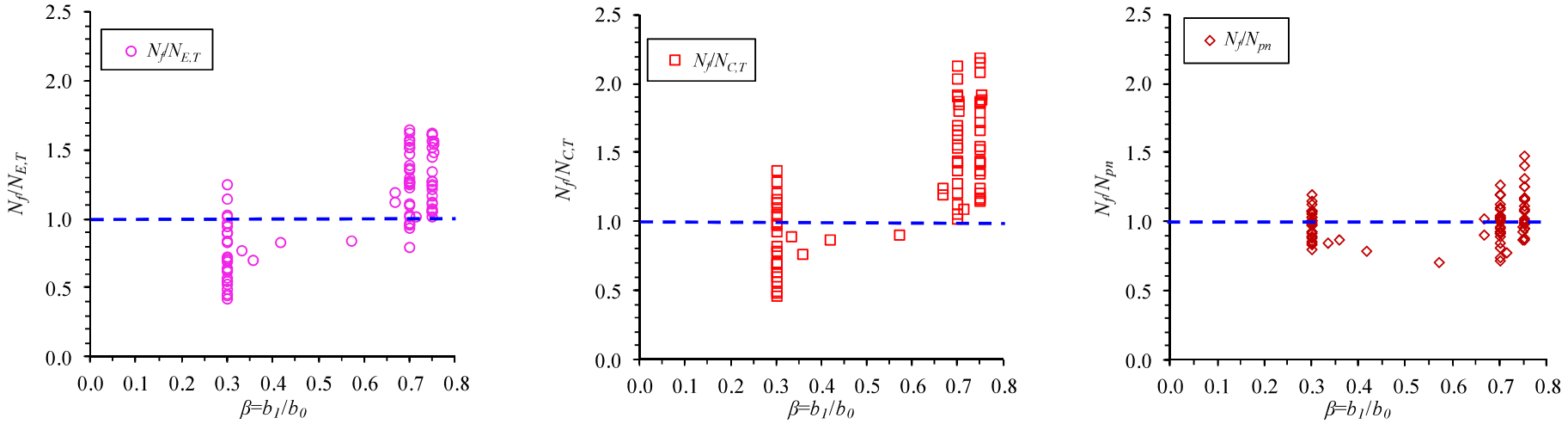

(a) For EC3 [2] (b) For CIDECT [3] (c) For proposed design rule

Fig. 54. Comparison of existing and proposed design rules for RHS-RHS T-joints failed in chord face failure mode

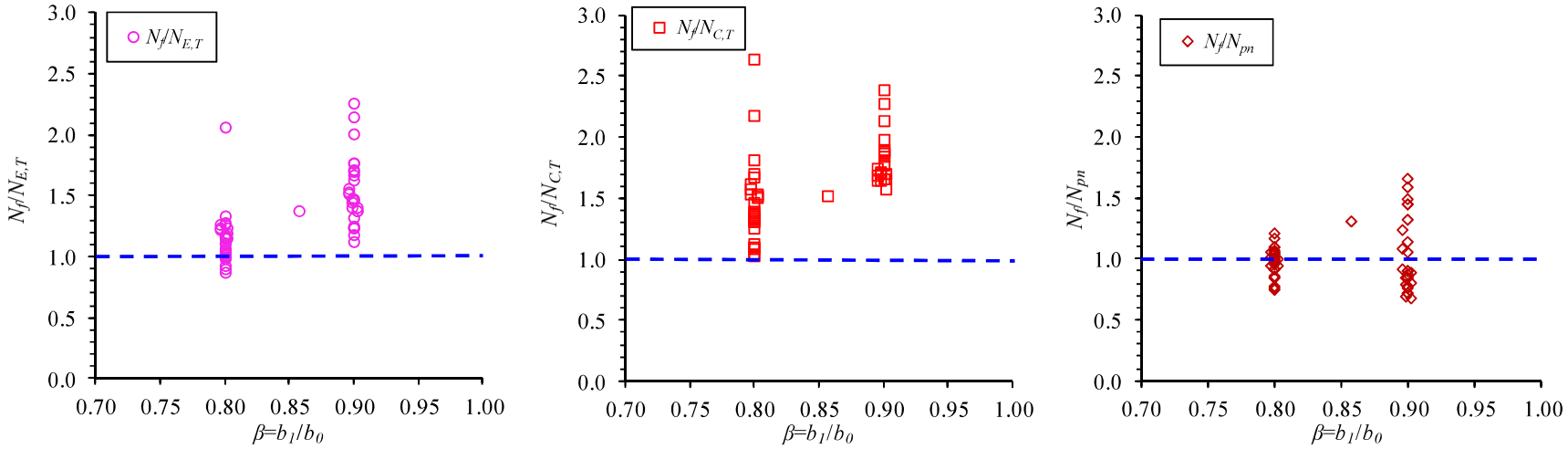

(a) For EC3 [2] (b) For CIDECT [3] (c) For proposed design rule

Fig. 55. Comparison of existing and proposed design rules for RHS-RHS T-joints failed in combined failure mode

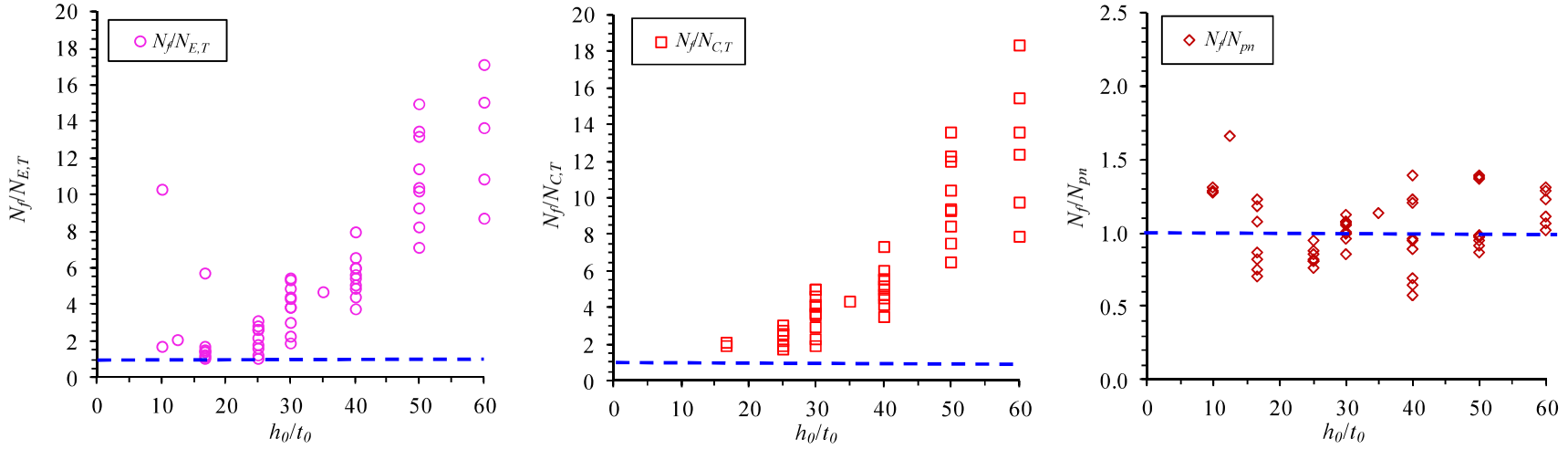

(a) For EC3 [2] (b) For CIDECT [3] (c) For proposed design rule

Fig. 56. Comparison of existing and proposed design rules for RHS-RHS T-joints failed in chord side wall failure mode

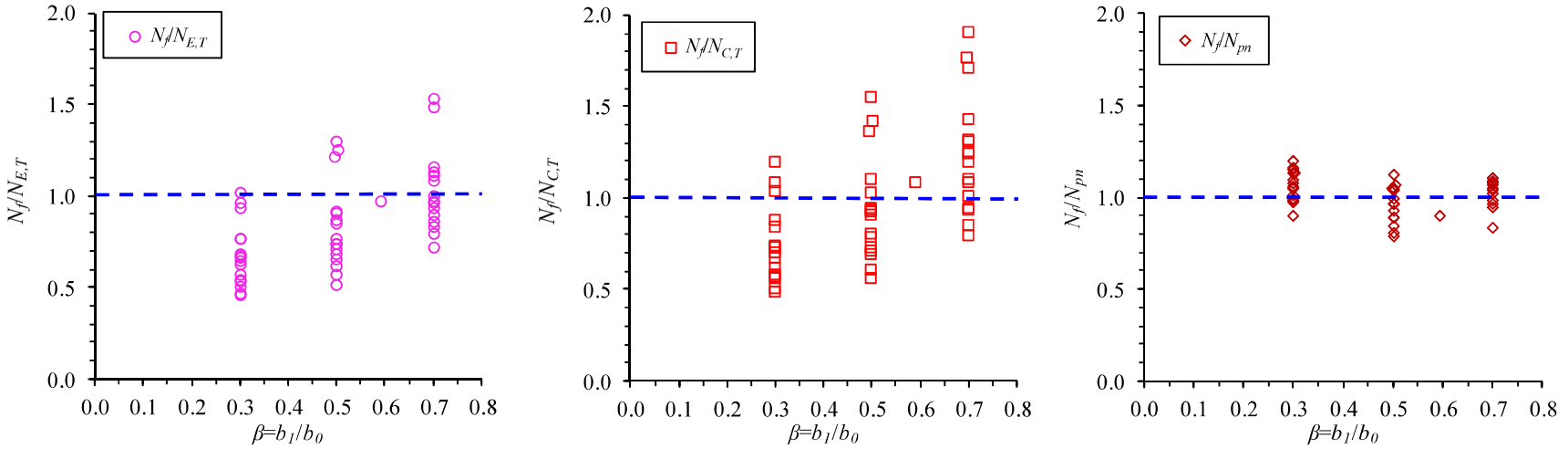

(a) For EC3 [2] (b) For CIDECT [3] (c) For proposed design rule

Fig. 57. Comparison of existing and proposed design rules for CHS-RHS T-joints failed in chord face failure mode

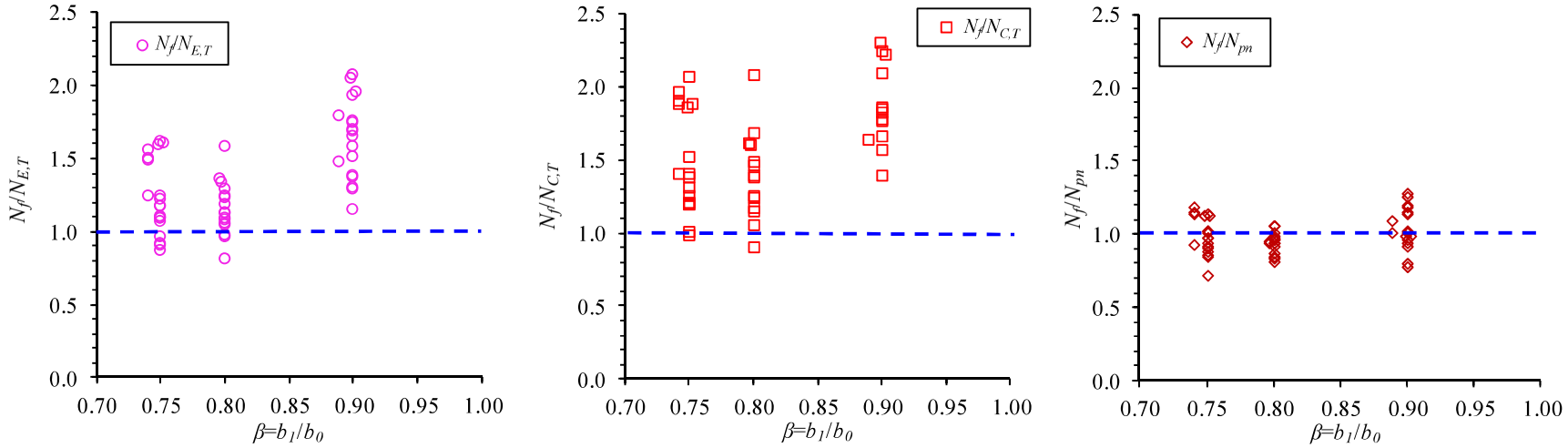

(a) For EC3 [2] (b) For CIDECT [3] (c) For proposed design rule

Fig. 58. Comparison of existing and proposed design rules for CHS-RHS T-joints failed in combined failure mode

Specimens T-b_1×h_1×t_1-b_0×h_0×t_0 or T-d_1×t_1-b_0×h_0×t_0	β	Test Strengths (kN) (a)	Numerical Strengths (kN) No Weld + No WHAR (b)	Weld + No WHAR (c)	Weld + WHAR (d)	Comparisons (b)/(a)	(c)/(a)	(d)/(a)
T-50×100×4-150×150×6	0.34	163.4	150.1	182.3	163.1	0.92	1.12	1.00
T-120×120×4-150×150×6	0.81	606.7	548.2	775.1	601.2	0.90	1.28	0.99
T-100×50×4-100×50×4	1.00	334.5	228.5	374.2	333.0	0.68	1.12	1.00
T-88.9×4-150×150×6	0.59	212.5	200.1	237.5	207.2	0.94	1.12	0.98
T-88.9×4-100×100×4	0.88	286.5	253.3	384.6	290.4	0.88	1.34	1.01

Table 1. Effect of weld and WHAR on typical RHS-RHS and CHS-RHS T-joint strengths

Specimens T-b_1×h_1×t_1-b_0×h_0×t_0 or T-d_1×t_1-b_0×h_0×t_0	Nominal Chord Widths (mm) b_0	Measured Maximum Chord Widths (mm) $b_{0,max}$	Maximum Convex Bulges (%) ($b_{0,max}$ - b_0)/b_0
T-50×100×4-150×150×6	150	154.80	3.20
T-50×100×4-140×140×4	140	144.70	3.36
T-50×100×4-120×120×4	120	124.80	4.00
T-80×80×4-140×140×4	140	144.90	3.50
T-80×80×4-120×120×4	120	124.45	3.71
T-80×80×4-120×120×3	120	124.10	3.42
T-100×50×4-140×140×4	140	144.30	3.07
T-80×80×4-100×50×4	100	102.21	2.21
T-120×120×4-150×150×6	150	153.84	2.56
T-120×120×4-150×150×6-R	150	154.33	2.89
T-120×120×3-150×150×6	150	154.15	2.77
T-120×120×4-140×140×4	140	144.23	3.02
T-100×50×4-100×50×4	100	102.98	2.98
T-120×120×4-120×120×4	120	123.02	2.52
T-140×140×4-140×140×4	140	143.07	2.19
T-120×120×3-120×120×3	120	123.10	2.58
T-88.9×4-150×150×6	150	154.15	2.77
T-88.9×3-120×60×4	120	123.26	2.72
T-88.9×3-120×60×4-R	120	122.91	2.43
T-88.9×4-120×60×4	120	122.87	2.39
T-88.9×4-120×60×4-R	120	122.93	2.44
T-88.9×4-120×120×6	120	123.67	3.06
T-88.9×4-100×60×4	100	102.74	2.74
T-88.9×4-100×100×4	100	103.15	3.15
		Average	2.90

Table 2. Measured maximum convex bulges in the chord members

Specimens	Geometric Ratios				Failure Mode(s)	Test Strengths (kN)	Numerical Strengths (kN)	Comparisons
T-b_1×h_1×t_1-b_0×h_0×t_0	β	τ	2γ	h_0/t_0		N_f	N_{FE}	$\frac{N_f}{N_{FE}}$
T-50×100×4-150×150×6	0.34	0.67	25.25	25.45	F	163.4	163.1	1.00
T-50×100×4-140×140×4	0.36	0.99	35.00	35.23	F	65.7	64.1	1.02
T-50×100×4-120×120×4	0.41	1.01	31.12	31.08	F	83.8	81.5	1.03
T-80×80×4-140×140×4	0.57	0.98	34.77	35.06	F	95.4	97.0	0.98
T-80×80×4-120×120×4	0.66	1.00	31.01	30.97	F	162.6	163.2	1.00
T-80×80×4-120×120×3	0.67	1.27	38.55	38.67	F	91.8	94.8	0.97
T-100×50×4-140×140×4	0.72	0.98	34.62	34.86	F	130.6	131.2	1.00
T-80×80×4-100×50×4	0.80	0.99	25.23	12.69	F+S	286.9	283.1	1.01
T-120×120×4-150×150×6	0.81	0.66	25.29	25.48	F+S	606.7	601.2	1.01
T-120×120×4-150×150×6-R	0.81	0.66	25.24	25.44	F+S	599.9	601.6	1.00
T-120×120×3-150×150×6	0.80	0.52	25.38	25.61	F+S	545.1	547.8	1.00
T-120×120×4-140×140×4	0.86	0.98	35.16	35.37	F+S	375.5	377.9	0.99
T-100×50×4-100×50×4	1.00	1.00	25.25	12.71	S	334.5	333.0	1.00
T-120×120×4-120×120×4	1.00	1.00	30.89	30.83	S	606.8	599.5	1.01
T-140×140×4-140×140×4	1.00	1.00	34.95	35.30	S	626.6	624.7	1.00
T-120×120×3-120×120×3	1.00	1.00	38.52	38.80	S	402.8	403.1	1.00
							Mean	1.00
							COV	0.014

Table 3. Comparison between test and FE strengths for RHS-RHS T-joints

Specimens	Geometric Ratios				Failure Mode(s)	Test Strengths (kN)	Numerical Strengths (kN)	Comparisons
T-d_1×t_1-b_0×h_0×t_0	β	τ	2γ	h_0/t_0		N_f	N_{FE}	$\frac{N_f}{N_{FE}}$
T-88.9×4-150×150×6	0.59	0.66	25.28	25.48	F	212.47	212.90	0.99
T-88.9×3-120×60×4	0.74	0.75	30.25	15.47	F+S	170.49	165.07	1.03
T-88.9×3-120×60×4-R	0.74	0.75	30.33	15.47	F+S	176.43	170.50	1.03
T-88.9×4-120×60×4	0.74	1.00	30.30	15.48	F+S	176.90	176.10	1.00
T-88.9×4-120×60×4-R	0.74	1.00	30.37	15.49	F+S	169.37	163.90	1.03
T-88.9×4-120×120×6	0.73	0.66	20.63	20.58	F+S	362.14	354.10	1.02
T-88.9×4-100×60×4	0.89	0.99	25.26	15.23	F+S	291.02	285.79	1.02
T-88.9×4-100×100×4	0.88	0.99	25.42	25.40	F+S	286.53	290.40	0.99
							Mean	1.02
							COV	0.018

Table 4. Comparison between test and FE strengths for CHS-RHS T-joints

Parameters	β					
	0.3	0.7	0.75	0.8	0.9	1
2γ (= b_1/t_0)	16.67, 30, 50	16.67, 30, 50	16.67, 30, 50	16.67, 30, 50	16.67, 30, 50	16.67, 30, 50
h_0/t_0	16.67, 30, 50	16.67, 30, 50	16.67, 30, 50	16.67, 30, 50	16.67, 30, 50	10, 16.67, 25, 30, 40, 50, 60
η (= h_1/b_0)	0.3, 0.6, 0.9	0.6, 0.9, 1.2	0.6, 0.9, 1.2	0.6, 0.9, 1.2	0.6, 0.9, 1.2	0.6, 0.9, 1.2
τ (= t_1/t_0)	0.75	1	1	0.75	1	0.75, 1, 1.25

Table 5. Parametric study planning for RHS-RHS T-joints

Parameters	β					
	0.3	0.5	0.7	0.75	0.8	0.9
2γ (= b_1/t_0)	16.67, 30, 40, 50	16.67, 30, 40, 50	16.67, 30, 40, 50	16.67, 30, 40, 50	16.67, 30, 40, 50	16.67, 30, 40, 50
h_0/t_0	16.67, 30, 40, 50	16.67, 30, 40, 50	16.67, 30, 40, 50	16.67, 30, 40, 50	16.67, 30, 40, 50	16.67, 30, 40, 50
τ (= t_1/t_0)	0.5, 0.75, 1	0.7, 1	0.9, 1	1	1	1

Table 6. Parametric study planning for CHS-RHS T-joints

Load Distributions in Chords	T-50x100x4-150x150x6 (β=0.34; 2γ=25.3)		T-120x120x4-140x140x4 (β=0.86; 2γ=35.2)		T-100x50x4-100x50x4 (β=1; h_0/t_0=12.7)		T-120x120x3-120x120x3 (β=1; h_0/t_0=38.8)	
(Vertical : Horizontal)	L_0/b_0	Strengths (kN)	L_0/b_0	Strengths (kN)	L_0/b_0	Strengths (kN)	L_0/b_0	Strengths (kN)
1:0.5	2.88	163.0	3.15	396.5	2.80	420.0	3.51	494.5
1:1	3.88	168.0	4.16	406.0	3.30	385.3	4.52	432.3
1:1.5	4.89	166.5	5.16	378.4	3.80	333.0	5.52	403.1
1:2	5.90	167.0	6.17	367.5	4.31	282.3	6.53	350.6
1:3	7.92	164.0	8.18	326.8	5.31	212.7	8.55	255.5
1:4	9.93	162.0	10.19	254.7	6.32	164.7	10.56	194.3
1:5	11.95	157.0	12.20	236.6	7.32	137.2	12.57	158.6

Table 7. Variation of typical RHS-RHS T-joint strengths with L_0/b_0 ratios

References	Chord Types	Brace Loadings	Boundary Conditions	L_e / max[b_0, h_0]	
				Minimum	Maximum
Kato and Nishiyama [38]	SHS and RHS	Compression	Simply Supported	2.28	3.33
Wardenier and Stark [39]	SHS	Compression	Simply Supported	3.00	3.00
Redwood [40]	SHS	Compression	Simply Supported	3.00	9.60
Korol and Mirza [41]	SHS	Compression	Simply Supported	7.20	7.20
Yu [42]	SHS	Compression	Simply Supported	3.00	20.00
Lu et al. [43]	SHS	Compression	Simply Supported	6.00	6.00
Wardenier [44]	SHS	Compression	Fully Supported	4.13	5.00
Yu and Wardenier [27]	SHS	Compression	Simply Supported	6.00	6.00
Wardenier and Koning [45]	SHS	Tension	Simply Supported	3.00	3.00
Crockett [16]	SHS	Compression	Simply Supported	3.00	8.33
Davies et al. [46]	SHS	Compression	Simply Supported	5.67	5.67
Zhao and Hancock [47]	SHS and RHS	Compression	Simply Supported	1.12	21.18
Pandey and Young [1]	SHS and RHS	Compression	Simply Supported	2.90	4.75
Bae et al. [48]	SHS	Compression	Fixed	3.00	3.00
Aguilera et al. [49]	SHS and RHS	Compression	Fixed	6.00	6.00
Sharaf and Fam [50]	SHS and RHS	Compression	Fixed	4.93	10.84
Chang et al. [51]	SHS	Compression	Fixed	6.50	6.50
			Average	4.16	7.61

Note: SHS denotes square hollow section; RHS denotes rectangular hollow section.

Table 8. Summary of chord span ratio from existing literature

Specimens	Geometric Ratios					Joint Failure Strengths (kN)	Comparisons					
T-b_1×h_1×t_1-b_0×h_0×t_0	β	2γ	h_0/t_0	τ	η	N_f	$\frac{N_f}{N^*_{E,T}}$	$\frac{N_f}{N_{E,T}}$	$\frac{N_f}{N^*_{C,T}}$	$\frac{N_f}{N_{C,T}}$	$\frac{N_f}{N_{pn}}$	$\frac{N_f}{N_{spn}}$
T-30×30×4.5-100×100×6	0.30	16.67	16.67	0.75	0.30	163.1	0.90	1.02	1.06	1.15	1.14	0.96
T-30×60×4.5-100×100×6	0.30	16.67	16.67	0.75	0.60	205.5	1.03	1.15	1.18	1.28	1.06	1.08
T-30×90×4.5-100×100×6	0.30	16.67	16.67	0.75	0.90	245.3	1.13	1.25	1.27	1.37	1.00	1.17
T-54×54×4.5-180×100×6	0.30	30.00	16.67	0.75	0.30	114.3	0.66	0.73	0.76	0.82	1.12	1.00
T-54×108×4.5-180×100×6	0.30	30.00	16.67	0.75	0.60	145.4	0.76	0.84	0.85	0.92	1.05	1.14
T-54×162×4.5-180×100×6	0.30	30.00	16.67	0.75	0.90	172.1	0.83	0.90	0.91	0.98	0.98	1.22
T-90×90×4.5-300×100×6	0.30	50.00	16.67	0.75	0.30	69.2	0.56	0.56	0.53	0.56	0.97	1.11
T-90×180×4.5-300×100×6	0.30	50.00	16.67	0.75	0.60	86.3	0.67	0.64	0.60	0.63	0.89	1.28
T-90×270×4.5-300×100×6	0.30	50.00	16.67	0.75	0.90	103.5	0.77	0.72	0.66	0.68	0.84	1.43
T-70×60×6-100×100×6	0.70	16.67	16.67	1.00	0.60	546.1	1.36	1.58	1.90	2.03	0.84	0.95
T-70×90×6-100×100×6	0.70	16.67	16.67	1.00	0.90	648.5	1.44	1.64	2.03	2.13	0.92	0.99
T-70×120×6-100×100×6	0.70	16.67	16.67	1.00	1.20	718.4	1.43	1.62	2.05	2.12	0.95	0.97
T-126×108×6-180×100×6	0.70	30.00	16.67	1.00	0.60	427.2	1.10	1.26	1.54	1.62	0.92	1.09
T-126×162×6-180×100×6	0.70	30.00	16.67	1.00	0.90	502.3	1.14	1.30	1.63	1.69	1.00	1.12
T-126×216×6-180×100×6	0.70	30.00	16.67	1.00	1.20	555.5	1.14	1.28	1.66	1.69	1.03	1.11
T-210×180×6-300×100×6	0.70	50.00	16.67	1.00	0.60	230.3	0.74	0.80	*	1.28	0.71	1.01
T-210×270×6-300×100×6	0.70	50.00	16.67	1.00	0.90	356.1	1.06	1.11	*	*	1.01	1.41
T-210×360×6-300×100×6	0.70	50.00	16.67	1.00	1.20	390.3	1.08	1.11	*	*	1.03	1.40
T-75×60×6-100×100×6	0.75	16.67	16.67	1.00	0.60	619.8	1.40	1.61	1.98	2.08	0.87	0.92
T-75×90×6-100×100×6	0.75	16.67	16.67	1.00	0.90	717.5	1.43	1.63	2.10	2.15	0.94	0.93
T-75×120×6-100×100×6	0.75	16.67	16.67	1.00	1.20	797.1	1.44	1.61	2.24	2.18	0.98	0.92
T-135×108×6-180×100×6	0.75	30.00	16.67	1.00	0.60	479.2	1.11	1.27	1.60	1.66	0.95	1.05
T-135×162×6-180×100×6	0.75	30.00	16.67	1.00	0.90	552.3	1.14	1.28	1.73	1.72	1.02	1.06
T-135×216×6-180×100×6	0.75	30.00	16.67	1.00	1.20	620.2	1.15	1.28	1.94	1.78	1.07	1.06
T-225×180×6-300×100×6	0.75	50.00	16.67	1.00	0.60	356.2	1.07	1.13	*	*	1.00	1.37
T-225×270×6-300×100×6	0.75	50.00	16.67	1.00	0.90	410.2	1.14	1.17	*	*	1.08	1.42
T-225×360×6-300×100×6	0.75	50.00	16.67	1.00	1.20	448.5	1.17	1.17	*	*	1.10	1.41
T-40×40×6-133×240×8	0.30	16.63	30.00	0.75	0.30	276.2	0.74	0.90	0.95	1.04	1.08	0.83
T-40×80×6-133×240×8	0.30	16.63	30.00	0.75	0.60	343.1	0.83	0.97	1.04	1.14	0.99	0.89
T-40×120×6-133×240×8	0.30	16.63	30.00	0.75	0.90	404.2	0.90	1.03	1.10	1.20	0.92	0.95
T-72×72×6-240×240×8	0.30	30.00	30.00	0.75	0.30	194.5	0.51	0.64	0.64	0.70	1.07	0.85
T-72×144×6-240×240×8	0.30	30.00	30.00	0.75	0.60	247.6	0.56	0.70	0.71	0.78	1.00	0.94
T-72×216×6-240×240×8	0.30	30.00	30.00	0.75	0.90	274.5	0.55	0.69	0.70	0.77	0.88	0.92
T-120×120×6-400×240×8	0.30	50.00	30.00	0.75	0.30	151.5	0.40	0.50	0.51	0.56	1.19	0.96
T-120×240×6-400×240×8	0.30	50.00	30.00	0.75	0.60	184.7	0.43	0.52	0.55	0.60	1.07	1.02
T-120×360×6-400×240×8	0.30	50.00	30.00	0.75	0.90	218.1	0.45	0.55	0.58	0.63	1.00	1.06
T-93×80×8-133×240×8	0.70	16.63	30.00	1.00	0.60	855.3	1.12	1.40	1.52	1.65	0.74	0.82
T-93×120×8-133×240×8	0.70	16.63	30.00	1.00	0.90	1131.6	1.27	1.57	1.77	1.91	0.90	0.92
T-93×160×8-133×240×8	0.70	16.63	30.00	1.00	1.20	1263.2	1.28	1.52	1.78	1.90	0.94	0.89
T-168×144×8-240×240×8	0.70	30.00	30.00	1.00	0.60	785.4	1.03	1.28	1.30	1.43	0.95	1.09
T-168×216×8-240×240×8	0.70	30.00	30.00	1.00	0.90	980.1	1.09	1.36	1.39	1.53	1.10	1.15
T-168×288×8-240×240×8	0.70	30.00	30.00	1.00	1.20	1140.2	1.10	1.37	1.42	1.56	1.19	1.16
T-280×240×8-400×240×8	0.70	50.00	30.00	1.00	0.60	592.5	0.77	0.97	1.02	1.12	1.02	1.20
T-280×360×8-400×240×8	0.70	50.00	30.00	1.00	0.90	742.7	0.82	1.03	1.11	1.21	1.19	1.27
T-280×480×8-400×240×8	0.70	50.00	30.00	1.00	1.20	844.9	0.81	1.02	1.11	1.21	1.26	1.26
T-100×80×8-133×240×8	0.75	16.63	30.00	1.00	0.60	1096.3	1.26	1.57	1.73	1.88	0.87	0.88
T-100×120×8-133×240×8	0.75	16.63	30.00	1.00	0.90	1280.4	1.28	1.54	1.78	1.91	0.94	0.86
T-100×160×8-133×240×8	0.75	16.63	30.00	1.00	1.20	1430.5	1.28	1.49	1.80	1.91	0.99	0.83
T-180×144×8-240×240×8	0.75	30.00	30.00	1.00	0.60	884.3	1.02	1.27	1.30	1.42	0.98	1.03
T-180×216×8-240×240×8	0.75	30.00	30.00	1.00	0.90	1109.5	1.08	1.35	1.39	1.52	1.15	1.09
T-180×288×8-240×240×8	0.75	30.00	30.00	1.00	1.20	1285.8	1.08	1.35	1.40	1.54	1.25	1.09
T-300×240×8-400×240×8	0.75	50.00	30.00	1.00	0.60	738.6	0.85	1.06	1.13	1.24	1.17	1.26
T-300×360×8-400×240×8	0.75	50.00	30.00	1.00	0.90	840.1	0.82	1.02	1.11	1.21	1.24	1.21

T-300×480×8-400×240×8	0.75	50.00	30.00	1.00	1.20	1063.4	0.89	1.11	1.24	1.34	1.47	1.32
T-50×50×7.5-167×500×10	0.30	16.70	50.00	0.75	0.30	403.5	0.69	0.85	0.88	0.97	1.02	0.76
T-50×100×7.5-167×500×10	0.30	16.70	50.00	0.75	0.60	495.4	0.77	0.90	0.96	1.05	0.92	0.81
T-50×150×7.5-167×500×10	0.30	16.70	50.00	0.75	0.90	579.6	0.82	0.95	1.01	1.10	0.85	0.86
T-90×90×7.5-300×500×10	0.30	30.00	50.00	0.75	0.30	272.8	0.46	0.57	0.57	0.63	0.96	0.74
T-90×180×7.5-300×500×10	0.30	30.00	50.00	0.75	0.60	343.4	0.50	0.62	0.63	0.69	0.89	0.81
T-90×270×7.5-300×500×10	0.30	30.00	50.00	0.75	0.90	389.1	0.50	0.62	0.64	0.70	0.80	0.81
T-150×150×7.5-500×500×10	0.30	50.00	50.00	0.75	0.30	203.2	0.34	0.43	0.41	0.46	1.02	0.81
T-150×300×7.5-500×500×10	0.30	50.00	50.00	0.75	0.60	245.4	0.36	0.45	0.44	0.48	0.91	0.85
T-150×450×7.5-500×500×10	0.30	50.00	50.00	0.75	0.90	283.8	0.36	0.46	0.45	0.49	0.83	0.87
T-117×100×10-167×500×10	0.70	16.70	50.00	1.00	0.60	1461.5	1.22	1.53	1.65	1.79	0.81	0.88
T-117×150×10-167×500×10	0.70	16.70	50.00	1.00	0.90	1735.8	1.24	1.54	1.73	1.86	0.89	0.88
T-117×200×10-167×500×10	0.70	16.70	50.00	1.00	1.20	1917.9	1.24	1.48	1.72	1.85	0.92	0.85
T-210×180×10-300×500×10	0.70	30.00	50.00	1.00	0.60	1173.5	0.98	1.23	1.24	1.37	0.91	1.02
T-210×270×10-300×500×10	0.70	30.00	50.00	1.00	0.90	1420.7	1.01	1.26	1.30	1.43	1.02	1.05
T-210×360×10-300×500×10	0.70	30.00	50.00	1.00	1.20	1625.9	1.00	1.25	1.31	1.44	1.09	1.04
T-350×300×10-500×500×10	0.70	50.00	50.00	1.00	0.60	897.8	0.75	0.94	0.92	1.01	0.99	1.14
T-350×450×10-500×500×10	0.70	50.00	50.00	1.00	0.90	1095.5	0.78	0.97	0.96	1.06	1.12	1.18
T-350×600×10-500×500×10	0.70	50.00	50.00	1.00	1.20	1245.2	0.77	0.96	0.95	1.05	1.19	1.16
T-125×100×10-167×500×10	0.75	16.70	50.00	1.00	0.60	1690.9	1.25	1.57	1.71	1.86	0.86	0.86
T-125×150×10-167×500×10	0.75	16.70	50.00	1.00	0.90	1947.8	1.25	1.52	1.74	1.87	0.93	0.84
T-125×200×10-167×500×10	0.75	16.70	50.00	1.00	1.20	2150.7	1.25	1.45	1.75	1.86	0.96	0.80
T-225×180×10-300×500×10	0.75	30.00	50.00	1.00	0.60	1320.9	0.97	1.22	1.24	1.36	0.94	0.97
T-225×270×10-300×500×10	0.75	30.00	50.00	1.00	0.90	1615.1	1.00	1.25	1.30	1.43	1.07	0.99
T-225×360×10-300×500×10	0.75	30.00	50.00	1.00	1.20	1855.6	1.00	1.24	1.32	1.44	1.15	0.99
T-375×300×10-500×500×10	0.75	50.00	50.00	1.00	0.60	1145.6	0.85	1.06	1.04	1.14	1.16	1.22
T-375×450×10-500×500×10	0.75	50.00	50.00	1.00	0.90	1384.7	0.86	1.08	1.06	1.17	1.31	1.25
T-375×600×10-500×500×10	0.75	50.00	50.00	1.00	1.20	1575.6	0.85	1.06	1.05	1.16	1.40	1.23
T-50×100×4-150×150×6	0.33	25.00	25.00	0.67	0.67	163.4	0.62	0.78	0.80	0.88	0.84	0.89
T-50×100×4-140×140×4	0.36	35.00	35.00	1.00	0.71	65.7	0.56	0.71	0.69	0.76	0.86	1.01
T-50×100×4-120×120×4	0.42	30.00	30.00	1.00	0.83	83.8	0.67	0.83	0.78	0.86	0.78	0.99
T-80×80×4-140×140×4	0.57	35.00	35.00	1.00	0.57	95.4	0.67	0.84	0.82	0.90	0.70	0.94
T-80×80×4-120×120×4	0.67	30.00	30.00	1.00	0.67	162.6	0.96	1.20	1.13	1.24	0.89	1.09
T-80×80×4-120×120×3	0.67	40.00	40.00	1.33	0.67	91.8	0.90	1.12	1.08	1.19	1.02	1.28
T-100×50×4-140×140×4	0.71	35.00	35.00	1.00	0.36	130.6	0.81	1.01	0.98	1.08	0.76	0.99
						Mean (P_m)	0.92	1.10	1.20	1.29	1.00	1.04
						COV (V_p)	0.309	0.304	0.385	0.364	0.145	0.167
						Resistance factor (ϕ)	0.80	0.80	0.80	0.80	0.80	0.80
						Reliability index (β_0)	1.54	1.98	1.97	2.21	2.51	2.54

Note: '$*$' denotes cases when k_n or $Q_f \approx 0$ or < 0.

Table 9. Comparison of test and numerical strengths with existing and proposed nominal strengths for RHS-RHS T-joints failed in chord face failure mode ($0.30 \leq \beta \leq 0.75$).

Specimens	Geometric Ratios					Joint Failure Strengths (kN)	Comparisons					
T-b_1×h_1×t_1-b_0×h_0×t_0	β	2γ	h_0/t_0	τ	η	N_f	$\frac{N_f}{N^*_{E,T}}$	$\frac{N_f}{N_{E,T}}$	$\frac{N_f}{N^*_{C,T}}$	$\frac{N_f}{N_{C,T}}$	$\frac{N_f}{N_{pn}}$	$\frac{N_f}{N_{spn}}$
T-80×60×4.5-100×100×6	0.80	16.67	16.67	0.75	0.60	551.5	1.11	1.27	1.66	1.67	0.92	1.07
T-80×90×4.5-100×100×6	0.80	16.67	16.67	0.75	0.90	640.2	1.15	1.28	2.15	1.81	0.98	1.08
T-80×120×4.5-100×100×6	0.80	16.67	16.67	0.75	1.20	747.3	1.21	1.33	*	2.18	1.05	1.13
T-144×108×4.5-180×100×6	0.80	30.00	16.67	0.75	0.60	458.1	0.95	1.08	1.52	1.46	0.86	1.01
T-144×162×4.5-180×100×6	0.80	30.00	16.67	0.75	0.90	542.5	1.01	1.11	*	1.69	0.92	1.05
T-144×216×4.5-180×100×6	0.80	30.00	16.67	0.75	1.20	543.8	0.91	0.99	*	2.63	0.85	0.94
T-240×180×4.5-300×100×6	0.80	50.00	16.67	0.75	0.60	349.6	0.98	1.01	*	*	0.75	1.10
T-240×270×4.5-300×100×6	0.80	50.00	16.67	0.75	0.90	392.4	1.05	1.03	*	*	0.77	1.12
T-240×360×4.5-300×100×6	0.80	50.00	16.67	0.75	1.20	430.8	1.11	1.04	*	*	0.78	1.13
T-90×60×6-100×100×6	0.90	16.67	16.67	1.00	0.60	604.2	1.08	1.23	2.14	1.65	0.72	0.78
T-90×90×6-100×100×6	0.90	16.67	16.67	1.00	0.90	758.3	1.19	1.32	*	*	0.85	0.84
T-90×120×6-100×100×6	0.90	16.67	16.67	1.00	1.20	864.9	1.22	1.33	*	*	0.91	0.84
T-162×108×6-180×100×6	0.90	30.00	16.67	1.00	0.60	640.0	1.12	1.24	*	*	0.85	0.87
T-162×162×6-180×100×6	0.90	30.00	16.67	1.00	0.90	710.3	1.12	1.18	*	*	0.88	0.83
T-162×216×6-180×100×6	0.90	30.00	16.67	1.00	1.20	757.5	1.11	1.12	*	*	0.88	0.79
T-270×180×6-300×100×6	0.90	50.00	16.67	1.00	0.60	497.9	1.49	1.26	*	*	0.77	1.03
T-270×270×6-300×100×6	0.90	50.00	16.67	1.00	0.90	539.9	2.69	1.47	*	*	0.78	1.20
T-270×360×6-300×100×6	0.90	50.00	16.67	1.00	1.20	535.7	*	1.77	*	*	0.72	1.44
T-106×80×6-133×240×8	0.80	16.63	30.00	0.75	0.60	1012.2	1.03	1.26	1.42	1.53	0.95	1.02
T-106×120×6-133×240×8	0.80	16.63	30.00	0.75	0.90	1182.4	1.05	1.23	1.48	1.56	1.01	0.99
T-106×160×6-133×240×8	0.80	16.63	30.00	0.75	1.20	1345.8	1.08	1.23	1.56	1.61	1.06	1.00
T-192×144×6-240×240×8	0.80	30.00	30.00	0.75	0.60	960.8	0.95	1.19	1.22	1.33	1.01	1.07
T-192×216×6-240×240×8	0.80	30.00	30.00	0.75	0.90	1148.3	0.94	1.18	1.23	1.35	1.10	1.07
T-192×288×6-240×240×8	0.80	30.00	30.00	0.75	1.20	1330.5	0.94	1.17	1.24	1.35	1.17	1.06
T-320×240×6-400×240×8	0.80	50.00	30.00	0.75	0.60	708.0	0.70	0.87	0.95	1.03	0.86	0.91
T-320×360×6-400×240×8	0.80	50.00	30.00	0.75	0.90	878.7	0.73	0.90	1.01	1.09	0.97	0.94
T-320×480×6-400×240×8	0.80	50.00	30.00	0.75	1.20	1030.3	0.75	0.91	1.04	1.12	1.04	0.94
T-120×80×8-133×240×8	0.90	16.63	30.00	1.00	0.60	1025.3	1.10	1.38	1.43	1.56	0.69	0.84
T-120×120×8-133×240×8	0.90	16.63	30.00	1.00	0.90	1286.9	1.13	1.41	1.53	1.65	0.81	0.85
T-120×160×8-133×240×8	0.90	16.63	30.00	1.00	1.20	1505.5	1.17	1.38	1.60	1.69	0.89	0.84
T-215×144×8-240×240×8	0.90	30.00	30.00	1.00	0.60	1235.8	1.21	1.51	1.49	1.64	0.93	1.02
T-215×215×8-240×240×8	0.90	30.00	30.00	1.00	0.90	1559.5	1.23	1.54	1.54	1.68	1.09	1.04
T-215×288×8-240×240×8	0.90	30.00	30.00	1.00	1.20	1899.1	1.25	1.56	1.58	1.73	1.25	1.06
T-360×240×8-400×240×8	0.90	50.00	30.00	1.00	0.60	1540.9	1.41	1.76	1.82	1.98	1.33	1.38
T-360×360×8-400×240×8	0.90	50.00	30.00	1.00	0.90	1804.2	1.31	1.63	1.76	1.89	1.46	1.27
T-360×480×8-400×240×8	0.90	50.00	30.00	1.00	1.20	1975.1	1.24	1.47	1.68	1.77	1.50	1.15
T-134×100×7.5-167×500×10	0.80	16.70	50.00	0.75	0.60	1580.9	1.00	1.24	1.39	1.50	0.95	0.96
T-134×150×7.5-167×500×10	0.80	16.70	50.00	0.75	0.90	1835.1	1.02	1.20	1.44	1.52	1.01	0.93
T-134×200×7.5-167×500×10	0.80	16.70	50.00	0.75	1.20	1995.2	1.01	1.15	1.47	1.51	1.01	0.90
T-240×180×7.5-300×500×10	0.80	30.00	50.00	0.75	0.60	1465.9	0.93	1.16	1.19	1.31	0.99	1.00
T-240×270×7.5-300×500×10	0.80	30.00	50.00	0.75	0.90	1745.2	0.92	1.15	1.21	1.32	1.07	0.99
T-240×360×7.5-300×500×10	0.80	30.00	50.00	0.75	1.20	1965.3	0.89	1.11	1.19	1.30	1.10	0.96
T-400×300×7.5-500×500×10	0.80	50.00	50.00	0.75	0.60	1261.1	0.80	1.00	0.98	1.08	0.98	1.00
T-400×450×7.5-500×500×10	0.80	50.00	50.00	0.75	0.90	1513.5	0.80	1.00	0.99	1.09	1.07	1.00
T-400×600×7.5-500×500×10	0.80	50.00	50.00	0.75	1.20	1645.2	0.74	0.93	0.93	1.02	1.07	0.93
T-150×100×10-167×500×10	0.90	16.70	50.00	1.00	0.60	1605.1	1.16	1.45	1.50	1.64	0.69	0.85
T-150×150×10-167×500×10	0.90	16.70	50.00	1.00	0.90	1985.1	1.18	1.47	1.58	1.71	0.80	0.86
T-150×200×10-167×500×10	0.90	16.70	50.00	1.00	1.20	2245.1	1.16	1.41	1.59	1.70	0.85	0.82
T-270×180×10-300×500×10	0.90	30.00	50.00	1.00	0.60	1894.8	1.36	1.70	1.66	1.83	0.91	1.10
T-270×270×10-300×500×10	0.90	30.00	50.00	1.00	0.90	2362.2	1.38	1.72	1.71	1.88	1.06	1.12
T-270×360×10-300×500×10	0.90	30.00	50.00	1.00	1.20	2738.6	1.34	1.68	1.70	1.86	1.15	1.09
T-450×300×10-500×500×10	0.90	50.00	50.00	1.00	0.60	2618.6	1.81	2.26	2.15	2.38	1.45	1.70

T-450×450×10-500×500×10	0.90	50.00	50.00	1.00	0.90	3084.4	1.72	2.15	2.05	2.27	1.59	1.61
T-450×600×10-500×500×10	0.90	50.00	50.00	1.00	1.20	3437.2	1.60	2.00	1.93	2.12	1.67	1.50
T-80×80×4-100×50×4	0.80	25.23	12.69	0.99	0.80	286.9	2.15	2.06	*	*	1.21	1.95
T-120×120×4-150×150×6	0.81	25.29	25.48	0.66	0.81	606.7	0.94	1.17	1.27	1.38	1.02	1.06
T-120×120×4-150×150×6-R	0.81	25.24	25.44	0.66	0.81	599.9	0.93	1.16	1.26	1.37	1.01	1.05
T-120×120×3-150×150×6	0.80	25.38	25.61	0.52	0.80	545.1	0.84	1.05	1.14	1.24	0.92	0.96
T-120×120×4-140×140×4	0.86	35.16	35.37	0.98	0.86	375.5	1.10	1.38	1.38	1.51	1.31	1.18
						Mean (P_m)	1.15	1.33	1.47	1.60	1.00	1.05
						COV (V_p)	0.293	0.234	0.219	0.221	0.218	0.211
						Resistance factor (ϕ)	0.70	0.70	0.70	0.70	0.70	0.75
						Reliability index (β_0)	2.47	3.19	3.70	3.94	2.59	2.57

Note: '*' denotes cases when k_n or $Q_f \approx 0$ or < 0.

Table 10. Comparison of test and numerical strengths with existing and proposed nominal strengths for RHS-RHS T-joints failed in combined failure mode ($0.80 \leq \beta \leq 0.90$).

Specimens	Geometric Ratios					Joint Failure Strengths (kN)	Comparisons					
T-b_1×h_1×t_1-b_0×h_0×t_0	β	2γ	h_0/t_0	τ	η	N_f	$\frac{N_f}{N^*_{E,T}}$	$\frac{N_f}{N_{E,T}}$	$\frac{N_f}{N^*_{C,T}}$	$\frac{N_f}{N_{C,T}}$	$\frac{N_f}{N_{pn}}$	$\frac{N_f}{N_{spn}}$
T-67×40×3-67×40×4	1.00	16.75	10.00	0.75	0.60	155.9	8.59	1.68	*	*	1.28	2.09
T-67×60×3-67×40×4	1.00	16.75	10.00	0.75	0.90	166.8	*	*	*	*	1.27	*
T-67×80×3-67×40×4	1.00	16.75	10.00	0.75	1.19	179.9	*	*	*	*	1.31	*
T-100×60×4.5-100×100×6	1.00	16.67	16.67	0.75	0.60	718.0	1.39	1.71	1.77	1.87	1.07	0.66
T-100×90×4.5-100×100×6	1.00	16.67	16.67	0.75	0.90	855.7	1.35	1.56	*	2.05	1.19	0.90
T-100×120×4.5-100×100×6	1.00	16.67	16.67	0.75	1.20	933.9	1.28	1.44	*	*	1.23	1.10
T-83×50×3.75-83×125×5	1.00	16.60	25.00	0.75	0.60	462.9	2.50	3.12	2.69	2.97	0.76	0.68
T-83×75×3.75-83×125×5	1.00	16.60	25.00	0.75	0.90	563.9	2.28	2.85	2.50	2.75	0.86	0.94
T-83×100×3.75-83×125×5	1.00	16.60	25.00	0.75	1.20	648.8	2.10	2.62	2.35	2.57	0.94	1.15
T-133×80×6-133×240×8	1.00	16.63	30.00	0.75	0.60	1462.4	4.32	5.40	4.52	5.01	0.85	0.83
T-133×120×6-133×240×8	1.00	16.63	30.00	0.75	0.90	1780.0	3.94	4.93	4.17	4.61	0.96	1.13
T-133×160×6-133×240×8	1.00	16.63	30.00	0.75	1.20	1934.8	3.43	4.28	3.66	4.04	1.00	1.31
T-50×30×3-50×120×3	1.00	16.67	40.00	1.00	0.60	164.1	5.97	7.46	6.13	6.80	0.58	0.79
T-50×45×3-50×120×3	1.00	16.67	40.00	1.00	0.90	200.8	5.48	6.85	5.65	6.26	0.64	1.06
T-50×60×3-50×120×3	1.00	16.67	40.00	1.00	1.20	212.5	4.64	5.80	4.80	5.32	0.69	1.28
T-167×100×7.5-167×500×10	1.00	16.70	50.00	0.75	0.60	2365.6	11.95	14.94	12.18	13.52	0.87	1.15
T-167×150×7.5-167×500×10	1.00	16.70	50.00	0.75	0.90	2785.2	10.56	13.20	10.79	11.97	0.95	1.52
T-167×200×7.5-167×500×10	1.00	16.70	50.00	0.75	1.20	3023.0	9.17	11.46	9.39	10.42	0.99	1.76
T-180×108×6-180×100×6	1.00	30.00	16.67	1.00	0.60	719.4	1.14	1.26	*	*	0.87	0.49
T-180×162×6-180×100×6	1.00	30.00	16.67	1.00	0.90	766.6	1.09	1.12	*	*	0.82	0.65
T-180×216×6-180×100×6	1.00	30.00	16.67	1.00	1.20	822.4	1.13	1.08	*	*	0.82	0.83
T-90×54×3-90×75×3	1.00	30.00	25.00	1.00	0.60	218.7	2.14	2.67	2.34	2.57	0.81	0.63
T-90×81×3-90×75×3	1.00	30.00	25.00	1.00	0.90	246.1	1.73	2.16	1.95	2.13	0.81	0.77
T-90×108×3-90×75×3	1.00	30.00	25.00	1.00	1.20	263.6	1.44	1.81	1.69	1.83	0.80	0.86
T-240×144×8-240×240×8	1.00	30.00	30.00	1.00	0.60	2233.6	4.30	5.38	4.50	4.99	1.05	0.82
T-240×216×8-240×240×8	1.00	30.00	30.00	1.00	0.90	2566.8	3.55	4.44	3.75	4.15	1.08	1.02
T-240×288×8-240×240×8	1.00	30.00	30.00	1.00	1.20	2871.8	3.10	3.88	3.31	3.65	1.12	1.19
T-120×72×4-120×160×4	1.00	30.00	40.00	1.00	0.60	477.9	6.38	7.97	6.54	7.26	0.94	1.00
T-120×108×4-120×160×4	1.00	30.00	40.00	1.00	0.90	546.6	5.24	6.55	5.41	5.99	0.96	1.23
T-120×144×4-120×160×4	1.00	30.00	40.00	1.00	1.20	546.5	4.09	5.11	4.24	4.70	0.89	1.28
T-300×180×10-300×500×10	1.00	30.00	50.00	1.00	0.60	3272.9	10.79	13.48	10.99	12.20	0.98	1.04
T-300×270×10-300×500×10	1.00	30.00	50.00	1.00	0.90	3450.1	8.17	10.22	8.36	9.27	0.91	1.18
T-300×360×10-300×500×10	1.00	30.00	50.00	1.00	1.20	3999.1	7.39	9.24	7.58	8.41	0.99	1.42

T-240×144×8-240×480×8	1.00	30.00	60.00	1.00	0.60	2213.8	16.30	20.37	16.52	18.35	1.02	1.36
T-240×216×8-240×480×8	1.00	30.00	60.00	1.00	0.90	2582.2	13.66	17.08	13.88	15.41	1.06	1.72
T-240×288×8-240×480×8	1.00	30.00	60.00	1.00	1.20	2911.7	12.02	15.03	12.24	13.59	1.11	2.01
T-300×180×7.5-300×100×6	1.00	50.00	16.67	1.25	0.60	511.9	2.89	1.39	*	*	0.75	0.54
T-300×270×7.5-300×100×6	1.00	50.00	16.67	1.25	0.90	554.4	*	*	*	*	0.70	*
T-300×360×7.5-300×100×6	1.00	50.00	16.67	1.25	1.20	609.1	*	*	*	*	0.71	*
T-200×120×5-200×100×4	1.00	50.00	25.00	1.25	0.60	350.9	1.27	1.58	1.57	1.67	0.88	0.36
T-200×180×5-200×100×4	1.00	50.00	25.00	1.25	0.90	376.8	1.06	1.22	*	*	0.82	0.42
T-200×240×5-200×100×4	1.00	50.00	25.00	1.25	1.20	406.6	0.97	1.08	*	*	0.81	0.49
T-400×240×10-400×240×8	1.00	50.00	30.00	1.25	0.60	1888.6	2.39	2.99	2.60	2.86	1.08	0.46
T-400×360×10-400×240×8	1.00	50.00	30.00	1.25	0.90	2048.6	1.81	2.27	2.05	2.24	1.01	0.52
T-400×480×10-400×240×8	1.00	50.00	30.00	1.25	1.20	2206.6	1.50	1.88	1.78	1.92	1.00	0.58
T-150×90×3.75-150×120×3	1.00	50.00	40.00	1.25	0.60	289.0	4.51	5.63	4.66	5.16	1.23	0.73
T-150×135×3.75-150×120×3	1.00	50.00	40.00	1.25	0.90	326.0	3.56	4.45	3.71	4.11	1.20	0.87
T-150×180×3.75-150×120×3	1.00	50.00	40.00	1.25	1.20	357.2	3.00	3.75	3.15	3.48	1.21	0.98
T-500×300×12.5-500×500×10	1.00	50.00	50.00	1.25	0.60	3835.4	8.31	10.38	8.46	9.40	1.38	0.80
T-500×450×12.5-500×500×10	1.00	50.00	50.00	1.25	0.90	4364.4	6.62	8.27	6.76	7.51	1.36	0.95
T-500×600×12.5-500×500×10	1.00	50.00	50.00	1.25	1.20	4870.9	5.68	7.10	5.82	6.46	1.40	1.09
T-250×150×6.25-250×300×5	1.00	50.00	60.00	1.25	0.60	884.4	10.95	13.69	11.10	12.33	1.31	1.03
T-250×225×6.25-250×300×5	1.00	50.00	60.00	1.25	0.90	998.0	8.65	10.81	8.79	9.76	1.28	1.22
T-250×300×6.25-250×300×5	1.00	50.00	60.00	1.25	1.20	1045.4	6.97	8.71	7.10	7.88	1.23	1.31
T-100×50×4-100×50×4	1.00	25.00	12.50	1.00	0.50	334.5	2.46	2.08	*	*	1.66	1.24
T-120×120×4-120×120×4	1.00	30.00	30.00	1.00	1.00	606.8	3.09	3.87	3.26	3.60	1.07	1.15
T-140×140×4-140×140×4	1.00	35.00	35.00	1.00	1.00	626.6	3.73	4.66	3.89	4.31	1.13	1.14
T-120×120×3-120×120×3	1.00	40.00	40.00	1.00	1.00	402.8	4.82	6.02	4.97	5.51	1.39	1.31
						Mean (P_m)	4.94	5.93	5.76	6.29	1.02	1.02
						COV (V_p)	0.750	0.793	0.639	0.653	0.219	0.374
						Resistance factor (ϕ)	0.70	0.70	0.70	0.70	0.70	0.50
						Reliability index (β_0)	2.99	3.06	3.70	3.75	2.63	2.66

Note: '*' denotes cases when k_n or $Q_f \approx 0$ or < 0.

Table 11. Comparison of test and numerical strengths with existing and proposed nominal strengths for RHS-RHS T-joints failed in chord side wall failure mode (β=1.0).

Parameters	Buckling Curves				
	a_0	a	b	c	d
No. of data	58	58	58	58	58
Mean (P_m)	0.98	1.02	1.08	1.16	1.28
COV (V_p)	0.230	0.219	0.208	0.199	0.192
Resistance factor (ϕ)	0.70	0.70	0.70	0.70	0.70
Reliability index (β_0)	2.45	2.63	2.88	3.12	3.48

Table 12. Comparison of test and numerical strengths with proposed nominal strengths obtained using different buckling curves for RHS-RHS T-joints failed in chord side wall failure mode (β=1.0).

Specimens	Geometric Ratios				Joint Failure Strengths (kN)	Comparisons					
T-d_1×t_1-b_0×h_0×t_0	β	2γ	h_0/t_0	τ	N_f	$\frac{N_f}{N^*_{E,T}}$	$\frac{N_f}{N_{E,T}}$	$\frac{N_f}{N^*_{C,T}}$	$\frac{N_f}{N_{C,T}}$	$\frac{N_f}{N_{pn}}$	$\frac{N_f}{N_{spn}}$
T-30×3-100×100×6	0.30	16.67	16.67	0.50	137.1	0.86	1.02	1.08	1.18	1.20	0.79
T-40×4-133×240×8	0.30	16.63	30.00	0.50	231.2	0.77	0.96	0.98	1.08	1.14	0.73
T-15×3-50×120×3	0.30	16.67	40.00	1.00	25.4	0.60	0.75	0.76	0.83	0.90	0.61
T-50×5-167×500×10	0.30	16.70	50.00	0.50	348.5	0.74	0.93	0.94	1.04	1.10	0.70
T-54×3-180×100×6	0.30	30.00	16.67	0.50	100.1	0.65	0.75	0.80	0.87	1.17	1.23
T-72×4-240×240×8	0.30	30.00	30.00	0.50	160.6	0.54	0.67	0.66	0.73	1.05	1.06
T-36×3-120×160×4	0.30	30.00	40.00	0.75	35.3	0.47	0.59	0.57	0.63	0.98	1.03
T-90×5-300×500×10	0.30	30.00	50.00	0.50	253.5	0.54	0.68	0.66	0.73	1.06	1.05
T-72×3-240×100×6	0.30	40.00	16.67	0.50	82.5	0.55	0.63	0.66	0.72	1.14	1.44
T-72×3-240×180×6	0.30	40.00	30.00	0.50	76.5	0.45	0.57	0.56	0.62	1.06	1.27
T-72×3-240×240×6	0.30	40.00	40.00	0.50	72.5	0.43	0.54	0.52	0.57	1.00	1.21
T-72×3-240×300×6	0.30	40.00	50.00	0.50	71.2	0.42	0.53	0.51	0.57	0.98	1.18
T-90×3-300×100×6	0.30	50.00	16.67	0.50	72.6	0.59	0.64	0.64	0.69	1.16	1.89
T-120×4-400×240×8	0.30	50.00	30.00	0.50	120.5	0.40	0.50	0.51	0.56	1.08	1.41
T-45×3-150×120×3	0.30	50.00	40.00	1.00	15.0	0.36	0.44	0.43	0.48	1.01	1.40
T-150×5-500×500×10	0.30	50.00	50.00	0.50	170.7	0.36	0.45	0.44	0.48	0.98	1.25
T-50×4.2-100×100×6	0.50	16.67	16.67	0.70	238.2	1.04	1.30	1.40	1.52	1.12	0.72
T-67×5.6-133×240×8	0.50	16.63	30.00	0.70	409.9	1.00	1.25	1.28	1.41	1.07	0.67
T-25×3-50×120×3	0.50	16.67	40.00	1.00	42.3	0.74	0.92	0.93	1.03	0.79	0.53
T-83×7-167×500×10	0.50	16.70	50.00	0.70	612.5	0.97	1.21	1.24	1.36	1.05	0.65
T-90×4.2-180×100×6	0.50	30.00	16.67	0.70	166.5	0.73	0.91	0.99	1.08	1.04	1.05
T-120×5.6-240×240×8	0.50	30.00	30.00	0.70	275.2	0.68	0.84	0.83	0.92	0.97	0.95
T-60×4-120×160×4	0.50	30.00	40.00	1.00	51.0	0.50	0.63	0.61	0.68	0.85	0.87
T-150×7-300×500×10	0.50	30.00	50.00	0.70	441.3	0.69	0.87	0.85	0.94	0.99	0.96
T-120×4.2-240×100×6	0.50	40.00	16.67	0.70	140.2	0.62	0.76	0.84	0.92	1.04	1.23
T-120×4.2-240×180×6	0.50	40.00	30.00	0.70	130.5	0.57	0.71	0.71	0.78	0.97	1.14
T-120×4.2-240×240×6	0.50	40.00	40.00	0.70	125	0.55	0.68	0.66	0.73	0.93	1.09
T-120×4.2-240×300×6	0.50	40.00	50.00	0.70	120.1	0.52	0.65	0.64	0.70	0.89	1.05
T-150×4.2-300×100×6	0.50	50.00	16.67	0.70	122.6	0.62	0.71	0.82	0.87	1.05	1.51
T-200×5.6-400×240×8	0.50	50.00	30.00	0.70	201.4	0.49	0.62	0.62	0.69	0.97	1.24
T-75×3-150×120×3	0.50	50.00	40.00	1.00	22.5	0.39	0.49	0.48	0.53	0.81	1.09
T-250×7-500×500×10	0.50	50.00	50.00	0.70	289.9	0.46	0.57	0.55	0.61	0.90	1.12
T-70×5.4-100×100×6	0.70	16.67	16.67	0.90	438.5	1.23	1.53	1.71	1.85	1.11	0.66
T-93×7.2-133×240×8	0.70	16.63	30.00	0.90	776.5	1.22	1.53	1.60	1.75	1.11	0.64
T-35×3-50×120×3	0.70	16.67	40.00	1.00	80.5	0.90	1.12	1.16	1.27	0.84	0.52
T-117×9-167×500×10	0.70	16.70	50.00	0.90	1186.9	1.19	1.49	1.55	1.70	1.08	0.62
T-126×5.4-180×100×6	0.70	30.00	16.67	0.90	319.4	0.91	1.11	1.27	1.36	1.08	1.00
T-168×7.2-240×240×8	0.70	30.00	30.00	0.90	576.6	0.90	1.13	1.12	1.24	1.09	0.99
T-84×3.6-120×160×4	0.70	30.00	40.00	0.90	127.5	0.80	1.00	0.99	1.09	0.97	0.92
T-210×9-300×500×10	0.70	30.00	50.00	0.90	859.8	0.86	1.08	1.07	1.18	1.04	0.93
T-168×5.4-240×100×6	0.70	40.00	16.67	0.90	272.4	0.79	0.95	1.10	1.18	1.09	1.20
T-168×5.4-240×180×6	0.70	40.00	30.00	0.90	278.5	0.78	0.97	0.97	1.07	1.11	1.21
T-168×5.4-240×240×6	0.70	40.00	40.00	0.90	267.7	0.75	0.93	0.91	1.00	1.07	1.17
T-168×5.4-240×300×6	0.70	40.00	50.00	0.90	246.5	0.69	0.86	0.84	0.93	0.98	1.07
T-210×5.4-300×100×6	0.70	50.00	16.67	0.90	221.5	0.75	0.84	1.11	1.12	1.02	1.43
T-280×7.2-400×240×8	0.70	50.00	30.00	0.90	420.8	0.66	0.83	0.85	0.93	1.09	1.29
T-105×3-150×120×3	0.70	50.00	40.00	1.00	51.4	0.57	0.72	0.71	0.78	0.95	1.19
T-350×9-500×500×10	0.70	50.00	50.00	0.90	630.4	0.63	0.79	0.77	0.85	1.05	1.21
T-88.9×4-150×150×6	0.59	25.00	25.00	0.67	212.47	0.77	0.97	0.97	1.07	0.91	0.79
				Mean (P_m)		0.69	0.85	0.87	0.96	1.02	1.04
				COV (V_p)		0.319	0.324	0.352	0.347	0.093	0.277
				Resistance factor (ϕ)		0.85	0.85	0.85	0.85	0.85	0.65
				Reliability index (β_0)		0.64	1.13	1.23	1.44	2.58	2.58

Table 13. Comparison of test and numerical strengths with existing and proposed nominal strengths for CHS-RHS T-joints failed in chord face failure mode ($0.30 \leq \beta \leq 0.70$).

Specimens	Geometric Ratios				Joint Failure Strengths (kN)	Comparisons					
T-$d_1 \times t_1$-$b_0 \times h_0 \times t_0$	β	2γ	h_0/t_0	τ	N_f	$\frac{N_f}{N^*_{E,T}}$	$\frac{N_f}{N_{E,T}}$	$\frac{N_f}{N^*_{C,T}}$	$\frac{N_f}{N_{C,T}}$	$\frac{N_f}{N_{pn}}$	$\frac{N_f}{N_{spn}}$
T-75×6-100×100×6	0.75	16.67	16.67	1.00	540.1	1.32	1.61	1.84	1.98	1.13	1.11
T-100×8-133×240×8	0.75	16.63	30.00	1.00	962.3	1.28	1.60	1.70	1.86	1.12	1.07
T-37.5×3-50×120×3	0.75	16.67	40.00	1.00	102.1	0.97	1.22	1.27	1.39	0.85	0.87
T-125×10-167×500×10	0.75	16.70	50.00	1.00	1480.1	1.28	1.60	1.69	1.84	1.12	1.06
T-135×6-180×100×6	0.75	30.00	16.67	1.00	383.2	0.96	1.14	1.34	1.43	0.94	1.16
T-180×8-240×240×8	0.75	30.00	30.00	1.00	740.4	0.99	1.24	1.24	1.37	1.02	1.20
T-90×4-120×160×4	0.75	30.00	40.00	1.00	162.3	0.87	1.09	1.08	1.19	0.89	1.10
T-225×10-300×500×10	0.75	30.00	50.00	1.00	1095.2	0.94	1.18	1.18	1.30	0.97	1.11
T-180×6-240×100×6	0.75	40.00	16.67	1.00	308.0	0.79	0.92	1.10	1.17	0.84	1.17
T-180×6-240×180×6	0.75	40.00	30.00	1.00	356.5	0.85	1.06	1.07	1.18	0.97	1.30
T-180×6-240×240×6	0.75	40.00	40.00	1.00	371.5	0.89	1.11	1.08	1.19	1.01	1.35
T-180×6-240×300×6	0.75	40.00	50.00	1.00	367.8	0.88	1.10	1.08	1.19	1.00	1.34
T-225×6-300×100×6	0.75	50.00	16.67	1.00	238.7	0.72	0.80	1.34	1.14	0.71	1.26
T-300×8-400×240×8	0.75	50.00	30.00	1.00	518.5	0.70	0.87	0.90	0.98	0.87	1.23
T-112.5×3-150×120×3	0.75	50.00	40.00	1.00	76.5	0.73	0.91	0.90	1.00	0.91	1.37
T-375×10-500×500×10	0.75	50.00	50.00	1.00	845.6	0.73	0.91	0.88	0.97	0.91	1.26
T-80×6-100×100×6	0.80	16.67	16.67	1.00	614.8	1.30	1.51	1.82	1.93	1.05	0.89
T-106×8-133×240×8	0.80	16.63	30.00	1.00	955.4	1.07	1.34	1.45	1.58	0.93	0.74
T-40×3-50×120×3	0.80	16.67	40.00	1.00	120.8	0.95	1.19	1.26	1.38	0.83	0.69
T-133×10-167×500×10	0.80	16.70	50.00	1.00	1512.9	1.09	1.36	1.47	1.60	0.94	0.74
T-144×6-180×100×6	0.80	30.00	16.67	1.00	468.6	1.01	1.17	1.44	1.51	0.94	1.01
T-192×8-240×240×8	0.80	30.00	30.00	1.00	933.4	1.03	1.29	1.30	1.43	1.05	1.03
T-96×4-120×160×4	0.80	30.00	40.00	1.00	202.6	0.90	1.12	1.12	1.24	0.91	0.93
T-240×10-300×500×10	0.80	30.00	50.00	1.00	1390.5	0.99	1.23	1.25	1.37	1.00	0.96
T-192×6-240×100×6	0.80	40.00	16.67	1.00	390.5	0.86	0.99	1.25	1.29	0.87	1.05
T-192×6-240×180×6	0.80	40.00	30.00	1.00	443.4	0.87	1.09	1.11	1.22	0.98	1.09
T-192×6-240×240×6	0.80	40.00	40.00	1.00	435.9	0.86	1.07	1.05	1.16	0.97	1.07
T-192×6-240×300×6	0.80	40.00	50.00	1.00	422.5	0.83	1.04	1.03	1.13	0.94	1.04
T-240×6-300×100×6	0.80	50.00	16.67	1.00	346.6	0.94	1.01	*	*	0.84	1.34
T-320×8-400×240×8	0.80	50.00	30.00	1.00	700.4	0.78	0.97	1.02	1.11	0.96	1.13
T-120×3-150×120×3	0.80	50.00	40.00	1.00	82.5	0.65	0.81	0.81	0.89	0.80	1.00
T-400×10-500×500×10	0.80	50.00	50.00	1.00	1090.9	0.77	0.97	0.94	1.04	0.96	1.10
T-90×6-100×100×6	0.90	16.67	16.67	1.00	765.4	1.35	1.55	1.98	1.97	0.96	0.68
T-120×8-133×240×8	0.90	16.63	30.00	1.00	1405.5	1.56	1.95	2.00	2.18	0.98	0.78
T-45×3-50×120×3	0.90	16.67	40.00	1.00	153.6	1.27	1.59	1.60	1.75	0.77	0.68
T-150×10-167×500×10	0.90	16.70	50.00	1.00	2169.2	1.64	2.05	2.09	2.29	0.98	0.81
T-162×6-180×100×6	0.90	30.00	16.67	1.00	636.1	1.06	1.19	*	*	0.93	0.78
T-216×8-240×240×8	0.90	30.00	30.00	1.00	1516.7	1.55	1.93	1.87	2.06	1.25	1.13
T-108×4-120×160×4	0.90	30.00	40.00	1.00	306.4	1.36	1.70	1.64	1.81	1.01	1.04
T-270×10-300×500×10	0.90	30.00	50.00	1.00	2235.2	1.66	2.07	2.02	2.22	1.18	1.18
T-216×6-240×100×6	0.90	40.00	16.67	1.00	559.3	0.94	1.01	*	*	0.91	0.84
T-216×6-240×180×6	0.90	40.00	30.00	1.00	705.2	1.21	1.51	1.48	1.62	1.15	1.11
T-216×6-240×240×6	0.90	40.00	40.00	1.00	705.6	1.35	1.68	1.59	1.76	1.15	1.24
T-216×6-240×300×6	0.90	40.00	50.00	1.00	694.1	1.40	1.75	1.67	1.84	1.13	1.28
T-270×6-300×100×6	0.90	50.00	16.67	1.00	440.8	1.17	1.03	*	*	0.79	1.21
T-360×8-400×240×8	0.90	50.00	30.00	1.00	1190.3	1.09	1.37	1.38	1.51	1.20	1.17
T-135×3-150×120×3	0.90	50.00	40.00	1.00	140.1	1.03	1.29	1.24	1.37	1.00	1.17
T-450×10-500×500×10	0.90	50.00	50.00	1.00	1984.6	1.41	1.76	1.66	1.84	1.28	1.47

T-88.9×3-120×60×4	0.74	30.00	15.00	0.75	170.5	1.24	1.42	1.65	1.71	1.14	1.59
T-88.9×3-120×60×4	0.74	30.00	15.00	0.75	176.4	1.29	1.47	1.71	1.77	1.18	1.64
T-88.9×4-120×60×4	0.74	30.00	15.00	1.00	176.9	1.29	1.47	1.71	1.78	1.18	1.65
T-88.9×4-120×60×4	0.74	30.00	15.00	1.00	169.4	1.24	1.41	1.64	1.70	1.13	1.58
T-88.9×4-120×120×6	0.74	20.00	20.00	0.67	362.1	1.00	1.25	1.25	1.37	0.92	0.99
T-88.9×4-100×60×4	0.89	25.00	15.00	1.00	291.0	1.49	1.59	*	*	1.08	1.00
T-88.9×4-100×100×4	0.89	25.00	25.00	1.00	286.5	1.18	1.48	1.45	1.59	1.01	0.82
					Mean (P_m)	1.08	1.31	1.39	1.50	0.99	1.10
					COV (V_p)	0.239	0.245	0.242	0.238	0.128	0.216
					Resistance factor (ϕ)	0.80	0.80	0.80	0.80	0.80	0.75
					Reliability index (β_0)	2.21	2.71	3.01	3.25	2.56	2.67

Note: '*' denotes cases when k_n or $Q_f \approx 0$ or < 0.

Table 14. Comparison of test and numerical strengths with existing and proposed nominal strengths for CHS-RHS T-joints failed in combined failure mode ($0.73 \leq \beta \leq 0.90$).